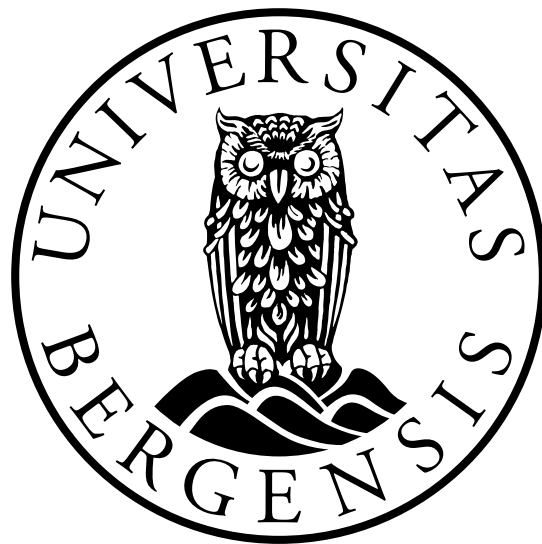# How to Improve Visibility in Turbid Water

Malin Stølsvik

Master's Thesis in Ocean Technology

University of Bergen

Department of Physics and Technology
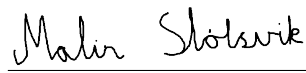
May 31, 2021

Preface

The work of this master's thesis is carried out at Department of Physics and Technology (IFT) at the University of Bergen (UiB). The thesis is a result of a 2 year master's degree in Ocean Technology within the field of optics. When I had to come up with ideas of what I wanted to study in my master's thesis in the autumn of 2019, it was challenging to develop ideas in a completely different field than what I was educated in. After discussion with my supervisors, I ended up with imaging underwater, and more specifically, how it is possible to utilize the polarizing properties of light to improve underwater imaging. Writing a master's thesis during a world pandemic may have been extra challenging, but it also has been an exciting and educational year.

As this thesis is coming to an end, I want to express my gratitude to my supervisors, Postdoctoral Fellow Arne Skodvin Kristoffersen and Professor Børge Hamre, for their good guidance and support in completing the project. I also would like to express my gratitude to Head Engineer Yi-Chun Chen for good guidance at the laboratory.

<div align="center">

Tysvær, May 2021

Malin Stølsvik

Malin Stølsvik

</div>

Abstract

The interest in the ocean and what happens below sea level has grown a lot in recent decades. Optical imaging under water has received increasing attention via applications such as target detection and recognition, both in aquaculture, marine rescue, and scientific research [1][2]. Scientists have been allowed to examine the ocean in ways one only could dream of before. It has been developed quite advanced camera systems which improve imaging under water, but because of the various optical phenomena occurring in underwater systems, photography on land is far less challenging. Visibility and detection of objects in water are limited to tens of meters and often less. The limitation results from a combination of different optical phenomena such as scattering, absorption, and masking of objects by veiling light. The particle content in the water is also crucial in determining the actual distance for detection. Although technology has evolved, there are still challenges with the optical phenomena affecting underwater imaging and reducing the detection distance. According to Carton et al. [3], polarization has shown to increase the contrast and detection range in scattering media both above and below water. Bohren et al. [4, p.381] also states that polarization can increase the contrast in a scattering medium considerably.

The main objective of the master's thesis is to study to what extent it is possible to improve imaging underwater by utilizing the polarization properties of light. CDOM's affection on underwater imaging is also studied. Polarized light emitted from small particles in the water retains its original polarization, while polarized light striking a large object with a rough surface, such as a fish, will be largely depolarized. By using two polarizing filters, one in front of the light source and one in front of the camera rotated 90° (cross-polarization), one will be able to remove the unwanted scattered light - while theoretically retain up to half of the light coming directly from the object. The use of polarizing filters in an underwater system is assumed to give the best effect when there is single scattering in the medium being examined, as multiple scattering ($\tau^* > 0.3$) causes the polarized incident light not to be preserved in backward direction [4, p.269].

Three experiments are conducted to study the effect of polarization filters in an underwater

system. The first experiment, Experiment A, consists of polystyrene spheres and Milli-Q water. The results from Experiment A indicates an apparent effect of using cross-polarization when there is single scattering in the container. For $\tau^* < 0.3$ the contrast has been improved by 22-105% when cross-polarization is used. Experiment B consists of algae and seawater. For $\tau^* < 0.3$ the contrast has been improved by 63-132% when cross-polarization is used. Although the object is not observable due to absorption at the highest concentrations, the contrast in the images is nevertheless improved using cross-polarization. Experiment C consists of studying how CDOM is affecting imaging in underwater systems. The results show an increase in contrast when cross-polarization is used. Results also show how CDOM is causing color degradation in the images.

List of Tables

List of Figures

Abbreviations

CDOM Colored dissolved organic matter

DOP Degree of polarization

IFT Department of Physics and Technology

LHC Left hand circular

RHC Right hand circular

UiB University of Bergen

Contents

1 Introduction

1.1 Background

The interest in the ocean and what happens below sea level has grown a lot in recent decades. Much of Norway's industry is related to the ocean, and optical imaging under water has received increasing attention via applications such as target detection and recognition, both in aquaculture, marine rescue, and scientific research [1][2].

Early scientists began to explore the ocean with optical systems designed to work on land. The first documented attempt to see underwater was Konrad Kyeser in 1405 [5, p. 19]. He entered the ocean in his diving leather suit, metal helmet, with glass windows around him. Around the 19th century, submarines were built to transport ocean researchers into the depths. Diving suits connected to an air source on land were also built. In 1893, a diver named Louis Boutan took a picture at a depth of 50m, using a photosensitive glass plate. In the late 19th and early 20th century - two inventions that have played a significant part in the development of underwater imaging were developed [6]. The development of the film camera beginning in 1890 with George Eastman, and the development of Aqua-Lung, which started in 1940 Cousteau and Gangnan. According to Jaffe [6] the first underwater color photographs were reported to have been taken in 1926-1927 by William Longely and Charles Martin. Underwater optical imaging has been through a significant revolution thanks to technological development in the latter part of the 1900s. It has been developed quite advanced camera systems which have improved the possibility of imaging under water, but because of the various optical phenomena occurring in underwater systems, photographing on land is far less challenging. Visibility and detection of objects in the water are limited to tens of meters and often less — the limitation results from a combination of scattering, absorption, and masking of objects by veiling light.

Absorption removes light rays from the path and causes the electromagnetic waves in the water to be quickly attenuated. The combined effect of absorption and scattering leads to light attenuation [7]. Absorption length is a measure that can be used to express how far light is transmitted

through the media before it is completely absorbed. For clear water, the absorption length is greatest for the shortest wavelengths and smallest for the longer wavelengths. This result in most of the objects underwater appearing blue-greenish. For water with Colored dissolved organic matter (CDOM), the short wavelengths disappear first, and the red survives the longest. In turbid water or places with a high concentration of plankton, red light is better transmitted [7]. As a result of scattering and light being attenuated, underwater images appear dark and suffer by low contrast.

Apart from the optical phenomena affecting visibility, various factors make the visibility decrease, some of them which are plankton blooms. During the summer, plankton blooms can reduce visibility in the ocean dramatically. Plankton usually requires specific temperature, salinity, and light conditions, and therefore only occur seasonally [8]. Another central factor affecting visibility is the particles in the water. The visibility is reduced depending on the density, type, and amount of sediment suspended in the water. Sediment particles get suspended when disturbed by water movement. Natural causes that lead to water movement include currents, runoff, and serve weather [8]. Turbid water is waters with large amounts of particles. The more particles the more scattering and absorption can be experienced.

Optical depth (τ) can be used as a measure of visibility. The more particles suspended in the water, the higher the optical depth. The optical depth of the medium also can be used as an indicator of whether the medium consists of single- or multiple scattering. According to Ugulen et al. [9] one can assume single scattering when $\tau < 0.1$, and multiple scattering when $\tau > 0.3$. Ugulen et al. [9] also states that "double-scattering corrections may be necessary for $0.1 < \tau < 0.3$". Waters containing multiple-scattering ($\tau > 0.3$) is known to have more reduced visibility than waters with single scattering ($\tau < 0.1$).

As discussed, there are several factors that, even though technology has developed considerably in the recent decades, still make it challenging to photograph underwater. According to Liu et al. [10], the loss of light problem is solved by using more sources of artificial lighting. A problem with this solution is that the use of artificial lighting also can complicate the image conditions as the amount of scattering depends on the illuminated volume of water in the camera's field

2

of view. The adverse effects increase when the distance between the camera and the object is increased. Reducing the distance between the camera and the object can reduce these effects to some extent. According to Cartron et al. [3] polarization is another method that has been shown to increase the contrast and detection range in scattering media both above and below water. Bohren et al. [4, p.381] also states that polarization can increase the contrast in a scattering medium considerably. Improving imaging underwater by utilizing the polarization properties of light will be further studied in this thesis.

1.2 Description of Problem

When imaging objects underwater, it is a known problem that the image gets blurred by light that is not just reflected from the object but scattered from particles in the water. Depending on the shape, size and refractive index of the particles, a significant portion of light from a source near the camera is scattered back and in through the lens. The result is an image formed by light, both from the object and the water between the camera and the object.

A method that can be used to overcome this problem is to utilize the polarization properties of light. Polarization is shown to increase the contrast and detection range in scattering media. According to Bohren et al. [4, p.381], polarized light emitted from small particles in the water retains its original polarization, while polarized light striking a large object with a rough surface, such as a fish, is largely depolarized. By using two linear polarizing filters, one in front of the light source and one in front of the camera (rotated 90°), one will be able to reduce the unwanted scattered light. At the same time, theoretically retain up to half of the light coming directly from the object. The use of polarizing filters in an underwater system is assumed to give the best effect when there is single scattering in the medium being examined, as multiple scattering causes the polarized incident light not to be preserved in backward direction [4, p.269].

The master's thesis will focus on finding out to what extent it is possible to achieve better imaging in different types of water utilizing the polarization properties of light. As well as studying how Colored dissolved organic matter (CDOM) is affecting underwater imaging.

2 Theory

2.1 Propagation of Light in Water

The visible light is a part of the electromagnetic spectrum (illustrated in Figure 2.1), and is ranging in wavelength from ≈400 nm to 700 nm.
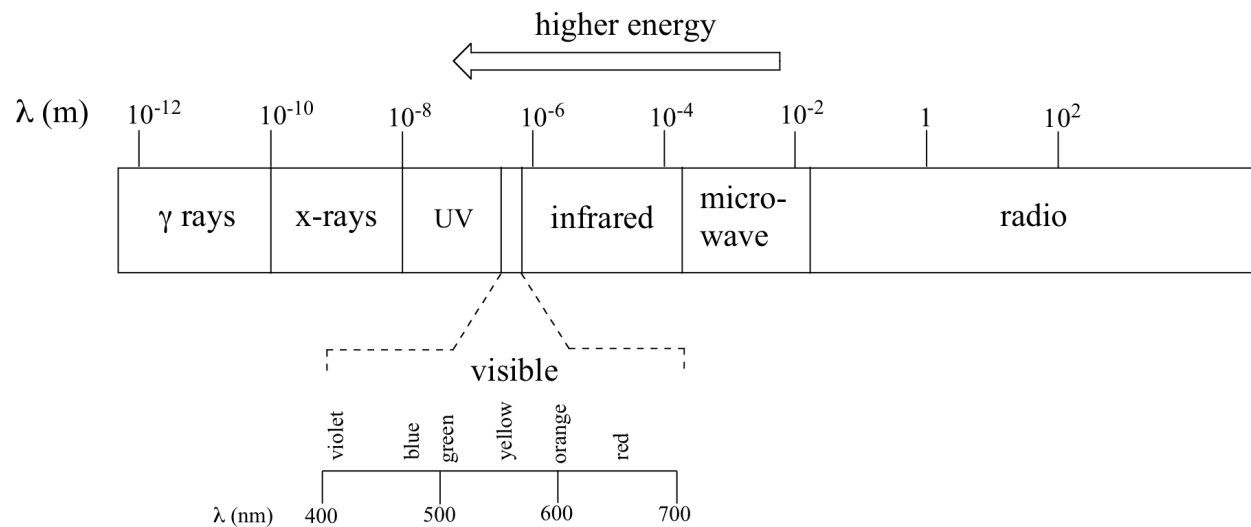
Figure 2.1: Electromagnetic spectrum. The illustration is obtained from [11].

Light has both wave- and particle properties. Which of these ways to describe light depends on the area of use. This thesis will focus on the wave properties of light. When electromagnetic waves propagate in a sub-aquatic medium, they interact with water molecules and with dissolved and particular matter [7, p. 25]. Figure 2.2 illustrates a simple underwater system. The light source, object and camera are placed in water. As can be seen, light rays are sent towards an object. When the light rays are propagating in the medium, the waves are interacting with particles that cause both forward- and backward scattering. Depending on the medium, a portion of the light will be absorbed, and the further the light rays are propagating into the medium, the more they get attenuated. When light rays pass through the camera housing, some of the light gets refracted due to different refractive index of the different mediums. As a result of the op-

tical phenomena occurring underwater images appear dark and suffer by low contrast. In this section, scattering, refraction, attenuation, and absorption will be further addressed.
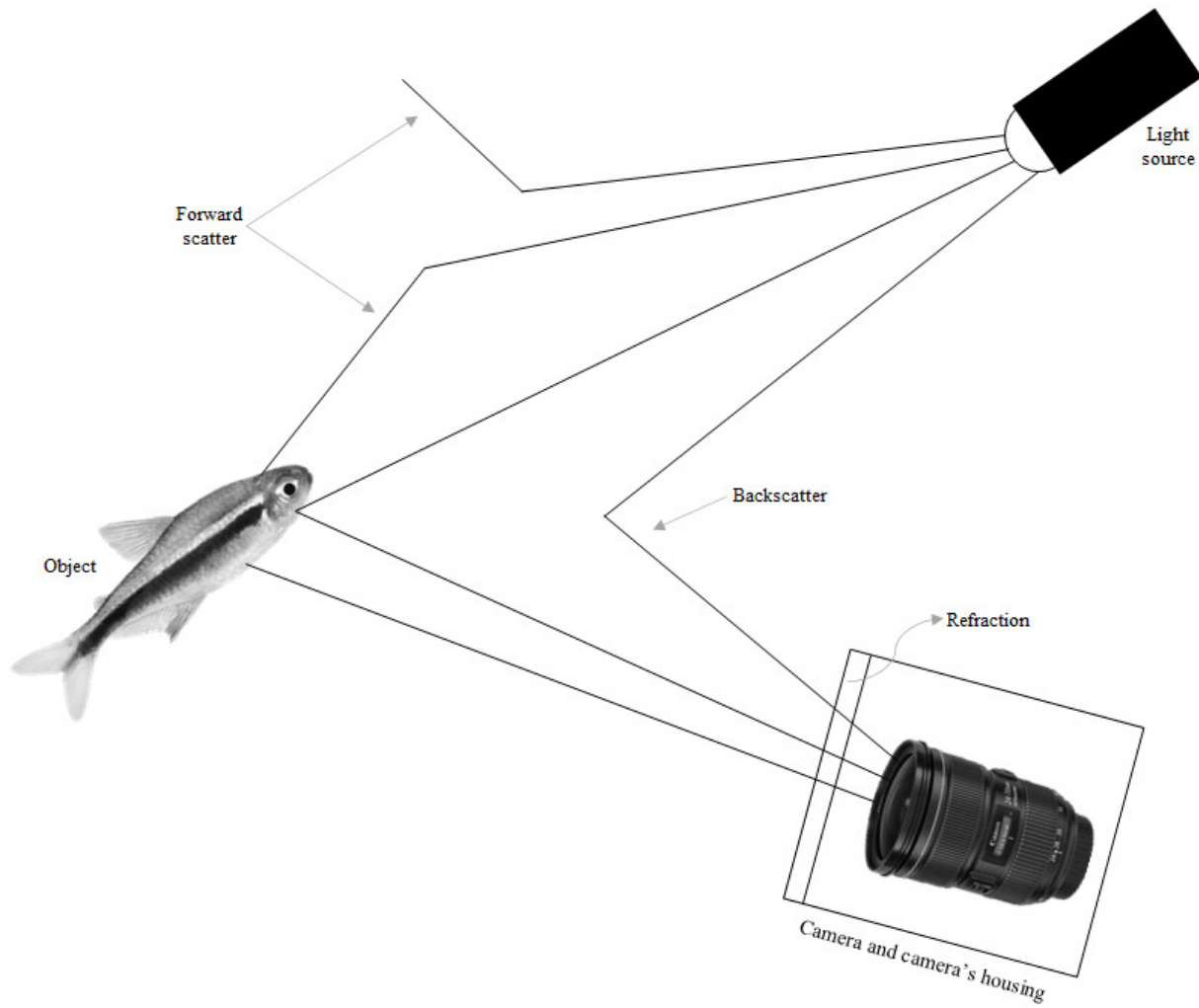
Figure 2.2: A simple underwater imaging system. The illustration is adapted from [7]

2.1.1 Reflection

When light is sent towards a surface, some of the light gets reflected when hitting the surface. In a natural environment, all light is rarely reflected. Some of the light may get absorbed, some transmitted, and some of the light may be scattered. How much of the light gets reflected, absorbed, and transmitted depends on the medium in which the light propagates.

There are two extremes of reflection: specular reflection and diffuse reflection. Reflection on a

smooth, such as a calm sea or a mirror, is known as specular reflection [12]. Specular reflection, illustrated in Figure 2.3a, occurs when the surface has irregularities in the same order for magnitude as the wavelength (λ), the result is reflected wavelets more or less in-phase [13, p. 107]. Specular reflection follows the law of reflection, which states that the angle of incidence θ_i is equal to the angle of reflection θ_r (Eq. 2.1). In order to follow the law of reflection, the incidence ray must be perpendicular to the surface, and the reflected ray must lay in the plane of incidence.

$$\theta_i = \theta_r \tag{2.1}$$

Reflection on uneven surfaces, for example a wavy sea, is known as diffuse reflection [12] (Illustrated in Figure 2.3b). Here the surface has irregularities that are large compared to the wavelength (λ).

(a)	(b)
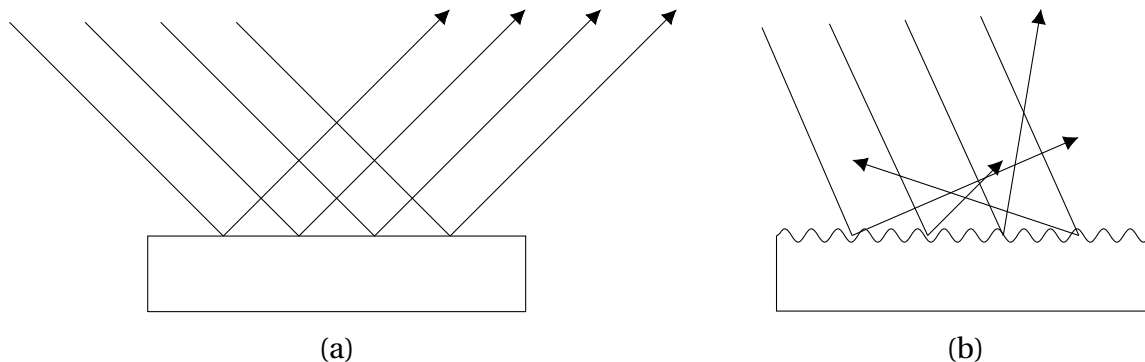
Figure 2.3: (a) Specular reflection (b) Diffuse reflection. The illustration is adapted from [13, p. 108]

2.1.2 Refraction

As mentioned in Section 2.1.1, it is not typical for all the light hitting a surface to be reflected. Some of the light rays also can be refracted. *Refraction* is an optical phenomenon in which the incident light ray changes the direction in the boundary transition between two different isotropic media. The law of refraction, also known as Snell's law, was derived by a Dutch mathe-

matician named Willebrord van Rojen Snell, i 1621. The law represents the relationship between the angle of incidence and angle of refraction when a light ray hits the boundary transition between the two media (Figure 2.4). The law is expressed in Eq. 2.2.

$$n_1 \sin\theta_i = n_2 \sin\theta_r \tag{2.2}$$

where n_1 is the refractive index of the incident medium, n_2 is the refractive index of the refracted medium, θ_i is the angle of incidence, and θ_r is the angle of refraction.
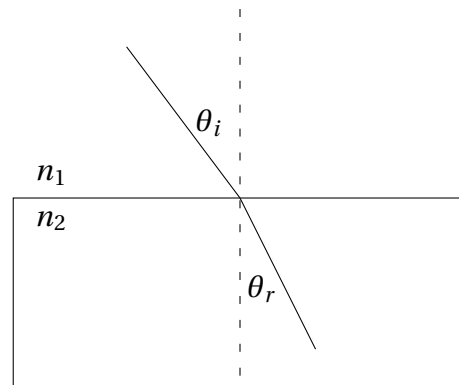
Figure 2.4: A light ray gets refracted when it goes from one medium to another.

When a light ray is sent from air (n_1) towards a water surface (n_2), the light ray will be refracted as it moves through the boundary between the air and water surface. This phenomenon has been known for almost 2000 years, as Claudius Ptolemy (c. 100 AD-c.170 AD) made a list describing the angle of the light ray in water for various angles of incidence [14]. The results are summarized in Table 2.1a. Snell's law, expressed in Eq. 2.2 makes it possible to predict how the light is refracted when moving from one medium to another. Table 2.1b, shows the different angles of incidence in air based on Snell's law. Comparing the results against Ptolemy's table, one can see great similarities. It was not until Snell's law was derived that they could mathematically connect these angles, but the similarities show that Ptolemy was impressively accurate for his time.

Table 2.1: (a) Ptolemy's table (b) Based on Snell's law (The tables are obtained from [14])

	(a)			(b)	
Angle in air	**Angle in water**		**Angle in air**	**Angle in water**	
10°	8°		10°	7°	
20°	15°		20°	15°	
30°	22°		30°	22°	
40°	29°		40°	29°	
50°	35°		50°	35°	
60°	40°		60°	40°	
70°	45°		70°	45°	
80°	50°		80°	48°	

2.1.3 Forward and Backward Scattering

When a light ray strikes a particle suspended in water, the original path of the light is refracted. Depending on the angle at which the light beam is bent, the phenomenon is known as *forward-* or *backscattering* [7]. This section will address how scattering affects an underwater imaging system, while Section *2.3.3 Scattering* will go into more details on how the light gets scattered.

Forward scattering occurs when the deflection angle is small ($0-90°$). A result of forward scattering is contrast reduction and blur in the image. Backward scattering occurs when the deflection angle is large ($90-180°$). Here the light ray is reflected back to the camera before reaching the object. The continuous shower of organic debris in the deep ocean, known as *marine snow*, produces strong backscatter, seen as bright spots in an image. However, the main problem with backscattering is veiling glare, which substantially reduces the image contrast [7].

The amount of forward- and backscattering depends on the illuminated volume of water in the camera's field of view. Due to light attenuation and poor lighting conditions in the ocean water, artificial lighting is needed in most cases. The use of artificial lighting increases the amount of backscatter in the scene [15]. The adverse effects increase when the distance between camera and object is increased [7]. These effects can be reduced by reducing the distance between the camera and object. Lighting systems, as well as which ones may be best suited for different desires, are studied in more detail in Section 2.2 *Illumination in Underwater Systems*.

Another method that can reduce backscattered light is to utilize the polarization properties of light. According to Bohren et al. [4], polarization is preserved in backward direction when polarized light is scattered by spherical particles. Using two linear polarizing filters, one in front of the light source and one in front of the camera rotated 90°, it should be possible to remove most of the unwanted scattered light. Polarization has been shown to improve the contrast of underwater images, as well as increase the observation distance [3]. Polarization and the polarization properties of light will be explained in more details in Section *2.4 Polarization*

2.1.4 Absorption and Attenuation

Absorbed light is a phenomenon in which some or all of the radiant energy is converted into another form of energy, for example, heat, by interaction with matter. The overall effect of absorption, scattering, and refraction leads to light attenuation.

Imagine a ray directed along the x-axis (Figure 2.5). The radiant energy crossing unit area per unit time at $x = 0$ is equal to F_0 [4, p. 51]. The distance x is divided into N similar pieces. The thickness of each piece is given by $\Delta x = \frac{x}{N}$. The irradiance of the light beam is attenuated when transmitted through the different pieces. If we start by studying N=1, the irradiance (F_0) is attenuated over the distance Δx, which gives us a new irradiance, called F_1. Then assume that if Δx is sufficiently small, the attenuation is proportional to Δx and F_0, where κ is the proportionality constant [4, p.51]. Each medium has its own absorption coefficient (κ).

$$F_0 - F_1 = F_0 \kappa \Delta x \qquad \Leftrightarrow \qquad F_1 = F_0 \, (1 - \kappa \Delta x)$$

For the next slice, the light ray get even more attenuated, and the irradiance is given by

$$F_2 = F_1 \, (1 - \kappa \Delta x) = F_0 \, (1 - \kappa \Delta x)^2$$

This continues in the same way for the Nth other slices as well, and the irradiance of the atten-

9

uated light when passing through a distance x, can therefore be expressed as

$$F_n = F_0 \, (1 - \kappa \Delta x)^n = F_0 \left(1 - \frac{\kappa x}{n} \right)^n \tag{2.3}$$
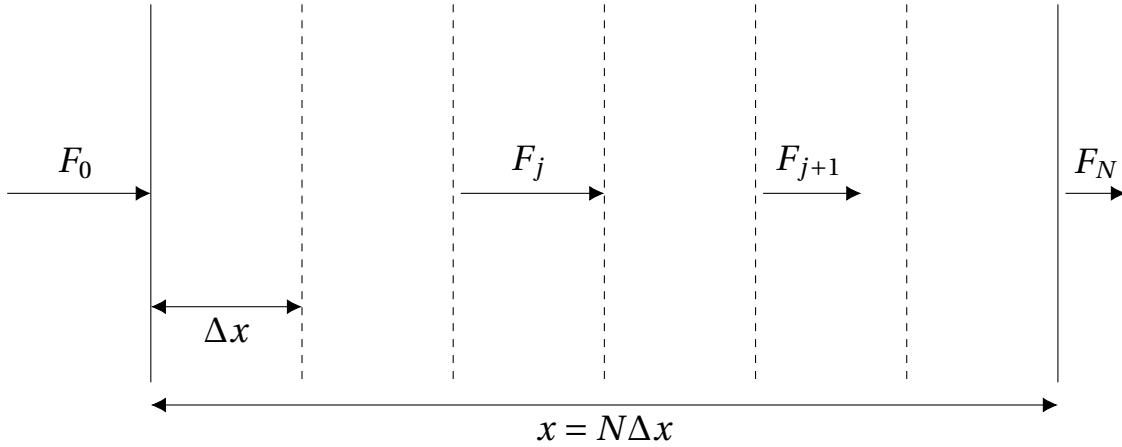
Figure 2.5: Absorbing medium made up of N similar slices, each slice have thickness Δx. Transmitted irradiance F_N decreases with increasing j. The illustration is adapted from [4, p.52].

By studying Eq. 2.3, for an infinitely large N, Lambert's law, also known as Beer's law, is obtained. It tells how much the light is attenuated over the distance x.

$$F = F_0 e^{-\kappa x} \tag{2.4}$$

When studying absorption, it is also essential to study the absorption length. The absorption length is a measure of how far light is transmitted through the media before it is completely absorbed. Figure 2.6 illustrates the dependency between absorption length and wavelength for liquid water and ice. The absorption length of can be calculated by using Eq. 2.5, which is the equation for average distance, where F is equal to F in beer's law (Eq. 2.4)

$$\overline{x} = \frac{\int_0^\infty x \, F \, dx}{\int_0^\infty F \, dx} \tag{2.5}$$

10

$$\overline{x} = \frac{\int_0^\infty x\, F_0\, e^{-\kappa x}\, dx}{\underbrace{\int_0^\infty F_0\, e^{-\kappa x}\, dx}_{\frac{1}{\kappa}}} = \kappa \int_0^\infty x\, e^{-\kappa x}\, dx = \kappa \left(\frac{1}{\kappa}\right)^2 = \frac{1}{\kappa} \tag{2.6}$$
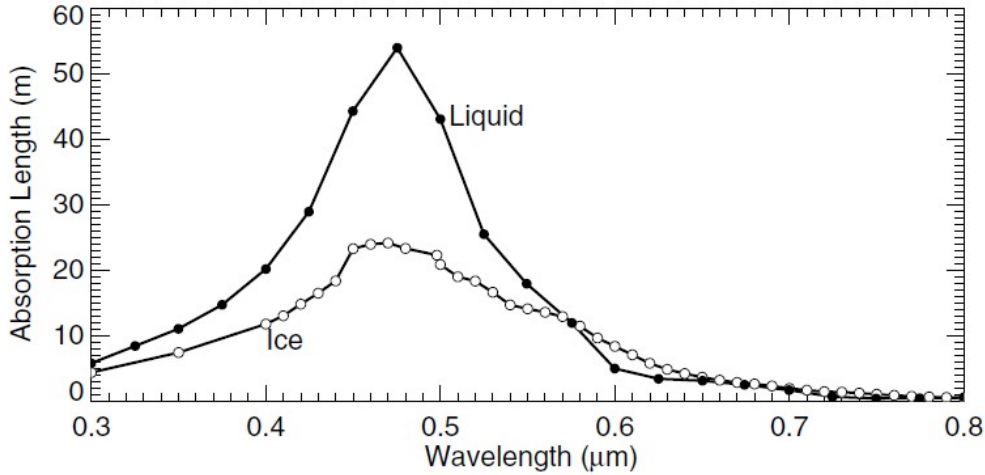
Figure 2.6: Absorption length versus wavelength for liquid water and ice. The illustration is obtained from Bohren et al. [4, p.53]

The illustration in Figure 2.6 shows how white light is attenuated when penetrating through ice and liquid water. It is observable that the absorption length is greatest for the shorter wavelengths region and least for the long wavelengths (both for ice and liquid water). It is especially for clear water, that the longer wavelengths are attenuated fastest, and the shorter wavelengths (blue and green wavelengths) are attenuated last. This explains why objects in the ocean often appear blue-greenish. In turbid water, or in places where there is a high concentration of plankton, yellow, or even red wavelengths, are better transmitted [7, p. 27].

The amount of light absorbed and attenuated depends on the medium, as each medium has a different absorption coefficient. Algae in the water are also affecting imaging underwater. Depending on the properties of the algae, the green wavelengths are usually absorbed first, causing color degradation in the images. Colored dissolved organic matter (CDOM), is also a type of material that affect imaging underwater. According to Nima et al. [16], CDOM is referred to "as a complex group of organic compounds dissolved in natural water". For CDOM, the absorption

11

length is highest for the long wavelengths and shortest for the short wavelengths. CDOM causes the objects to appear yellow-brownish.

Absorption and attenuation have adverse effects on an underwater imaging system and causes the images taken underwater to appear dark and suffer by low contrast. Because of poor lighting conditions underwater, artificial lighting is often needed. When choosing the right lighting system for an underwater system, the attenuation length is used as a measure to determine a practical distance between camera and object. This is explained in more detail in Section 2.2. Attenuation length is known as the distance where the light intensity has fallen by a factor of $1/e$. Thus, it is the distance where approximately 64 % of the light intensity is lost. The visibility in clear water is usually between one to two attenuation lengths [7, p. 27].

2.2 Illumination in Underwater Systems

Due to the fact that light gets scattered in the water, the field of view in underwater images is often limited. Other elements, such as reflection from underwater objects, scattering and camera settings, also affects the field of view. According to Jaffe [17], an imaging system is said to be *contrast-limited* when there occurs light scattering in the volume of water where the field of view of the camera and the light source intersects. Jaffe also states that when the power falling on the reception sensor is too small to be perceived, the system is said to be *power-limited*.

Advances in optical imaging have allowed researchers to study ocean water in a way one only could dream of before. However, there are still significant challenges associated with underwater imaging. One of the biggest problems is backscatter. No technology has yet made it possible to remove the backscatter completely, but various factors can help reduce it. As mentioned, polarization filters can reduce the backscatter to some extent. However, another factor contributing to reducing backscatter is the choice of light system and light source position. The choice of light system and light source position also helps to reduce another challenge with underwater imaging: attenuation of light.

2.2.1 Lighting Systems

Lighting systems underwater can be classified based on different concepts. The simplest classification is to distinguish between *passive* and *active* lighting systems. Some techniques utilize light with specific frequencies to reduce negative effects, such as scattering, absorption, refraction [7].

Passive Lighting Systems

A passive lighting system is a system that uses natural light sources, such as sunlight or a bioluminescence light source. It can also be a system that uses artificial lighting from, e.g. a nearby ship or platform [7, p.28]. Because of attenuation of light, it is not wise to choose a passive lighting system if it is desirable to photograph in deeper environments. According to Reynaud [7, p. 28], this type of lighting system is particularly suitable for use in operations such as "fish seeking, defense, or surveillance tasks".

Active and Structured Lighting Systems

Active and Structured lighting systems use artificial lighting to illuminate the desired area. An advantage of such a system is that it is possible to choose the amount of lights sources needed, as well as how illuminated the area and the surroundings should be. If it is desirable to photograph in deeper environments, these types of lighting systems are best suited [7, p. 28]. As discussed in Reynaud [7, p.28], there is for such a system possible to decide how the light beam should be emitted, for example, as a narrow or wide beam, flash, or continuously emitted.

2.2.2 Selection of Lighting System

According to Jaffe [18], underwater imaging systems can roughly be divided into three groups (illustrated in Figure 2.7):

1. Conventional systems

2. Systems where there is an increase in separation between camera and light source

3. Exotic systems
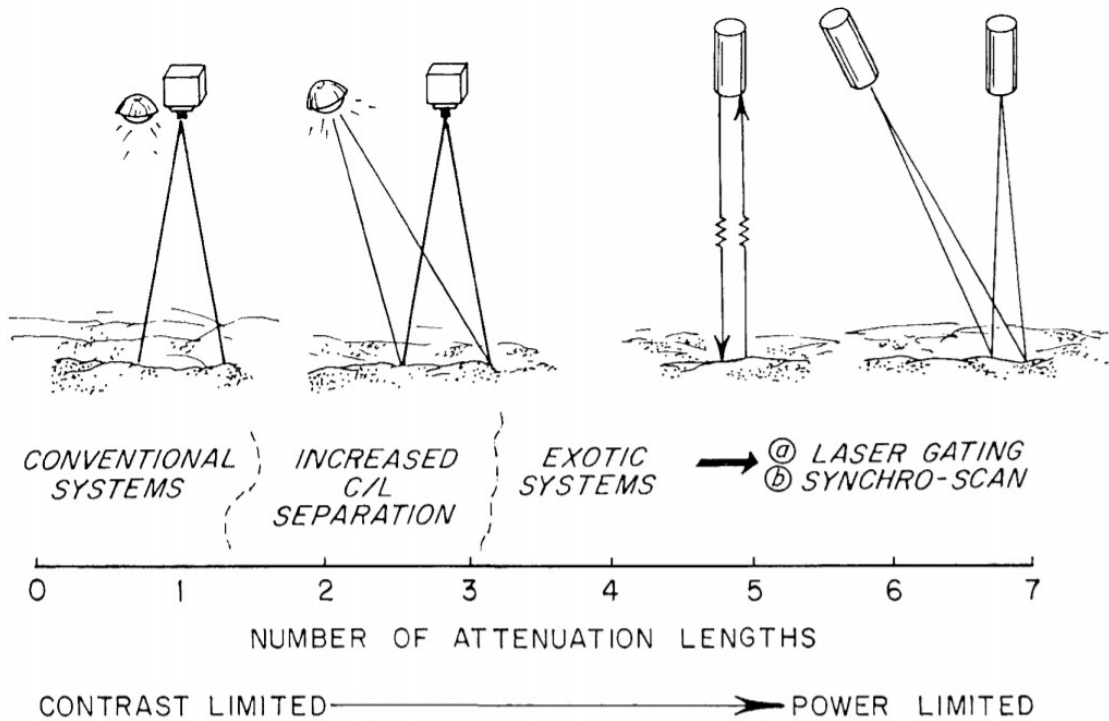
Figure 2.7: Different types of lighting systems versus number of attenuation lengths. The illustration is obtained from[17].

A practical measure of the performance of a lighting system is the attenuation length at which the system provides acceptable images. Therefore, it is essential to think of the desired attenuation length when choosing a lighting system. For a conventional system, the camera and light source position coincides. Such a system is said to take acceptable images at one attenuation length. Images captured further away may suffer by contrast limitation. [17].

If it is desirable to photograph with a longer distance to the object, another system should be chosen. Another factor that can be important to think about is the location of the light source in relation to the camera, as the wrong choice can cause unnecessary backscattering. According Reynaud [7], "the amount of backscatter in lighting systems depends on the volume at which

the light field and the camera's field of view intersect". In order to reduce backscatter, one can separate the light source as much as possible from the camera, which reduces the illuminated volume where the camera and light field intersect. By increasing the separation between camera and light source, capturing images of objects further away than one attenuation length will also be possible. Systems where the camera and the light source are separated capture images with acceptable quality up to a distance of 2-3 attenuation lengths. According to Jaffe [17], images captured further away than 2-3 attenuation length is more affected by backscattering. According to Harris et al. [19], a separation of 3-5 meter is typical when mounted on a remote-operated platform. Suppose it is desirable to photograph an object further away than three attenuation lengths; more exotic systems are needed. Some examples are laser gating and synchro-scan. These types of systems are more complex and also more expensive.

2.2.3 Separation Between Light Source and Camera

In Jaffe [17][18], the behaviour of light in water is modelled in relation to the image formation process. The camera is adjusted to point down towards the seabed, and the image contrast is evaluated for different separations between the camera and the light source [7]. The light source is moved both horizontally and vertically. The results from the modelling are depicted in Figure 2.8. It illustrates how a change in horizontal separation from 10-20 meters increases the image contrast. It also illustrates that for larger distances, the image contrast decreases. One reason for this is due to light attenuation.

Figure 2.8 also illustrates that the contrast increases if the distance between the camera and the light source increases vertically. According to Jaffe [18], the reason is that the area in front of the camera is not as well lit as it would be if their position were coinciding. The amount of backscattering is therefore reduced.
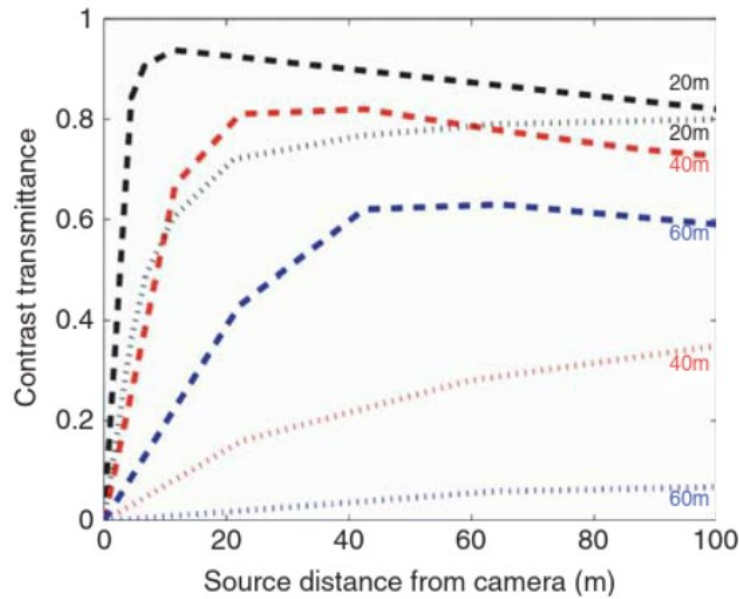
Figure 2.8: Change in contrast transmittance with with difference separations between the light source and the camera. ||, indicates vertical separation. −, indicates horizontal separation. The illustration is obtained from Reynaud [7].

2.3 Scattering

In Section 2.1.3, scatterings impact on an underwater system were studied. Here scattering will be studied in further details. *Scattering* is an optical phenomenon that makes non-luminous objects visible. When light hits an object, light is scattered differently depending on the wavelength of the incident light and the material of the object.

All matter consists of discrete electrical charges: electrons and protons [20, p. 3]. We can start by concentrating on a single particle or molecule and calling it an obstacle. When the obstacle is illuminated by an electromagnetic wave, illustrated in Figure 2.9, the electrical charges of the obstacle are set in an oscillating motion. The accelerated electric charges radiate electromagnetic energy in all directions. The radiation emitted from the obstacle is called *secondary radiation*, and is the radiation scattered by the obstacle [20, p.4]:

Scattering = excitation + reradiation

16
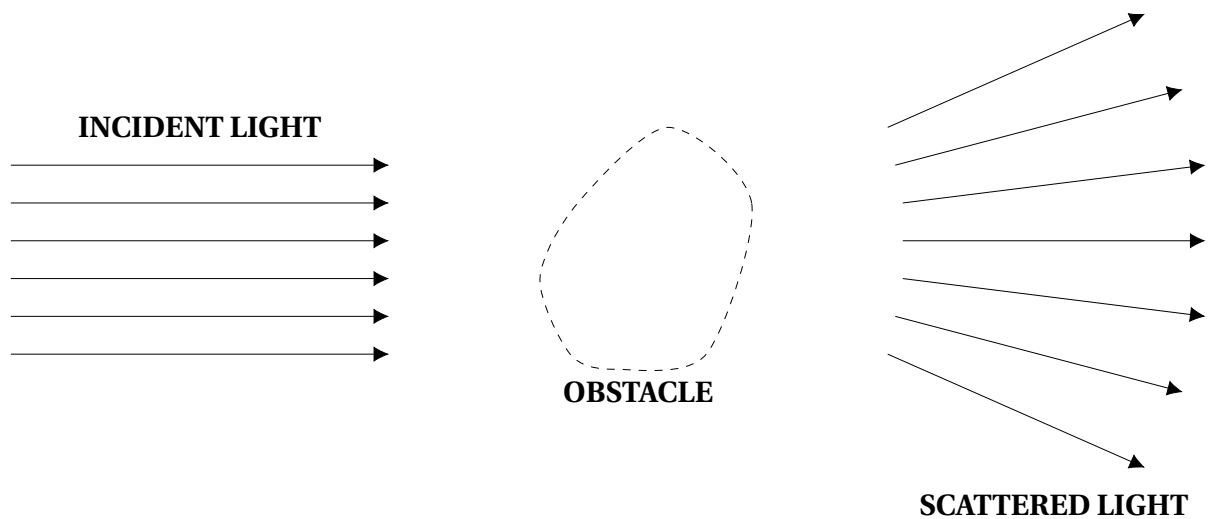
Figure 2.9: Scattering by an obstacle. The illustration is adapted from Bohren et. al [20]

Each medium has its own scattering coefficient (β), given by

$$\beta = N \cdot C_{Sca} \tag{2.7}$$

where N is the number of particles per volume, and C_{Sca} is the scattering cross-section. The mean free path for scattering (l_s) can be calculated based on the scattering coefficient. l_s is given by $1/\beta$ and is a measure of the mean distance a light wave travels before it gets scattered. Imagine a container filled with spherical particles and water. A light source is aimed towards one side of the container. The scattering coefficient of the mixture is known. If the mean free path is greater than the length of the container, it is assumed that there is mostly *single scattering* within the container. If the mean free path is less than the length of the container, it is assumed that there is dominating *multiple scattering* inside the container.

2.3.1 Model for Light Scattering and Absorption

As discussed in the previous section, when electric charges are exposed to oscillating electric fields, the charges in the matter are set in motion. The charge emits new waves that move at the speed of light. When a dipole is set in motion, it oscillates at the same frequency as the incident

17

wave. As a result, it scatters electric waves with the same frequency as the incident light. In cases where the scattered electric waves have the same frequency as the incident light, the scattering is called elastic scattering. Can start by setting up a model for what happens when a dipole, in this case, an electron, is set into motion by an incident electric field. Different forces are acting on the electron. There will be a binding force, a damping force, and a driving force. There will also be a dissipative force that acts on the dipole [4]. Using Newton's second law: $\sum F = ma$, we can set up an expression of which forces act on the electron in Figure 2.10.
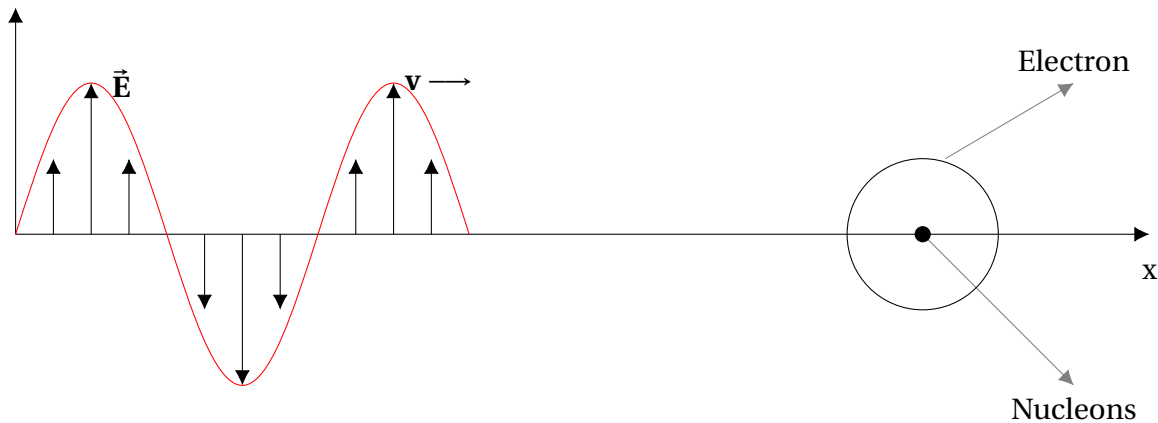
Figure 2.10: Dipole oscillator.

$$F_{\text{bidning}} + F_{\text{damping}} + F_{\text{driving}} + F_{\text{radiative reaction}} = m \frac{d^2 x}{dt}$$

Which gives

$$-kx - b\frac{dx}{dt} + eE_o \exp(-i\omega t) + \omega \frac{d^3 x}{dt^3} + = m\frac{d^2 x}{dt^2} \tag{2.8}$$

where k is the spring constant ($k = \omega_o \cdot m$), γ is the damping coefficient, and e is the charge of the electron. After an adequately long time, x is time-harmonic with the same frequency as the electrical field, here x is equal to $x_0 \exp(-i\omega t)$ [4, p. 127]. Replaces x in Eq. 2.8 with the new expression, the result is the steady-state solution, the complex amplitude is given by

18

$$x_o = \frac{e}{m_o} \frac{E_o}{\omega_o^2 - \omega^2 - i\gamma\omega 0} \tag{2.9}$$

where $\gamma = \gamma_a + \gamma_s \frac{\omega^2}{\omega_o^2}$, $\gamma_a = \frac{b}{m}$, and $\gamma_s = \frac{\omega_o \omega}{m}$.

Work done on the electron by the incident field is given by Eq. 2.10. The work can be divided into two parts; absorbed and scattered (Eq. 2.3.1).

$$P = \mathbf{F} \cdot \frac{dx}{dt} = e\mathbf{E} \cdot \frac{dx}{dt} \tag{2.10}$$

$$\langle P \rangle = \langle P_a \rangle + \langle P_s \rangle$$

$$\langle P_a \rangle = \frac{e^2}{2m} E_o^2 \frac{\omega^2 \gamma_a}{(\omega_o^2 - \omega^2)^2 + \gamma^2 \omega^2} \tag{2.11}$$

$$\langle P_s \rangle = \frac{e^2}{2m} \frac{E_o^2}{\omega_o^2} \frac{\omega^4 \gamma_s}{(\omega_o^2 - \omega^2)^2 + \gamma^2 \omega^2} \tag{2.12}$$

$\langle P_a \rangle$ is power absorbed (Eq. 2.11), and is a result of transforming radiant energy into other forms [4, p.128]. $\langle P_s \rangle$ is power scattered by the dipole (Eq. 2.12), and is a result of the incident electric field exciting scattered light (radiation) in all directions. Scattering do not transform radiant energy into other forms such as for absorption, scattering radiate energy into different directions, radiant energy is conserved [4, p.128]. Maximum absorption and scattering occurs at ω_o. ω_o is know as resonant frequency, and is the frequency at which the oscillator oscillates when there are no forces acting on the oscillator [4, p.72].

2.3.2 Rayleigh Scattering

The scattering law, first derived by Lord Rayleigh in 1871, is obtained if $\omega << \omega_o$ in Eq. 2.12.

$$\langle P_s \rangle \approx \frac{e^2}{2m} \frac{E_o^2}{\omega_o^6} \gamma_s^2 \omega^4 \tag{2.13}$$

As stated in Borhen et al. [4, p.128], "frequency to the fourth power is proportional to wavelength to the inverse fourth power."

Rayleigh scattering typically occurs when the particle size is much smaller than the wavelength of the incident light ($d << \lambda$). The intensity (I) of the scattered light is proportional to $1/\lambda^4$ for this type of scattering ($I \propto 1/\lambda^4$). By studying Figure 2.11, it can be seen that this type of scattering results in about the same amount of back- and forward scattering. Rayleigh particles scatter the short wavelengths more than the long wavelengths for an equal incident intensity.
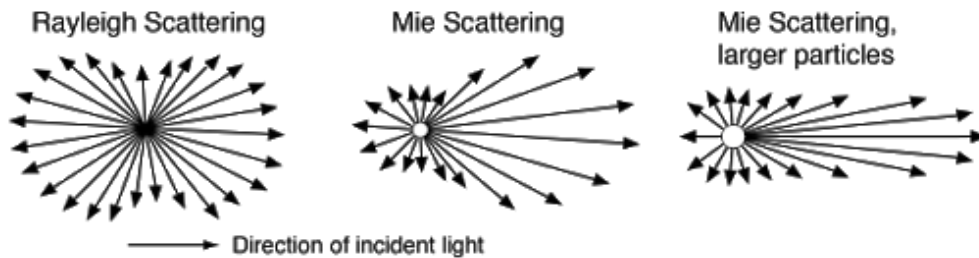
Figure 2.11: Light scattered on different particle sizes. The illustration is obtained from [21]

2.3.3 Scattering by a Sphere

The simplest finite scatter is an isotropic homogeneous sphere. Scattering by a sphere is associated with Gustav Mie and is known as *Mie scattering*. Mie scattering is known to occur in situations where the particles exposed to scattering are larger or comparable to the wavelength of the incident light (d$\geqslant \lambda$). By studying Figure 2.11, it can be observed that there for a Mie particle will be more forward-scattering than backscattering. As stated in Borhen et al. [4, p.166], there is no absolute limit to whether a particle is a Mie or Rayleigh particle. A particle can go

from Rayleigh to Mie by changing the wavelength of the incident light.

Gustav Mie was in 1908 able to use Maxwell's equations to describe the scattering that occurs when an electromagnetic plane wave hits an isotropic homogeneous sphere. As stated in Bohren et al. [4, p. 166], Gustav Mie's solution "is based on expanding the incident, scattered and internal electric and magnetic field in series of vector spherical harmonics". In the expansions of the scattered electric and magnetic field, observable quantities are expressed in the form of the complex scattering coefficients a_n and b_n. Bohren et al. [4, p. 166] also states that "the coefficients are determined so that the tangential components of the fields are continuous across the surface of the sphere". The following formulas give extinction- and scattering cross-section based on these coefficients.

$$C_{ext} = \frac{2\pi}{k^2} \sum_{n=1}^{\infty} (2n+1) \, \mathbb{R} \{a_n + b_n\} \tag{2.14}$$

$$C_{sca} = \frac{2\pi}{k^2} \sum_{n=1}^{\infty} (2n+1) \left\{|a_n|^2 + |b_n|^2\right\} \tag{2.15}$$

where k is the wavenumber of the incident light. The scattering coefficients a_n and b_n is given by

$$a_n = \frac{[D_n(mx)/m + n/x]\psi_n(x) - \psi_{n-1}(x)}{[D_n(mx)/m + n/x]\xi_n(x) - \xi_{n-1}(x)} \tag{2.16}$$

$$b_n = \frac{[mD_n(mx)/m + n/x]\psi_n(x) - \psi_{n-1}(x)}{[mD_n(mx)/m + n/x]\xi_n(x) - \xi_{n-1}(x)} \tag{2.17}$$

where x is the size parameter given by $k \cdot a$, k is the wavenumber of the incident light, a is the radius of the sphere, m is the complex refractive index of the sphere [4, p. 167], and ψ_n and ξ_n are Riccati-Bessel functions. The logarithmic derivative (D_n) is given by

$$D_n(\rho) = \frac{d}{d\rho} \ln \psi_n(\rho) \qquad (2.18)$$

Particles smaller than the wavelength

For particles $\leqslant \lambda$, and am adequately small x, the extinction- and scattering cross section is given by

$$C_{\text{ext}}/v \approx \frac{6\pi}{\lambda} \Im\left\{\frac{m^2 - 1}{m^2 + 2}\right\} \qquad (2.19)$$

$$C_{\text{sca}}/v \approx \frac{24\pi^3 v}{\lambda^4} \left|\frac{m^2 - 1}{m^2 + 2}\right|^2 \qquad (2.20)$$

where v is the particle volume and λ is the wavelength in the material around the sphere [4, p. 168].

Particles larger or equal to the wavelength

For particles $\geqslant \lambda$, the extinction cross section is given by,

$$\lim_{a \to \infty} C_{ext} = 2G \qquad (2.21)$$

where a is the linear dimension of the particle being illuminated, for a sphere, the linear dimension is its radius. As stated in Bohren et al. [4, p. 169] G is the "projected geometrical cross-sectional area".

2.4 Polarization

Understanding how to utilize the polarizing properties of light is an advantage and can be crucial in optical applications underwater. It can help reduce unwanted reflections and backscatter [22]. As discussed in Section 2.1.3, backscattering reduced the image contrast in underwater imaging systems. As discussed in Section 2.1.3, there is a disagreement in the research community about how polarization works in an underwater system. What is agreed upon is that by using a polarizing filter, one can increase the quality of the image. As discussed in Bohren et al. [4, p. 381], we assume that linearly polarized light scattered on spheres larger than the wavelength is preserved in the backward direction. This topic will be studied in more detail in Section 2.4.7, but will first start by looking at the principle of polarization.

An electromagnetic wave consists of both an electric (**E**) and magnetic (**H**) field. As discussed in Bohren et al. [4, p. 346], the fields are not necessarily perpendicular to each other or the direction of propagation. However, Bohren et al. [4, p. 346] states that "they lie in a plane to which the Poynting vector is perpendicular". When studying polarization of light, one can focus on both the electric and magnetic field. However, the most common is to study the electric field when studying the effects of polarization. Figure 2.12 illustrates the electric field component perpendicular to the plane of incident ($\vec{E}_\perp$), and the electric field component parallel to the plane of incidence ($\vec{E}_\parallel$). The perpendicular component is often called the s-component; s is for senkrecht, which means perpendicular in German. The parallel component is often called the p-component; p stands for parallel.
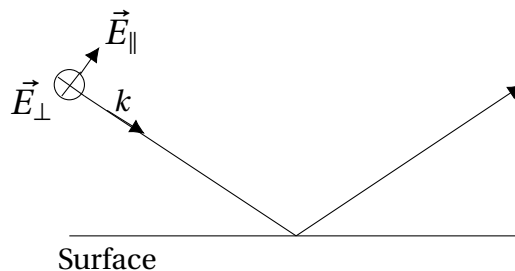
Figure 2.12: Reflection on a straight surface

A plane monochromatic wave is given by

$$\widetilde{\vec{E}} = \widetilde{E}_\perp \hat{e}_\perp + \widetilde{E}_\parallel \hat{e}_\parallel \qquad (2.22)$$

where

$$\widetilde{E}_\perp = \widetilde{a}_\perp e^{i(\vec{k}\cdot\vec{r}-\omega t)} \qquad \text{and} \qquad \widetilde{E}_\parallel = \widetilde{a}_\parallel e^{i(\vec{k}\cdot\vec{r}-\omega t)},$$

$$\widetilde{a}_\perp = a_\perp e^{-i\theta_\perp} \qquad \text{and} \qquad \widetilde{a}_\parallel = a_\parallel e^{-i\theta_\parallel}.$$

$\widetilde{E}$ is the complex electric field, and $\widetilde{a}$ is the complex amplitude. For simplicity, it is chosen to study the wave at $\vec{r} = 0$, and $a_\perp = a_\parallel = 1$,

$$\widetilde{E_\perp} = e^{-i\theta_\perp} \cdot e^{-i\omega t} = e^{-i(\theta_\perp + \omega t)} \qquad \widetilde{E_\parallel} = e^{-i\theta_\parallel} \cdot e^{-i\omega t} = e^{-i(\theta_\parallel + \omega t)}$$

The real electric field (force per charge) for a monochromatic wave is given by

$$\vec{\mathbf{E}} = Re\{\vec{E}\} = Re\{\widetilde{E_\perp}\}\hat{e}_\perp + Re\{\widetilde{E_\parallel}\}\hat{e}_\parallel$$

$$\vec{\mathbf{E}} = \overbrace{\cos(\theta_\perp + \omega t)\hat{e}_\perp}^{E_\perp = E_s} + \overbrace{\cos(\theta_\parallel + \omega t)\hat{e}_\parallel}^{E_\parallel = E_p} \qquad (2.23)$$

A monochromatic wave has different properties, one of which is *state of polarization*. By using eq. 2.23, the different states of polarization can be studies. Two waves with identical frequency and irradiance can behave differently as a result of the polarization state of the wave [23, p. 44]. The states of polarization will be further studied in the following section.

2.4.1 States of Polarization

Different states of polarization are unpolarized, linearly polarized, circularly polarized, and elliptically polarized. Light can also be slightly polarized. In this section, the different states of polarization will be studied.

Unpolarized light

Almost all types of natural and artificial lighting produce unpolarized light waves. Unpolarized light, illustrated in Figure 2.13, occurs when the electric field vibrates randomly in all planes perpendicular to the direction of propagation.
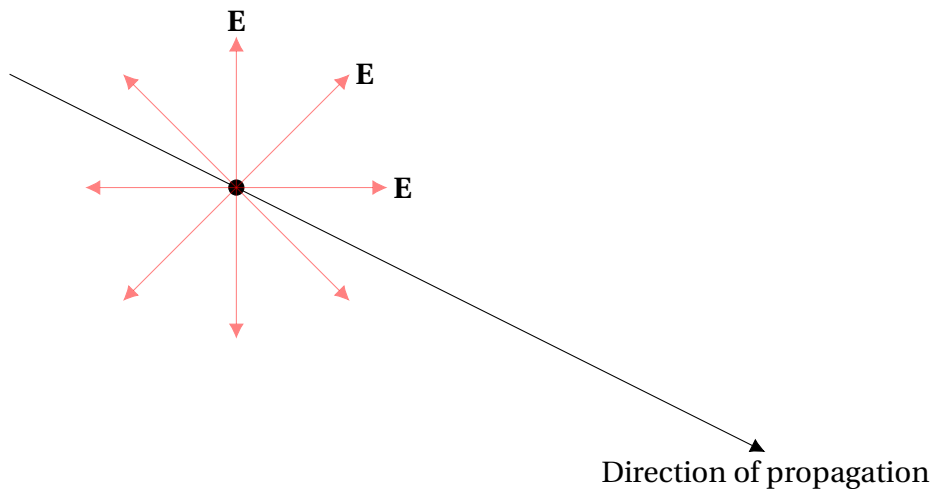
Figure 2.13: Unpolarized light. The illustration is adapted from [24].

Linearly polarized light

Linearly polarized light illustrated in Figure 2.14, occurs when there is no phase difference between the electric components in Eq. 2.23 ($\theta_\perp = \theta_\parallel = 0$). The electric field oscillates in a linear direction perpendicular to the direction of propagation. It can oscillate at certain angles, at which angle it oscillates with is determined by the tilt angle θ, given by Eq. 2.24, and is determined by the amplitudes of the original orthogonal waves [13, p. 338]. In this case

$$\tan \theta = \frac{E_\perp}{E_\parallel} \qquad (2.24)$$

As mentioned in Section 2.4, the amplitude being studied is given by $a_\perp = a_\parallel = 1$, which give an electric field oscillating at $\theta = +45°$.

ωt	$E_\perp$	$E_\parallel$
0	1	1
$\frac{\pi}{2}$	0	0
π	-1	-1

<div style="display:flex; justify-content:space-between;">

Table 2.2: Linear polarization
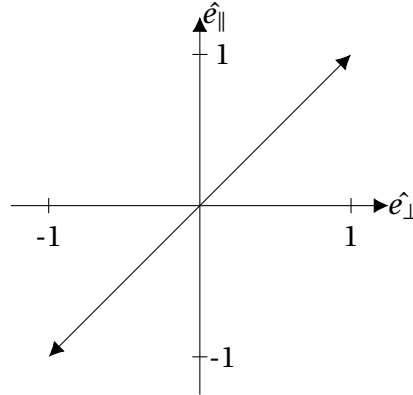
Figure 2.14: Linear polarized light

</div>

Circularly polarized light

Circularly polarized light, illustrated in both Figure 2.15 and Figure 2.16, occurs when we have two linear components with same amplitude, but with a phase difference of $\pm\pi/2$. Here the electric field is rotating in a circle around the direction of propagation. Depending on the direction of the rotation, the light is said to be left- or right-hand circularly polarized [25]. Right hand circular (RHC) polarized light occurs when the s-component is $\pi/2$ behind p-component ($\theta_\perp = 0$ and $\theta_\parallel = \frac{\pi}{2}$). Left hand circular (LHC) polarized light occurs when the s-component is $\pi/2$ in front of the p-component ($\theta_\perp = 0$, $\theta_\parallel = -\frac{\pi}{2}$).

ωt	$E_\perp$	$E_\parallel$
0	1	0
$\frac{\pi}{2}$	0	-1
π	-1	0

Table 2.3: RHC
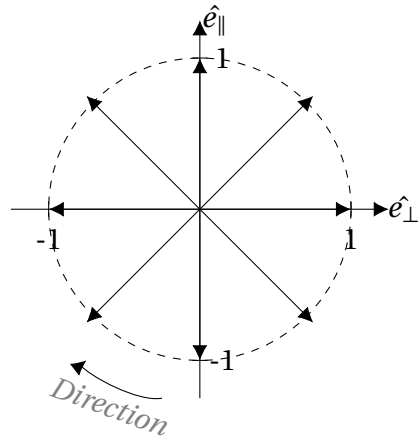
Figure 2.15: Right hand circular polarized light

ωt	$E_\perp$	$E_\parallel$
0	1	0
$\frac{\pi}{2}$	0	1
π	-1	0

Table 2.4: LHC
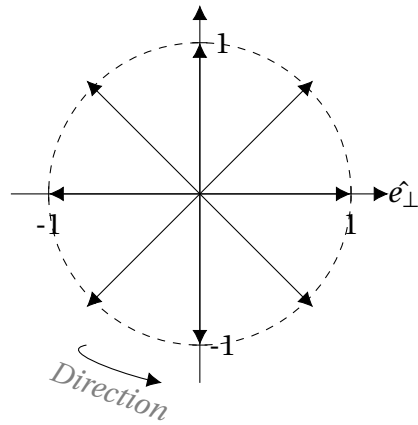
Figure 2.16: Left hand circular polarized light

Elliptically polarized light

When light consists of two electric components with different amplitudes or a phase difference that differ from $\pm\frac{\pi}{2}$, the light is said to be elliptically polarized. The electric field traces out an ellipse. When the electric field rotates, it is also changing its magnitude. As for circularly polarized light, elliptical polarization can also be right- or left-handed. Both circular and linear polarized light can be viewed as exceptional cases of elliptically polarized light [13].

27

2.4.2 Stokes Vector

Stokes vector is used to describe the polarization state of light. George G. Stokes introduced four parameters for the observability of the electromagnetic wave in 1852 [13, p. 387]. These parameters are also known as *Stokes parameters*. The stokes parameters together make up the stokes vector presented in Eq. 2.25.

$$
\begin{bmatrix} I \\ Q \\ U \\ V \end{bmatrix} = \begin{bmatrix} E_\parallel E_\parallel^* + E_\perp E_\perp^* \\ E_\parallel E_\parallel^* - E_\perp E_\perp^* \\ E_\parallel E_\perp^* + E_\perp E_\parallel^* \\ i\left(E_\parallel E_\perp^* + E_\perp E_\parallel^* \right) \end{bmatrix} = \begin{bmatrix} a_\parallel^2 + a_\perp^2 \\ a_\parallel^2 - a_\perp^2 \\ 2 a_\parallel a_\perp \cos\delta \\ 2 a_\parallel a_\perp \sin\delta \end{bmatrix} \tag{2.25}
$$

where $a_\parallel$ and $a_\perp$ are amplitudes, and δ is the phase difference $(\theta_\parallel - \theta_\perp)$. I is the time-averaged irradiance, and is calculated by the sum of squares of the amplitudes. Q and U describe the orientation of the line/ellipse relative to the x- and y-axis. V is the measure of the circularity of the polarisation [4, p.350]. The Stokes vector for the different states of polarization is illustrated in Figure 2.17.

Figure 2.17: Stokes vector for the different polarisation states. The figure is obtained from [26]

2.4.3 Degree of Polarization

Bohren et. al defines Degree of polarization (DOP), as "the ratio of the irradiance of the polarized component to the total irradiance" [4, p. 357]. A completely polarized light wave has a DOP of 100%, while an unpolarized light wave has a DOP of 0%. If a light wave is partially polarized, it is said to have a DOP between 0 and 100%. As discussed Bohren et al. [4, p. 357], any light beam can be considered an incoherent superposition of two beams. The stoke vector therefore can be divided into one unpolarized and one polarized part.

$$
\begin{bmatrix} I \\ Q \\ U \\ V \end{bmatrix} = \begin{bmatrix} I_u \\ 0 \\ 0 \\ 0 \end{bmatrix} + \begin{bmatrix} I_p \\ Q \\ U \\ V \end{bmatrix} = \text{Unpolarized part} \quad + \quad \text{Polarized part} \tag{2.26}
$$

From Eq. 2.26;

$$
I_p^2 = Q^2 + U^2 + V^2 \qquad I = I_u + I_p
$$

In general $I_p \leq I$, so that $I^2 \geq Q^2 + U^2 + V^2$. The degree of elliptical polarization is given by

$$
\frac{I_p}{I} = \frac{\sqrt{Q^2 + U^2 + V^2}}{I} = \frac{\sqrt{Q^2 + U^2 + V^2}}{I_p + I_u} \tag{2.27}
$$

By further developing Eq. 2.26, a light beam also can be expressed with a linearly polarized and circularly polarized part:

$$
\begin{bmatrix} I \\ Q \\ U \\ V \end{bmatrix} = \begin{bmatrix} I_u \\ 0 \\ 0 \\ 0 \end{bmatrix} + \begin{bmatrix} I_{lp} \\ Q \\ U \\ 0 \end{bmatrix} + \begin{bmatrix} I_{cp} \\ 0 \\ 0 \\ V \end{bmatrix} \tag{2.28}
$$

Degree of Linear Polarization

From Eq. 2.28:

$$I_{lp}^2 = Q^2 + U^2 + 0^2 \qquad I = I_u + I_{lp} + I_{cp}$$

Degree of linear polarization is expressed by

$$\frac{I_{lp}}{I} = \frac{\sqrt{Q^2 + U^2 + 0^2}}{I} = \frac{\sqrt{Q^2 + U^2}}{I_u + I_{lp} + I_{cp}} \tag{2.29}$$

Degree of Circular Polarization

From Eq.2.28:

$$I_{cp}^2 = 0^2 + 0^2 + V^2 \qquad I = I_u + I_{lp} + I_{cp}$$

Degree of circular polarization is expressed by

$$\frac{I_{cp}}{I} = \frac{\sqrt{0^2 + 0^2 + V^2}}{I} = \frac{|V|}{I_u + I_{lp} + I_{cp}} \tag{2.30}$$

2.4.4 Mueller Matrix

As discussed in 2.4.2, a light beam with an arbitrary polarization can be expressed using Stokes parameters. The polarization state of a light beam typically changes when the polarized light is interacting with optical elements, such as polarizers, particles, etc.. The optical elements can be described using a 4x4 matrix, called the *Mueller matrix* [23, p. 53]. A Mueller matrix describes the relation between the input and output beam after interacting with the optical element. A typical Mueller matrix is based on reflection on a surface (illustrated in Figure 2.18). The Matrix is expressed in Eq. 2.31.
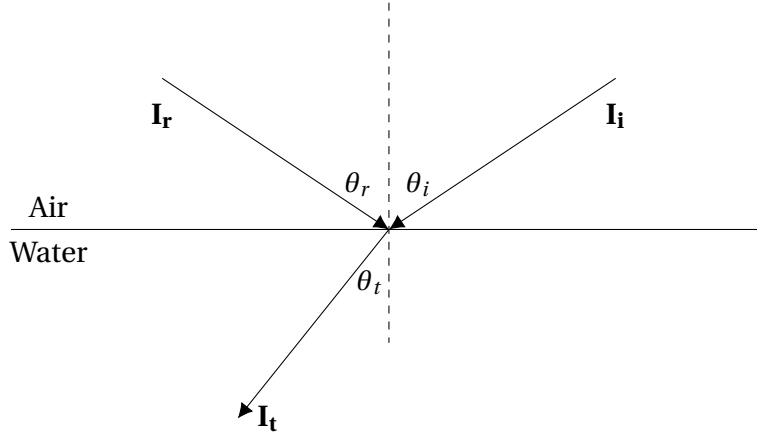
Figure 2.18: Incident and reflected Stokes vector

$$
\begin{bmatrix} I_r \\ Q_r \\ U_r \\ V_r \end{bmatrix} = \overbrace{\begin{bmatrix} R_{11} & R_{12} & 0 & 0 \\ R_{12} & R_{11} & 0 & 0 \\ 0 & 0 & R_{33} & R_{34} \\ 0 & 0 & -R_{34} & R_{33} \end{bmatrix}}^{Mueller\ matrix} \begin{bmatrix} I_i \\ Q_i \\ U_i \\ V_i \end{bmatrix} \tag{2.31}
$$

where $R_{ij} = R_{ij}(\theta)$ depends on angle. Their four different elements are expressed by,

$$
R_{11} = \frac{1}{2} \left(|\tilde{r}_\parallel|^2 + |\tilde{r}_\perp|^2 \right) \qquad R_{12} = \frac{1}{2} \left(|\tilde{r}_\parallel|^2 - |\tilde{r}_\perp|^2 \right)
$$

$$
R_{33} = \mathrm{Re}\{\tilde{r}_\parallel \tilde{r}_\perp{}^*\} \qquad R_{34} = \mathrm{Im}\{\tilde{r}_\parallel \tilde{r}_\perp{}^*\}
$$

where $\tilde{r}_\parallel$ and $\tilde{r}_\perp$ is the Fresnel coefficients for reflection;

$$
\tilde{r}_\parallel = \frac{E_{\parallel r}}{E_{\parallel i}} = \frac{\tan(\theta_i - \theta_t)}{\tan(\theta_i + \theta_t)} \qquad \tilde{r}_\perp = \frac{E_{\perp r}}{E_{\perp i}} = \frac{\sin(\theta_i - \theta_t)}{\sin(\theta_i + \theta_t)}
$$

where θ_i is the angle of incidence, and θ_t is the angle of transmission.

2.4.5 Methods for Achieving Polarized Light

In underwater optical applications, one can benefit from polarized light since polarized light reduces unwanted reflections. Using polarized light also results in a reduction of backscatter captured by the camera. The process by which light transforms from unpolarized to polarized light is called *polarization*. Polarized light can be achieved in various ways, some of which are by transmission, reflection, refraction, and scattering. These cases will be studied in further in the following sections.

Polarization by transmission

The most common way to achieve polarized light is by using polarizing filters. A polarizing filter consists of long-chained molecules that can be adjusted vertically or horizontally. As a result of the chemical composition of the filter material, the electromagnetic vibrations vibrating in the direction parallel to the molecules get absorbed. What comes out of the polarizing filter is polarized light [27].

When unpolarized light is being sent towards a polarizing filter, the intensity of the resulting electric field gets reduced. Polarizing filters do not affect the shape or dimension of the object [27]. Each polarizing filter has an associated polarization axis, which is determined based on the alignment of the molecules. The axis extends over the length of the filter, allowing only vibrations in the electric field parallel to the axis to pass through the filter. The filter blocks vibrations perpendicular to the axis of polarization. As illustrated in Figure 2.19, a polarizing filter with long-chained molecules aligned vertically has a polarizing axis aligned horizontally and vice versa.

If unpolarized light is sent towards an ideal linear polarizer, the incident intensity I_0 is reduced by half ($I = I_0/2$) [22]. If linearly polarized light with intensity I_0 is sent through an ideal polarizer, the intensity is described by Malus' law [13, p. 346],

$$I = I_0 \cos^2 \theta \qquad (2.32)$$

where θ is the angle between the incident linear polarization and the axis of polarization. If the axes of the two polarization filters perpendicular to each other (also known as cross-polarizers), there is 0% transmission. However, if the axes of the polarization filters are parallel ($\theta = 0°$), there is 100% transmission [22].
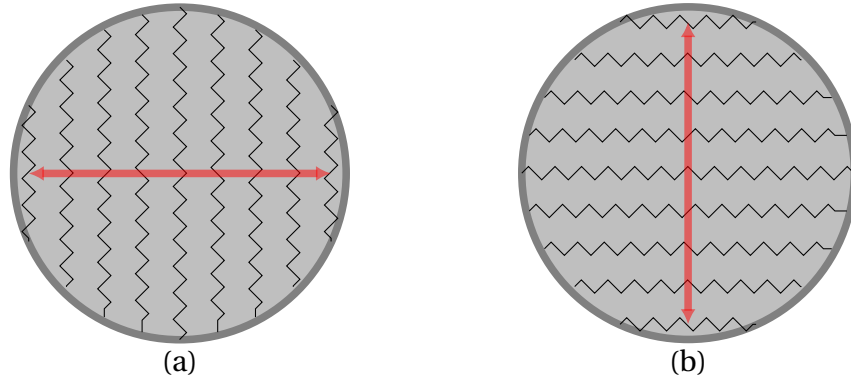
Figure 2.19: (a) Molecules aligned vertically results in horizontal polarization axis. (b) Molecules aligned horizontally results in vertical polarization axis. The illustration is adapted from [27].

Polarization by Reflection

When unpolarized light strikes a non-metallic surface, it gets polarized. To which extent polarization happens depends on the angle at which the light strikes the surface, and the surface material [27]. When unpolarized light gets polarized in this way, most of the resulting electric field will vibrate in a plane parallel to the reflecting surface. At a given angle, known as *Brewster angle* or the *polarization angle*, the light is completely p-polarized. At other angles of incident, the reflected light gets partially polarized.

Brewster's angle depends on the refractive indexes of the two media, illustrated in Figure 2.20, and is calculated using Brewster's law (Eq. 2.33). At the Brewster angle, the angle of incident is equal to the angle of reflectance, and the angle between the reflected and refracted rays is 90°, which gives:

$$\theta_p + \theta_2 = 90° \Rightarrow \theta_2 = 90° - \theta_p$$

By using Snell's law (Eq. 2.2), we get Brewster angle (θ_p) to be:

$$n_1 \sin\theta_p = n_2 \sin\theta_2 \quad \Rightarrow \quad n_1 \sin\theta_p = n_2 \sin\left(90° - \theta_p\right) = n_2 \cos\theta_p$$

$$\theta_p = \arctan\left(\frac{n_2}{n_1}\right) \tag{2.33}$$

where n_1 is the refractive index of the incident medium, and n_2 is the refractive index of the refracted medium.
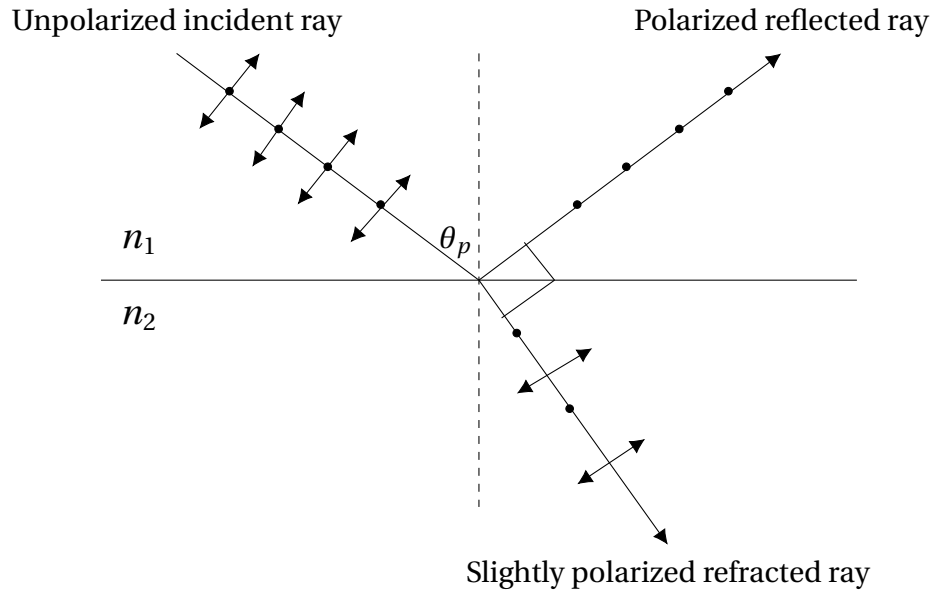
Figure 2.20: Brewster angle. The illustration is adapted from [28]

When light gets reflected on non-metallic surfaces, the light can have a high degree of polarization on specific points. Here a strong reflection, also known as glare, can be experienced. Glare on water surfaces occurs when light from a light source (sun, moon or artificial) undergoes specular reflection [29]. As shown in Figure 2.20, the incident light on the surface contains both s- and p-polarized light. The reflected light is p-polarized, and the refracted right is slightly polarized. By studying Figure 2.21, it can be seen that the reflectivity of p-polarization is approx-

34

imately zero at Brewsters angle.
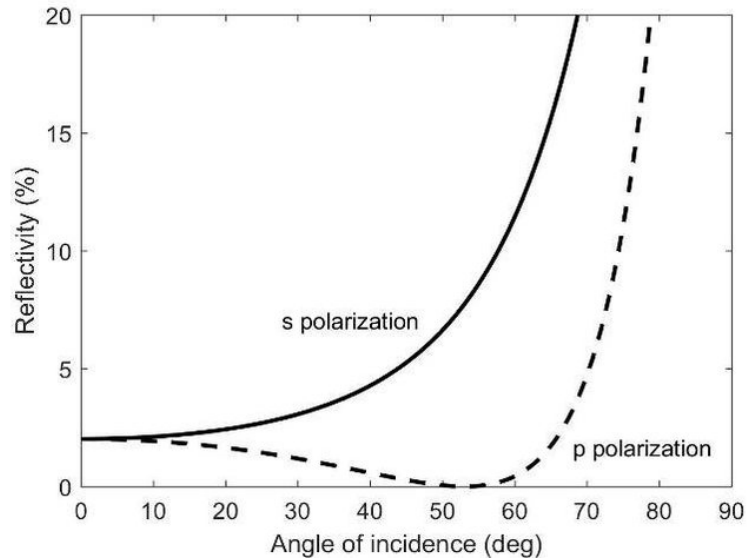
Figure 2.21: Reflection of s- and p-polarized light at different angles of incidence on a water surface. The refractive index (n_i) is equal to 1.33. The figure is obtained from Shaw et. al [29]

Polarization by refraction

As discussed in Section 2.1.2, refraction occurs when a beam of light is propagating from one material into another. As illustrated in Figure 2.20, the refractive ray is slightly polarized. For a birefringent surface, the incident beam gets refracted into two rays with different polarization when a light ray strikes a surface. A material is called birefringent when the refractive index of the material depends on the direction of the incident light, as well as the polarization of light [27].

Polarization by scattering

When light rays hit the atoms in a material, the electrons start to vibrate. The vibrating electrons produce their own electromagnetic wave, which in turn radiates in all directions. The newly generate wave will again hit nearby atoms, causing the electrons to vibrate at the same original frequency. The light scattering causes the light to spread around the medium. The scattered light will be partially or entirely plane-polarized [27]. The following sections will explain

polarization by scattering in further detail.

2.4.6 Polarization by Dipole Scattering

Figure 2.22 illustrates polarization by dipole scattering. The incident light wave and the Poynting vector of the scattered light wave determines a plane called the scattering plane. The incident and scattered electric field can be divided into components perpendicular ($\perp$) and parallel ($\parallel$) to the scattering plane.
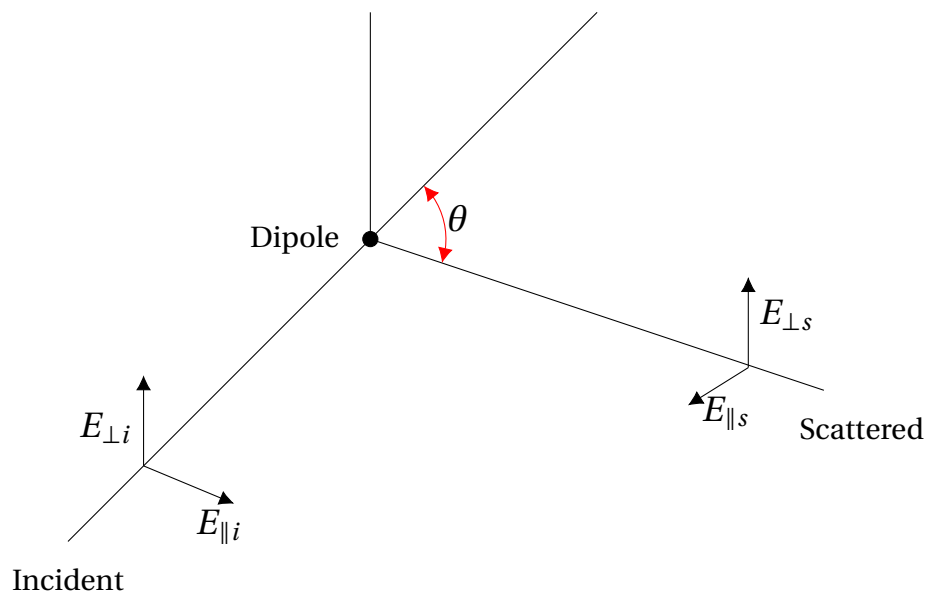
Figure 2.22: Polarization by Dipole scattering

The electric field components for the scattered field is given by Eq. 2.34, and Eq. 2.35. The perpendicular component is independent of θ. For the the parallel component there will be no scattering at 90°.

$$E_{\perp s} = kE_{\perp i} \tag{2.34}$$

$$E_{\parallel s} = kE_{\parallel i}\cos\theta \tag{2.35}$$

The Fresnel coefficient is defined in the same way as in Section 2.4.4,

$$\widetilde{r}_\perp = \frac{E_{\perp s}}{E_{\perp i}} = k \qquad \widetilde{r}_\parallel = \frac{E_{\parallel s}}{E_{\parallel i}} = k\cos\theta$$

where k as stated in Bohren et al. [4, p. 373] "incorporates all factors irrelevant to the polarization state of the scattered field (but not magnitude)". The mueller matrix can be determined based on the mueller matrix presented in Eq. 2.31. The mueller matrix for polarization by dipole scattering is given by,

$$\begin{bmatrix} I_t \\ Q_t \\ U_t \\ V_t \end{bmatrix} = \overbrace{\begin{bmatrix} \frac{1}{2}\left(\cos^2\theta+1\right) & \frac{1}{2}\left(\cos^2\theta-1\right) & 0 & 0 \\ \frac{1}{2}\left(\cos^2\theta-1\right) & \frac{1}{2}\left(\cos^2\theta+1\right) & 0 & 0 \\ 0 & 0 & \cos\theta & 0 \\ 0 & 0 & 0 & \cos\theta \end{bmatrix}}^{Mueller\ matrix} \begin{bmatrix} I_i \\ Q_i \\ U_i \\ V_i \end{bmatrix} \tag{2.36}$$

For incident unpolarized light the mueller matrix is given by

$$\begin{bmatrix} I \\ Q \\ U \\ V \end{bmatrix} = \begin{bmatrix} \frac{1}{2}\left(\cos^2\theta+1\right) \\ \frac{1}{2}\left(\cos^2\theta-1\right) \\ 0 \\ 0 \end{bmatrix} \tag{2.37}$$

Here the degree of linear polarization is given by

$$\frac{I_{lp}}{I} = \frac{\sqrt{(\frac{1}{2}(\cos^2\theta-1))^2+0^2}}{\frac{1}{2}(\cos^2\theta+1)} = \frac{|\frac{1}{2}(\cos^2\theta-1)|}{\frac{1}{2}(\cos^2\theta+1)}$$

2.4.7 Mueller Matrix for Spheres

In the previous section, polarization by scattering on a dipole was studied. In this section, polarization by particles that can be compared to or are larger than the wavelength is studied.

Mueller matrix for scattering a homogeneous sphere has the same symmetry as for reflection on a surface, described in Eq. 2.31), as discussed in Bohren et al.[4, p.378], this is because the polarized incident light perpendicular to the plane of scattering only gives rise to the scattered light perpendicular to the scattering plane. The same case with incident light parallel to the plane of scattering. The scattering matrix of an arbitrarily homogeneous sphere is therefore given by

$$
M = \begin{bmatrix}
S_{11} & S_{12} & 0 & 0 \\
S_{12} & S_{11} & 0 & 0 \\
0 & 0 & S_{33} & S_{34} \\
0 & 0 & -S_{34} & S_{33}
\end{bmatrix}
\tag{2.38}
$$

where $S_{ij} = S_{ij}(\theta)$ is the different scattering functions, related to the sums over a_n (Eq. 2.16) and b_n (Eq. 2.17). As stated in Bohren et al. [4, p. 378], "S_{ij} depends on the size of the sphere relative to the wavelength of the illumination and its composition (i.e., complex refractive index)".

Degree of linear polarization of scattered radiation and incident unpolarized radiation is given by

$$
\frac{I_{lp}}{I} = \frac{\sqrt{S_{12}^2}}{S_{11}}
\tag{2.39}
$$

often set to

$$
-\frac{S_{12}}{S_{11}}
\tag{2.40}
$$

38

For a particle to be able to act as a polarizer the size of the particle must be large compared to the wavelength. By studying Figure 2.23 one can observe the vibration ellipse of when visible light is scattered in different directions by a water droplet with a size of 0.5 micrometres [4, p.379]. By studying $\theta = 0°$, and $\theta = 180°$, one can see that the linear polarization is preserved in backward direction. At other observing angles the incident polarization is not preserved.

For an underwater system where light is sent towards an object (illustrated in Figure 2.2), the light gets reflected and scattered back towards the camera. If the incident light is linearly polarized, the light scattered in backward direction by the particles in the water also is linearly polarized. By studying Figure 2.23, it can be seen that if the camera is placed at a different angle, deviating from 180°, the backward scattered light is not fully preserved. Thus, not all the backscattered light will be removed by a linear polarizing filter. This master's thesis will study this effect in more detail by studying to what extent it is possible to achieve better imaging underwater by using polarizing techniques.
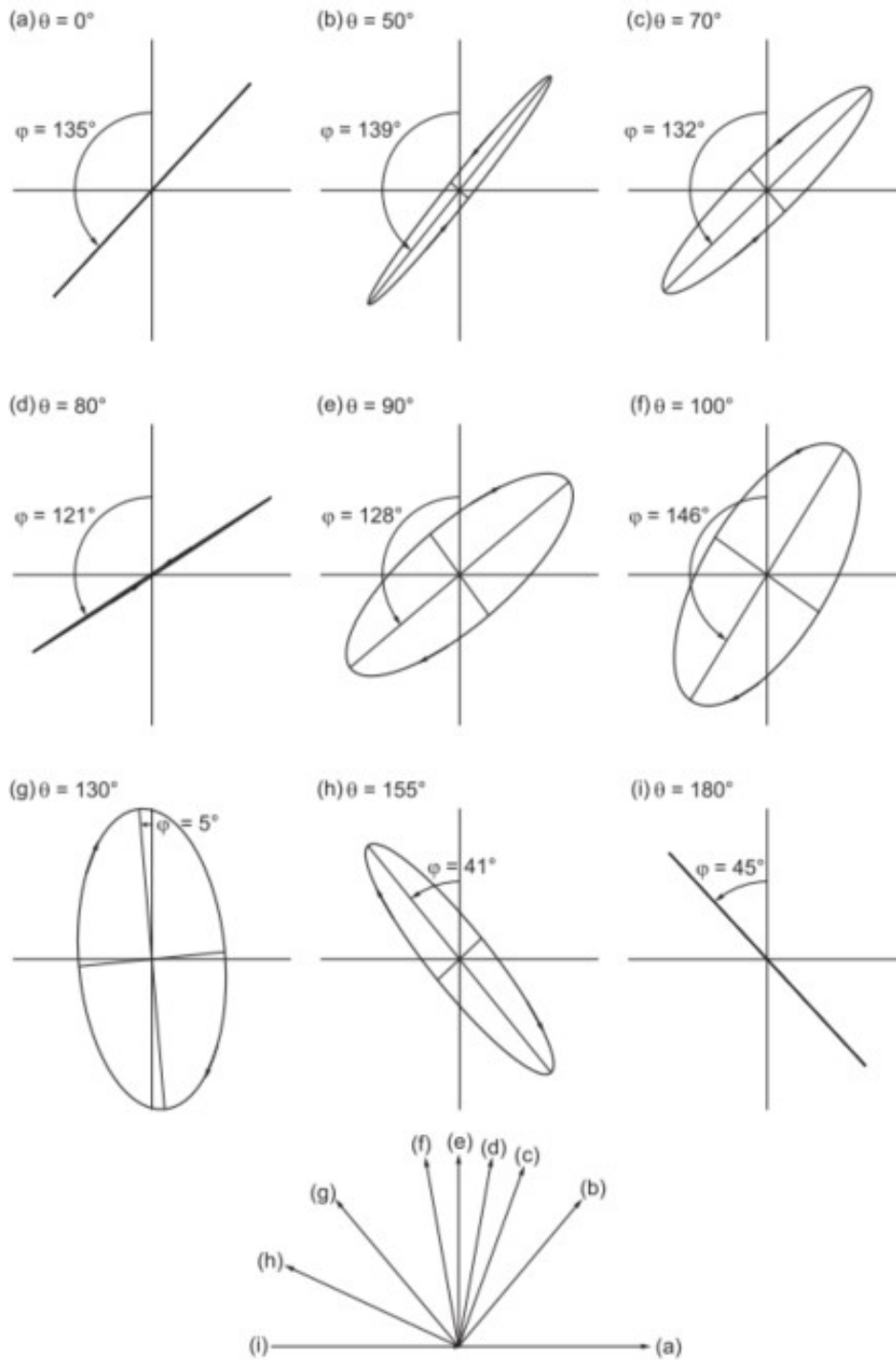
Figure 2.23: Light scattered in different directions by a water droplet ($0.5 \, \mu m$) for different observing angles. The incident light is 100% linearly polarized. The illustration is obtained from [4, p. 380]

3 Method

Three experiments, listed in Table 3.1, have been conducted in order to study to what extent it is possible to achieve better imaging underwater by using polarization techniques, as well as to study how CDOM affects underwater imaging. This section addresses the different experimental setups and procedures. It also addresses the data processing used to obtain the results presented in Section 4 - results and discussion. All MATLAB code used to obtain the different results is in the GitHub attached to the thesis [30].

Table 3.1: List of experiments

Experiment	Variable	Purpose
A	Polystyrene spheres & Milli-Q water	Study to what extent polarization techniques can be used to improve underwater imaging in such a medium
B	Algae & Sea water	Study to what extent polarization techniques can be used to improve underwater imaging in such a medium
C	Colored dissolved organic matter (CDOM)	Study how CDOM affects optical imaging, as well as whether polarization techniques can be used to achieve better imaging in such a medium

3.1 Experiment A & Experiment B

The purpose of these experiments is to study to what extent it is possible to achieve better imaging underwater by utilizing light's polarization properties. By using two polarization filters, one in front of the light source and one in front of the camera rotated 90° (cross-polarization), it should be possible to reduce most of the unwanted scattered light and theoretically obtain up to 50% of the scattered light intensity.

As discussed in Section 2.4.7, polarization is preserved in backward direction when polarized light is scattered by a particle. The amount of backscattering depends on the particle properties, and the concentration of particles in the medium. Suppose the concentration is so high that multiple scattering can be assumed. In that case, it is assumed that the effect of cross-polarization is not as good - this is because the polarization of the backscattered light is no longer preserved if it is scattered several times. Thus, it is assumed that one sees the best effect of cross-polarization if there is single scattering in the medium being examined. According to Ugulen et al. [9], one can assume single scattering when the optical depth $\tau < 0.1$, and multiple scattering when $\tau > 0.3$. Ugulen et al. [9] also states that "double-scattering corrections may be necessary for $0.1 < \tau < 0.3$". Since we are interested in scattering in backward direction, scaled optical depth (τ^*) is selected as a indicator for when multiple scattering can be expected. Multiple scattering is assumed if $\tau^* > 0.3$, as the concentration needs to be greater in order to get multiple scattering. Scaled means scaled to isotropic scattering.

The setup used in these experiments is described in Section 3.1.2. Briefly explained, the setup consists of a container filled with water. The scattering particles are added to the container to achieve the concentration that gives the scaled optical depths one wants to study. Two images are taken for the different concentration; one with polarization filters parallel to each other and one with cross-polarization. The images are studied and set as input parameters to the contrast code presented in section 3.3 to study how the contrast of the images changes with increasing concentration.

The difference between these experiments is the different scattering particles and waters used.

In order to observe the effect of polarization filters the best possible way, it is believed that it is best to use spherical particles since the polarization is perceived in backward direction for such a particle. The algae are not entirely spherical, so the state of polarization may not be fully perceived in backward direction for such types of particles.

Experiment A is performed with different shutter speeds and apertures in order to study which effect camera settings will have on the result. The best-suited combination of shutter speed and aperture is used for the other experiments in this thesis.

3.1.1 List of Equipment

Table 3.2: Experiment A & B: List of equipment

Equipment	Value
Camera	Panasonic Lumix DMC-GH3
2x Polarizing filter	Linear
LED	MBB1L3 - 470-850 nm Mounted Broadband LED, 70 mW (Min), 500 mA
LED power supply	DC2200, High-Power1-Channel LED Driver with Pulse Modulation, 10.0 A Max, 50.0 V Max
Container	Plexiglas, size: 11.5 cm x 11.5 cm
Milli-Q water	1 L
Seawater	1 L
Polystyrene spheres	510 nm polystyrene sphere. The certified batch:3500-005. The production batch:3500-035. Manufacturer: Thermo Fisher Scientific. More info can be found in Table 3.3.
Algae	250 ml Nannochloropsis. Concentration $4 \cdot 10^7$ 1/ml
Pipette	
Magnetic stirrer	
Magnetic stirring bar	

Table 3.3: Physical data for the 510nm polystyrene sphere. The certified batch:3500-005. The production batch:3500-035. The data is obtained from the manufacturer.

Variables	Value
Certified Mean Diameter	510 nm + 7 nm, $k = 2$
Standard Deviation	9.2 nm
Coefficient of Variation	1.8%
Microsphere Composition	Polystyrene
Microsphere Density	1.05 g/cm^2
Index of Refraction	1.59 @ 589 nm
Approximate Concentration	1% solids

3.1.2 Setup

The setup used is depicted in Figure 3.1. The camera is the main element of data collection. The camera output is an sRGB image. The initial parameters for the camera settings are shown in Table 3.4. In order to study the optical phenomena happening in underwater images in the best possible way, it is desirable to use constant manual settings when performing the experiment.

The LED light is a *Mounted Broadband LED* and emits light with wavelengths in the range 470-850 nm. The LED must be supplied with a constant current that cannot exceed 500 mA. The power is supplied to the LED using a LED power supply (DC2200).

The polarizing filters used in the setup are both linear polarizing filters. One filter is mounted directly at the camera lens, while the other is placed right in front of the LED light. The setup also consists of a magnetic stirrer and a magnetic stirring bar that mixes the water and particles, which prevents the particles from sticking together. 1L of the correct type of water is added to the container. The right amount of scattering particles is gradually added to the container by pipette, based on the desired scaled optical depth. The seawater and Milli-Q water are from UiB's Department of Biology.
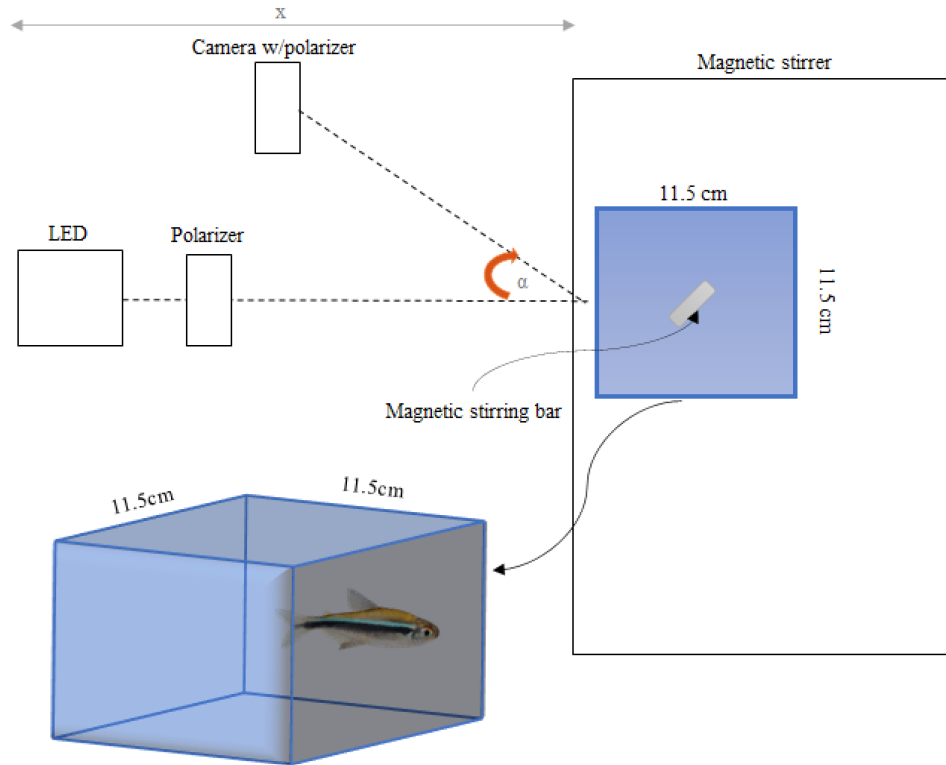
Figure 3.1: Experiment A: Illustration of setup. $x = 0.5m$, and is the distance between the container and the LED. $\theta = 20°$, and is the angle between the camera and the LED.

Table 3.4: Camera settings

Parameter	Value
Resolution	4608 x 3456
Shutterspeed	1 s & 4 s
ISO	200
Aperture value	f/4 & f/7.1
Color mode	sRGB
Bit depth	24
White balance	Constant

3.1.3 Experiment A: Calculations in Advance of Serial Dilution

As discussed in section 3.1, it is assumed that using cross-polarization does not give an equally good effect when it is multiple scattering in the container. In order to know when multiple scattering can be expected, it is desirable to know the concentration and scaled optical depth of the medium being examined. Prior to knowing the concentration in the container, the volume of a single microsphere is calculated. The volume is calculated according to the formula for a sphere, and the microspheres used, is as mentioned in section 3.1.1, is the 510nm polystyrene sphere. Which gives a particle volume of

$$V = \frac{4}{3} \cdot \pi \cdot r^3 = \frac{4}{3} \cdot \pi \cdot (0.255 \mu\text{m})^3 = 0.069 \mu\text{m}^3 = 0.069 \cdot 10^{-12} \text{ ml} \tag{3.1}$$

Furthermore, the data from the polystyrene spheres, in Table 3.3, is entered into a scattering code created by Børge Hamre [30]. The code calculates the number of scattering particles per volume based on the radius, approximate standard deviation and complex refractive index of the particle, and the complex refractive index of the water. The datasheet for the spheres does not state the imaginary part of the complex refractive index. Therefore, the imaginary part (k) is obtained from Kandilian et al. [31], and is said to be $3 \cdot 10^{-4}$. Since it is desirable to study when the number of scattering particles per volume is equal to a scaled optical depth of 0.3, some implementations have been made on the code. Scaled optical depth is given by

$$\tau^* = \tau(1 - g) \tag{3.2}$$

Where τ is the optical depth, and g is the asymmetry parameter. The optical depth is calculated by Eq. 3.3,

$$\bar{\tau} = \int_0^h \beta dz = \beta \cdot h \tag{3.3}$$

where h is the length of the container used. The asymmetry parameter is calculated by Eq. 3.4

46

$$g = \langle\cos\theta\rangle = \int_0^{2\pi} p(\theta)\cos\theta\sin\theta\,d\theta \tag{3.4}$$

where $p(\theta)$ is the phase function, and θ is the scattering angle. The asymmetry parameter g has a value between 1 (no reflection) and -1 (no transmission); $0 < g < 1$ indicates forward scattering, $g = 0$ indicates isotropic scattering, and $-1 < g < 0$ indicates backscattering. After running the script for the specific values, scaled optical depth versus scattering particles per volume is plotted. The plot is shown in Figure 3.2. By studying the plot it is assumed that it occurs multiple scattering in the container when the concentration in container is equal to to $8.6 \cdot 10^{13}\,1/\,\text{m}^3 = 8.6 \cdot 10^7\,1/\text{ml}$. Here the scaled optical depth is equal to 0.3.
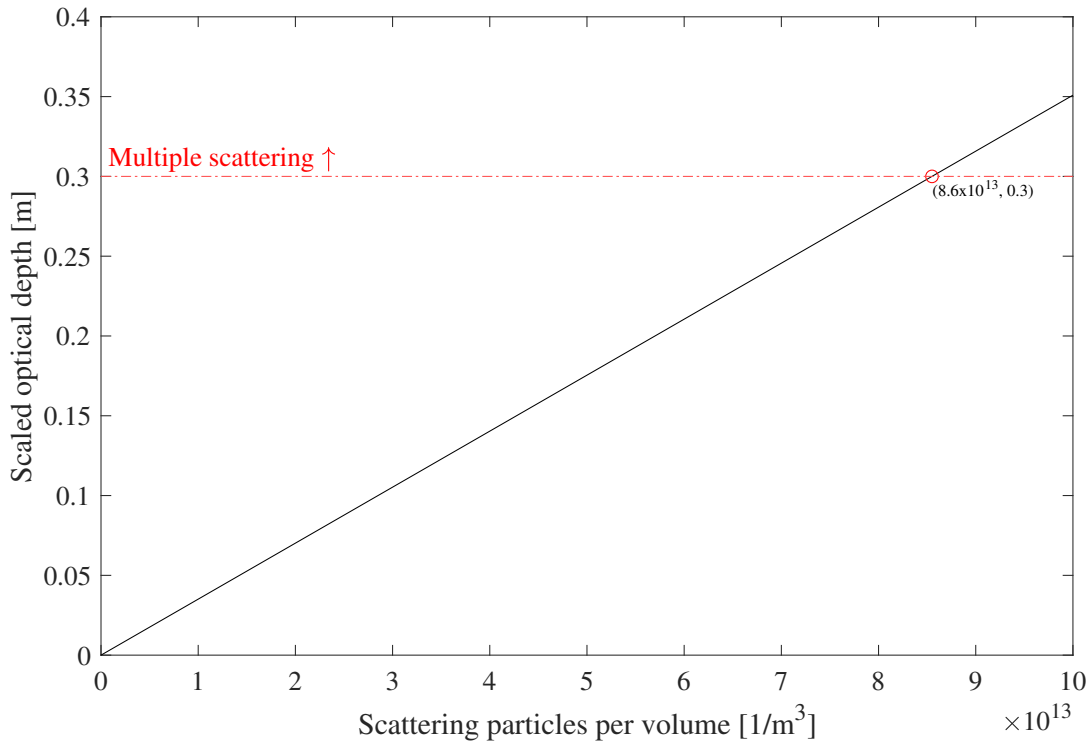
Figure 3.2: Scaled optical depth versus scattering particles per volume

In advance of the serial dilution, the volume percentage of scattering particles at this point is calculated using Eq. 3.5.

$$\text{\% Scattering volume} = \text{Volume of a single microsphere} \cdot \text{Scattering particles per volume} \quad (3.5)$$

$$\text{\% Scattering volume} = 0.069 \cdot 10^{-12} \text{ ml} \cdot 8.6 \cdot 10^{7} \text{ 1/ml} = 5.9 \cdot 10^{-6}$$

For %Scattering volume equal to $5.9 \cdot 10^{-6}$, the scaled optical depth is approximately 0.3. Since the limit for multiple scattering is not entirely set, it is in the region around this volume percentage that multiple scattering can be expected.

3.1.4 Experiment A: Serial Dilution

The aim of serial dilution is to calculate the concentration, the number of scattering particles per volume in the container at any given time to know when multiple scattering can be expected. The serial dilution sheet is shown in Table 3.5. Here the concentration is given as %Scattering volume. Added Milli-Q water (W), added sample volume ($V2$), and starting %Scattering volume ($N2$) are entered into the sheet's red cells. From the previous section, the calculations gave a scaled optical depth equal to 0.3 when the %Scattering volume is equal to $5.9 \cdot 10^{-6}$. By comparing this value up to the values in Table 3.5, it can be observed that the scaled optical depth is greater than 0.3 for addition number seven and onwards. From here, it is assumed a great extent of multiple scattering in the container.

The values in the serial dilution sheet are calculated based on the following equations. The dilution function is given in Eq. 3.6, and the total volume i calculated according to Eq. 3.7.

$$N1 \cdot V1 = N2 \cdot V2 \quad (3.6)$$

$$V1 = V2 + W \quad (3.7)$$

48

Table 3.5: Experiment A: Serial dilution

No.	Concentration N1	Total volume V1 (ml)	Original concentration N2	Total sample volume V2 (ml)	Add sample volume S (ml)	Added Milli-Q volume W (ml)
1	5.99E-08	1000.006	0.01	0.006	0.006	1000
2	1.06E-06	1000.106	0.01	0.106	0.1	1000
3	2.06E-06	1000.206	0.01	0.206	0.1	1000
4	3.06E-06	1000.306	0.01	0.306	0.1	1000
5	4.06E-06	1000.406	0.01	0.406	0.1	1000
6	5.06E-06	1000.506	0.01	0.506	0.1	1000
7	6.06E-06	1000.606	0.01	0.606	0.1	1000
8	7.06E-06	1000.706	0.01	0.706	0.1	1000
9	8.06E-06	1000.806	0.01	0.806	0.1	1000

Now all the calculations necessary in advance of Experiment A have been made. Experimental procedure is presented in Section 3.1.7.

3.1.5 Experiment B: Calculations in Advance of Serial Dilution

The algae used in Experiment B is *Nannochloropsis.* Nannochloropsis is a single-celled alga and is related to microalgae. The shape of the algae can be spherical or oblong and usually measure 2-5 μm in diameter [32]. The algae can be found both in freshwater and ocean water.

The concentration of algae in the mixture is counted by flow cytometry and is estimated to be $4 \cdot 10^7$ 1/ml. The algae used are imaged in Figure 3.3 (here, the mixture is diluted so that it is easier to study them).
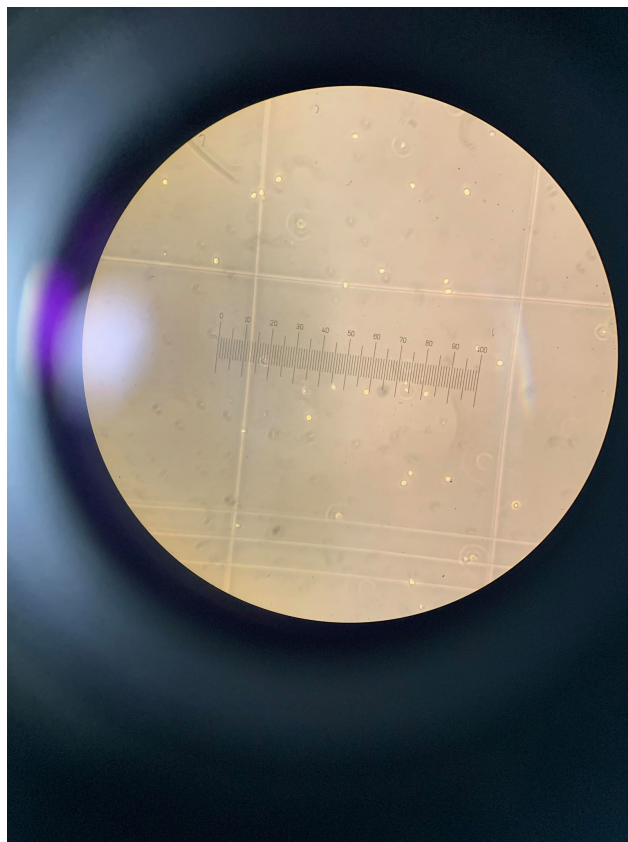
Figure 3.3: Microscopic image of nannochloropsis. The mixture is diluted so it is easier to study the algae.

In order to calculate the %Scattering volume, it is necessary to know the volume of a single alga. The alga is assumed spherical. In order to calculate the volume, it is necessary to know the radius of the algae. The diameter of 20 algae from Figure 3.3 was measured to get a good estimate. A software called *ImageJ* was used to measure the diameter. The algae were displayed in a Fuchs Rosenthal Counting chamber. Each large square in the counting chamber had a surface area of 1.0mm^2. One of the large squares is shown in Figure 3.3, one of the 1mm lines was used as a reference when measuring the diameter of the algae. The result of the algae measuring is $\bar{X} = 4.4$ and $\sigma = 0.73$.

It can be determined an uncertainty in the diameter measurements based on the mean and standard deviation. Standard deviation is a common measure of the uncertainty in each measurement, and is the average deviation from the most probable value. 68.2% of the observations will be within $\pm\sigma$, while 95.4% of the observations will be within $\pm 2\sigma$. 99.8% of the measure-

ments will be within $\pm 3\sigma$. The most common is to state the uncertainty with 1 σ, 68.2% of the algae diameters will lay between this area:

$$\text{Diameter} = 4.4 \pm 0.73 \ \mu\text{m}$$

Based on the mean diameter, the volume of one single alga is calculated,

$$V = \frac{4}{3} \cdot \pi \cdot r^3 \ = \ \frac{4}{3}\pi \, (2.2 \ \mu\text{m})^3 \ = \ 44.6 \ \mu\text{m}^3 = 44.6 \cdot 10^{-12} \ \text{ml}$$

Based on the volume of one single alga and the estimated concentration, the volume percentage of the algae in the algae mixture is calculated to be

$$\% \text{ Scattering volume} \ = \ V \cdot \rho \ = \ 44.6 \cdot 10^{-12} \ \text{ml} \cdot 4 \cdot 10^7 \ 1/\text{ml} = \ 1.8 \cdot 10^{-3} \tag{3.8}$$

The algae diameter, standard deviation and complex refractive index of both the water and the algae are added to the scattering script. The complex refractive index is obtained from Kandilian et al. [31]. The real part of the refractive index (n) is equal to 1.371, and the imaginary part (k) is equal to 0.0005. The result from the scattering script is shown in Figure 3.4. By studying the plot in Figure 3.4, the amount of scattering particles per volume at a scaled optical depth equal to 0.3, is equal to $4.1 \cdot 10^{12}$ $1/\text{m}^3 = 4.1 \cdot 10^6$ $1/\text{ml}$. In advance of the serial dilution, %Scattering volume at this point is calculated using Eq. 3.5,

$$\% \text{ Scattering volume} \ = \ 44.6 \cdot 10^{-12} \ \text{ml} \cdot 4.1 \cdot 10^6 \ 1/\text{ml} = \ 1.8 \cdot 10^{-4}$$

For %Scattering volume equal to $1.8 \cdot 10^{-4}$, the scaled optical depth is equal to 0.3, and thus there is expected multiple scattering around this region. If the %Scattering volume is greater than $1.8 \cdot 10^{-4}$, a greater extent of multiple scattering is expected.
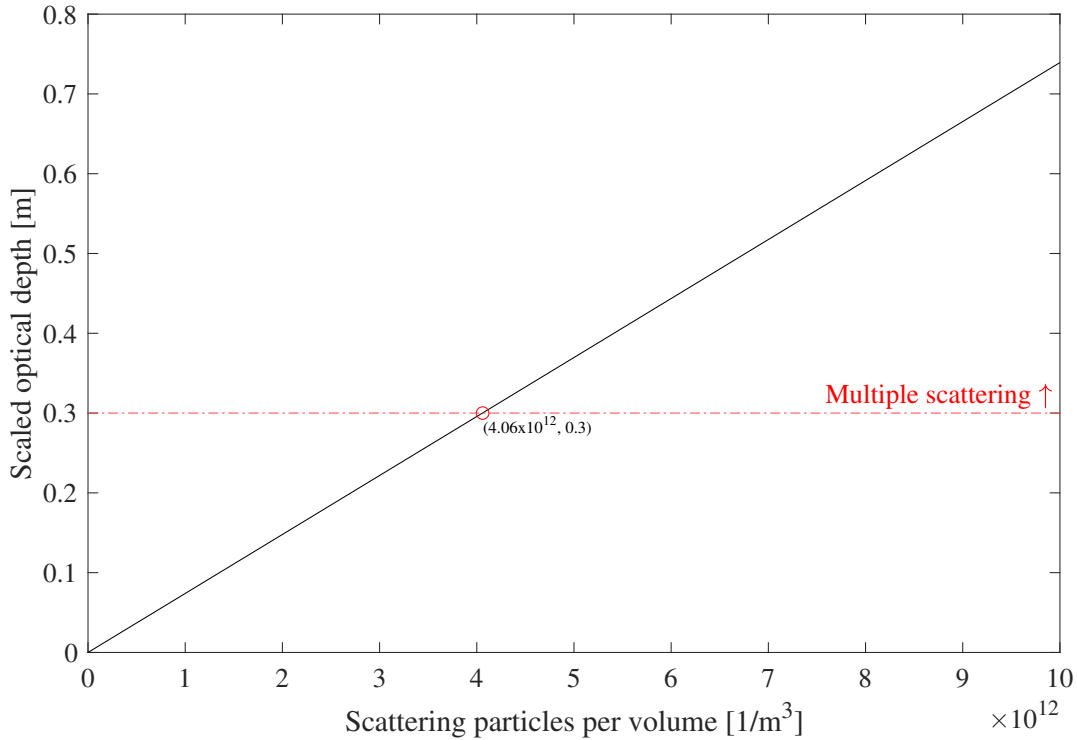
Figure 3.4: Scaled optical depth versus scattering particles per volume. Multiple scattering is expected when the scaled optical depth is equal to 0.3.

3.1.6 Experiment B: Serial Dilution

As for Experiment A, the purpose of serial dilution is to control the concentration in the container at any given time so that one knows when one can expect multiple scattering in the container. Based on the calculations in the previous section, it is assumed that there is multiple scattering in the container when the %Scattering volume is greater than, or in the range around $1.8 \cdot 10^{-4}$. For this scattering volume, the scaled optical depth is equal to 0.3. Since this is not a complete set limit, multiple scattering can occur for other scattering volumes as well.

The serial dilution sheet used is presented in Table 3.6. The original concentration ($N2$), calculated in Eq. 3.8, added sample volume (S) and added seawater (W) are entered in the red cells. The dilution function in Eq. 3.6 is used to calculate the concentration ($N1$), and Eq. 3.7 is used to calculate the total volume ($V1$). The concentration is in the serial dilution sheet given as %Scattering volume.

By comparing the calculated %Scattering volume $(1.8 \cdot 10^{-4})$ up against the different scattering volumes in Table 3.6, it can be seen that one can expect multiple scattering in the container after addition number five. Here the scaled optical depth is greater than 0.3. For an increasing scaled optical depth, there will be a higher degree of multiple scattering in the container.

Table 3.6: Serial dilution

No.	Concentration N1	Total volume V1 (ml)	Original concentration N2	Total sample volume V2 (ml)	Add sample volume S (ml)	Added Seawater volume W (ml)
1	7.20E-06	1004	0.0018	4	4	1000
2	2.14E-05	1012	0.0018	12	8	1000
3	4.92E-05	1028	0.0018	28	16	1000
4	1.02E-04	1060	0.0018	60	32	1000
5	1.99E-04	1124	0.0018	124	64	1000
6	3.64E-04	1252	0.0018	252	128	1000

3.1.7 Experimental Procedure

The following steps explain how the two experiments were conducted

1. Arrange the setup based on Figure 3.1. Ensure that the LED light is directed towards the middle of the container. Also, ensure that the light illuminates the fish attached to the container.

2. Arrange one of the polarizing filters in front of the LED and one in front of the camera lens.

3. Depending on the experiment being performed, add 1L of Milli-Q water or Seawater to the container. Also, add a magnetic stirring bar to the container so that the particles are stirred around. Place the container on the magnetic stirrer.

4. Start by taking images with just Milli-Q water in the container, both with the polarization filter in front of the camera parallel and perpendicular to the polarizing filter in front of the LED. Do this by switching between the two shutter speeds and aperture values presented in Table 3.4.

5. Use a pipette to add the correct amount of the sample volume (ml). For Experiment A, the correct amount of polystyrene sphere is added based on Table 3.5. For Experiment B, the correct amount of algae is added based on Table 3.6.

6. For each concentration; take two images, both with the polarization filter in front of the camera parallel and perpendicular to the polarizing filter in front of the LED. (For experiment A, perform the experiment by switching between the two shutter speeds and aperture values presented in Table 3.4.)

7. Repeat 5 to 6, until the serial dilution is finished.

The result is now two images for each concentration, both with and without cross-polarization. The next step will be to analyze the images and study how the imaging is affected when the concentration and the probability for multiple scattering in the container increases. As polarization is known to increase the contrast and detection range in a scattering media [3], it is chosen to study how the contrast of the images changes with increasing concentration, both with and without cross-polarization. The data processing used to study the contrast is described in further details in Section 3.13. The images taken and the result after the data processing is presented and discussed in Section 4.

3.2 Experiment C: Milli-Q Water and CDOM

This experiment aims to study how Colored dissolved organic matter (CDOM) affects imaging underwater by determining the absorption coefficient and absorption length of the CDOM material used, as well as studying how polarization filters affect imaging in a CDOM medium. CDOM is known to absorb the shorter wavelengths first, and the long ones are the ones that

survive the longest. Water with little or no CDOM typically looks bluish, while water with a high concentration of CDOM may look yellow-brownish.

The experiment is divided into three different cases, as shown in Table 4.12. The CDOM used is tea made under two different conditions and fun light iced tea. The reason tea can be used is because it is a type of color dissolved organic matter. It is assumed that there is not a large enough concentration of particles in the CDOM materials used to experience a significant backscatter. Based on this assumption, it is assumed that one will not see as clear an effect by using cross-polarization as for the other two experiments.

Table 3.7: Experiment C: The CDOM used

Case	CDOM	Amount
1	Earl Gray Tea (100 °C, 15min)	1:5 + 1:10
2	Earl Gray Tea (37 °C, 15min)	1:5 + 1:10
3	Fun light Iced tea	1:5 + 1:10

The calculated absorption coefficients will be compared with typical CDOM parameterization to study how the selected CDOM materials are in relation to typical CDOM. CDOM is, per definition, what passes through a filter with a pore size of 0.02 μm [33].

3.2.1 List of Equipment

The equipment used in Experiment C is listed in Table 3.8.

Table 3.8: Experiment C: List of equipment

Variables	Value
Camera	Panasonic Lumix DMC-GH3
2x Polarizing filter	Linear. One in front of the camera, and one in front of the LED
LED	MBB1L3 - 470-850 nm Mounted Broadband LED, 70 mW (Min), 500 mA
LED power supply	DC2200, High-Power1-Channel LED Driver with Pulse Modulation, 10.0A Max, 50.0V Max
Container	Plexiglass, size: 11.5cm x 11.5cm
Milli-Q water	1.5 L
Earl Gray Tea 100 °C 15 min	0.1 L
Earl Gray Tea 37 °C, 15 min	0.1 L
Fun light iced tea	0.1 L
Spectrometer	USB2000+UV-VIS, Ocean Optics, Inc.
Fiber optics cable	QR400-7-UV-BX, Ocean Optics, Inc.
Diffuse reflectance standard	SRT-99-050, Labsphere, Inc.
Ocean View	
Pipette	
Magnetic stirrer	
Magnetic stirring bar	

3.2.2 Setup

The setup used is shown in Figure 3.5. There are two main elements of data collection in this experiment. The first element is the fiber optics cable connected to Ocean View via the spectrometer. The second element is the camera. The output of the camera is an sRGB image. The

software Ocean View is used to obtain transmission data from the spectrometer. The spectrometer (USB2000+UV-VIS) measure light intensity of a sample, based on reference intensity and background intensity of the setup. The reference spectrum was set to an empty container. After being calibrated to the setup, the transmittance in Ocean View is calculated using Eq. 3.9,

$$\%T_\lambda = \frac{S_\lambda - D_\lambda}{R_\lambda - D_\lambda} \cdot 100\% \tag{3.9}$$

Where S_λ is the sample intensity at wavelength lambda, D_λ is the background intensity, and R_λ is the reference intensity.
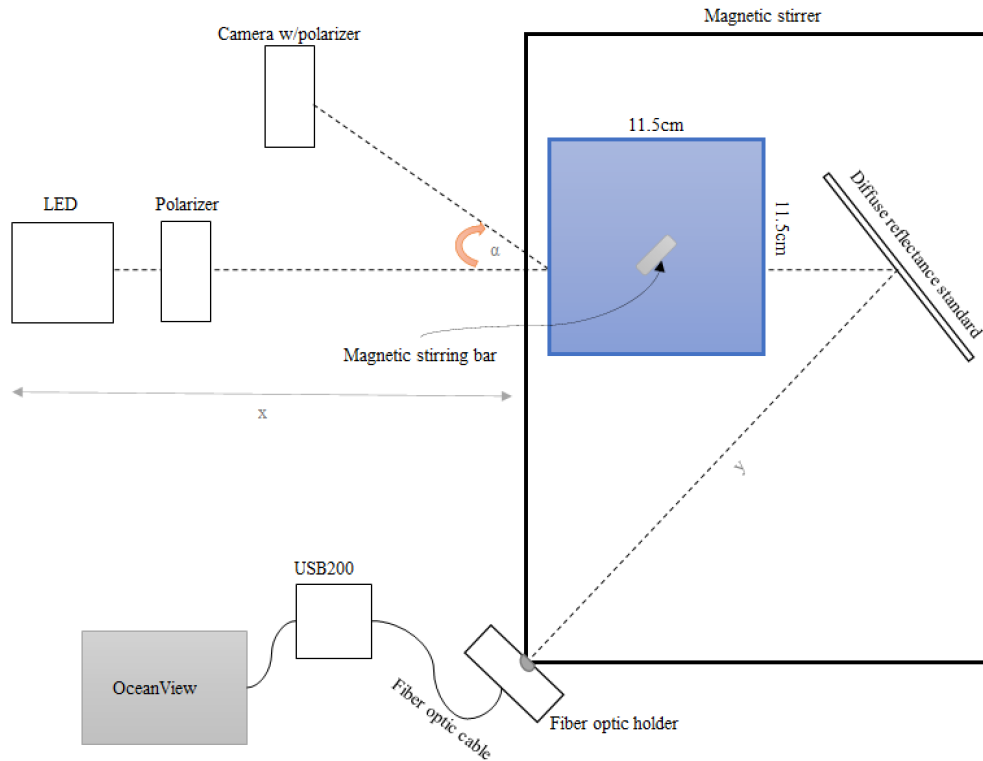
Figure 3.5: Illustration of the setup. $x = 0.5'$ m, and is the distance between the container and the LED. $\theta = 20°$, and is the angle between the camera and the LED. $y = 0.20$ m. and is the distance between the diffuse reflectance standard and the optics cable.

57

When arranging the setup, it is essential to ensure that the fiber cable is directed towards the right area of diffuse reflectance standard so that it does not pick up unwanted light. A plate was used to make sure that no unwanted light passed through the sides of the container and was caught up by the fiber cable. A diffuse reflectance standard was used because the reflection is the same in all directions for such a plate. It absorbs extremely little, so it is ideal to use when studying the transmitted light through the container.

A magnetic stirrer, and stirring bar was used to mix the CDOM material with the Milli-Q water. As for the other experiments, two polarization filters were used, one in front of the camera and one in front of the LED.

3.2.3 Experimental Procedure

The following steps explain how the experiment were conducted:

1. Arrange the setup based on Figure 3.5. Ensure that the LED is directed towards the middle of the container. Also, ensure that the optics cable is directed towards the right area of the diffuse reflectance standard.

2. Arrange one of the polarizing filters in front of the LED and one in front of the camera lens.

3. Calibrate spectrometer to the setup.

   - Open OceanView.

   - Click "Spectroscopy Application Wizards" → Click "Transmission" → Select "Set Acquisition Parameters ()" and click "Next".

   - Set the Integration time to "Automatic", and set Scans to Average to 100 → Wait for the Automatic process to finish → click "Next".

   - Make sure that the LED is on. Wait for the spectrum to show in the "Reference Spectrum Preview" -→ click "next".

   - Turn of the LED. Wait for the spectrum to show in the "Background Spectrum Preview" → click "next".

- Now the spectrometer is calibrated to the setup.

4. For each of the cases (Table 3.7), measure transmittance versus wavelength for each of these following points. Remember to click on the "save data" icon to save the transmission data for each of the following points. Also capture images for each of the points, both with polarizing filter in front of the camera parallel and perpendicular to the polarizing filter in font of the LED.

    - Container empty

    - Container filled with 0.5L Milli-Q water

    - Container filled with 0.5L Milli-Q water + 0.1L Tea

    - Container filled with 0.5L Milli-Q water + 0.1L Tea + 0.6L Milli-Q water

5. Repeat the experimental procedure for each of the three different cases.

After performing the experimental procedure for each of the cases in Table 3.7, the result is different transmission measurements. Each transmission measurement has its own .txt file, and each file contains wavelengths and the associated transmission for each wavelength. The transmission data are analyzed and processed according to what is presented in Section 3.2.4. The images taken are presented in Section 4.3.

3.2.4 Absorption Coefficient and Absorption Length

Figure 3.6 illustrates a clip of the setup used. As explained, the transmittance is measured for the different contents in the container. This is done because it is desirable to study how much of the light that is moving through the container for the three different cases. Based on the transmittance, the absorption coefficient and absorption length are calculated. The absorption coefficient can be calculated using Beer's law (Eq. 2.4). As discussed in section 2.1.4, Beer's law express the irradiance of the attenuated light ray. The irradiance of the attenuated light ray is calculated based on the incident irradiance, the thickness x of the slab, and the absorption coefficient κ. By making some changes to Eq. 2.4, we get

$$T = \frac{T_T}{T_W} = e^{-\kappa x} \tag{3.10}$$

Where T_T is transmission measured when there is tea in the container, and T_W is transmission measured when there is only water in the container.
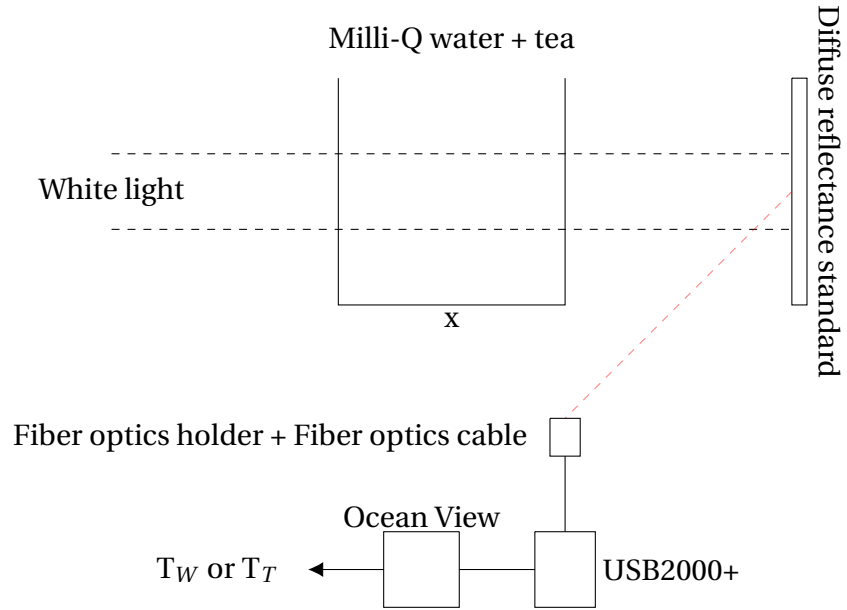
Figure 3.6: Transmittance setup

By making an adaption on Eq. 3.10, the absorption coefficient κ, can be calculated by:

$$\kappa = -\frac{\ln\left(\frac{T_T}{T_W}\right)}{x} \tag{3.11}$$

Since absorption length is the inverse absorption coefficient, absorption length is given by

$$\bar{x} = \frac{1}{\kappa}$$

A MATLAB script is written to study the absorption coefficient and absorption length of the CDOM materials used. Eq. 3.11 and Eq. 3.2.4 is implemented to the script. The script plots the absorption coefficient and absorption length versus the wavelength. The equation for typical CDOM paramterization [33] is also included to the MATLAB script,

$$\kappa(\lambda) = \kappa(500) \cdot \exp(-0.016 \cdot (\lambda - 500)) \tag{3.12}$$

Where $\kappa(500)$ is κ measured at 500 nm, and λ is the wavelength of the absorption coefficient being calculation. The MATLAB script can be found in the GitHub attached to this thesis [30]. The results are presented in Section 4.3 .

3.3 Data Processing: Image Contrast

Contrast is a difference in luminance or color that distinguishes an object from another object within the same field of view [4]. As stated in Bohren et al. [4, p.416], "The distance at which a black object cannot be distinguished from the horizon sky depends on the contrast threshold". The contrast threshold is typically set as 2%, and is the smallest absolute contrast difference that can be perceived by a human observer. Bohren et al. [4, p.416] also states that the contrast threshold depends on "the angular size of the object observed, the presence of nearby objects, and the absolute luminance". By comparing an image with low contrast, and an image with high contrast, one can see that the details of the image with high contrast are more visible than details in the image with lower contrast. One way to study whether an image has high or low contrast is by studying the image histogram. According to Pietka [34], "an image histogram is a gray-scale value distribution showing the frequency of occurrence of each gray-level value" [34]. If the pixel intensity is within a narrow range, it is said to have low contrast (Figure 3.7a). Here, it is more difficult to distinguish between approximately the same intensity value. For an image with high contrast, the intensity values are spread more outwards (Figure 3.7b).
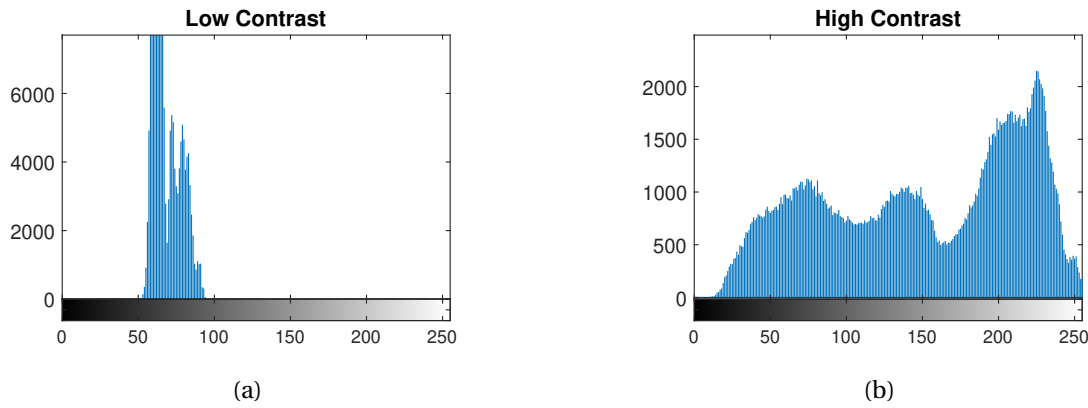
Figure 3.7: A image histogram is illustrating the frequency occurrence of each gray-level value [34]. (a) Low contrast (b) High contrast

Although this is a way to study whether one image has better contrast than another, it is desirable to put a number on the contrast. This is because it should be possible to study how much better it is to use polarizing filters rotated perpendicular to each other versus parallel to each other. So that one can numerically study the effect of cross-polarization. Bohren et al. [4] defines the contrast between a object with luminance B, and a background with luminance B_∞, as

$$C = \frac{B - B_\infty}{B_\infty} \tag{3.13}$$

Where B_∞ is the horizon luminance. There are different ways of calculating contrast in an image, this type of contrast is known as *Weber contrast*, and makes calculations based on the object and the background. According to Nasa Research centre, [35], the contrast is given by a value between zero and -1 when the background is lighter than the object. When the background is darker than the object, the contrast is between zero and potentially very high numbers.

The contrast is here used as a measure of the image quality. Eq. 3.13 is implemented in a MAT-LAB script created to calculate the contrast of the different images. The input parameters are the images taken for the given experiment, as well as the concentration in the container for the various images. The code retrieves one area of the object and one area of the background. Fur-

thermore, the contrast is calculated by Eq. 3.13. The result is an array with associated contrast for each image. Furthermore, a ratio is calculated that tells how much better or worse it is to photograph with cross-polarization. By using the plot function in MATLAB, the results can be plotted graphically. The code created to calculate the contrast can be found GitHub attached to this master's thesis [30]. GitHub also contains a contrast code that calculates the average contrast and standard deviation based on four different areas of the object and background.

4 Results and Discussion

This chapter aims to study the results of the experiments that have been conducted. As explained in Section 3, three experiments were conducted in order to study to what extent it is possible to achieve better imaging underwater using polarization techniques. Experiment A and Experiment B study the effect of polarizing filters with increasing concentration of particles. Images are taken at different concentrations, both with the polarizing filters parallel and with cross-polarization. In order to study how the image quality changes for increasing concentration, the contrast of the images are calculated. The higher contrast, the more details of the object can be seen. Experiment C studies the effect of CDOM in an underwater imaging system and calculates the image contrasts. In order to study the effect of CDOM, the absorption coefficient and absorption length for the CDOM materials used are calculated. The aim of each experiment is explained in further detail in Section 3.

As discussed in Section 3.1, it is assumed that the use of cross-polarization will give the best effect in Experiment A, where polystyrene spheres have been used. This is because these particles are spherical, and as discussed in Section 2.4.7, linear polarization is preserved in backward direction when a sphere scatters light. Since the algae used in Experiment B not are spherical, polarization is not preserved in backward direction. The fact that polarization is not preserved in backward direction can affect the result, in that light is transmitted through the filter in front of the camera when using cross-polarization. In cases where linearly polarized light is preserved in backward direction, the unwanted backscattered light will be blocked when using cross-polarization (More details on polarizing filter can be read in Section 2.4.5). It is also assumed that the use of polarizing filter will give the best effect when there is single scattering in the container. The limit for multiple scattering is set to when the scaled optical depth is greater than 0.3 ($\tau^* > 0.3$). Another thing that is assumed is that the algae will absorb more than the polystyrene spheres, which may be evident in the results. For Experiment C, it is assumed that one will not see an equally evident effect of cross-polarization since it is assumed that the concentration of CDOM used is not high enough to cause a great extent of backscatter.

Section 4.1 presents the results from experiment A, Section 4.2 presents the results from experiment B and Section 4.3 presents the results from experiment C. The different sections will also contain a discussion of the results. Possible sources of error that may have affected the results will be presented along the way. Section 4.4 will summarize the possible sources of error, as well as discuss other potential sources.

4.1 Experiment A: Polystyrene Spheres and Milli-Q Water

In this experiment, the effect of polarizing filters in an underwater imaging system is studied. The aim of the experiment is explained in further details in Section 3.1. The setup used to obtain the results is described and illustrated in Section 3.1.2. Briefly explained, the setup consists of a container filled with Milli-Q water and polystyrene spheres. The spheres were added to the container with a pipette according to Table 3.5. For each addition of particles, a new concentration was calculated. Based on calculations made in Section 3.1.3, it is known for what concentration multiple scattering can be expected.

As shown in Table 4.1, the images were taken with four different combinations of camera settings. The other camera settings, such as ISO, resolution, bit depth, are specified in Table 3.4. For each of the concentrations in Table 3.5, two images were taken. In the first image, the polarizing filter in front of the camera is rotated parallel to the polarizing filter in front of the light source. In the second image, the polarizing filter in front of the camera is rotated perpendicular to the polarizing filter in front of the light source (also known as cross-polarization). The images taken with the camera settings in *case 1* is presented in Figure 4.1. The other cases will be studied later in this section.

Table 4.1: The different cases of camera settings

	Shutter speed	Aperture value
Case 1	1s	f/4
Case 2	4s	f/4
Case 3	1s	f/7.1
Case 4	4s	f/7.1

(a) C0 ∥   (b) C0 ⊥   (c) C1 ∥   (d) C1 ⊥

(e) C2∥   (f) C2⊥   (g) C3 ∥   (h) C3 ⊥

(i) C4 ∥   (j) C4 ⊥   (k) C5 ∥   (l) C5 ⊥

(m) C6 ∥   (n) C6 ⊥   (o) C7 ∥   (p) C7 ⊥

(q) C8 ∥   (r) C8 ⊥   (s) C9 ∥   (t) C9 ⊥
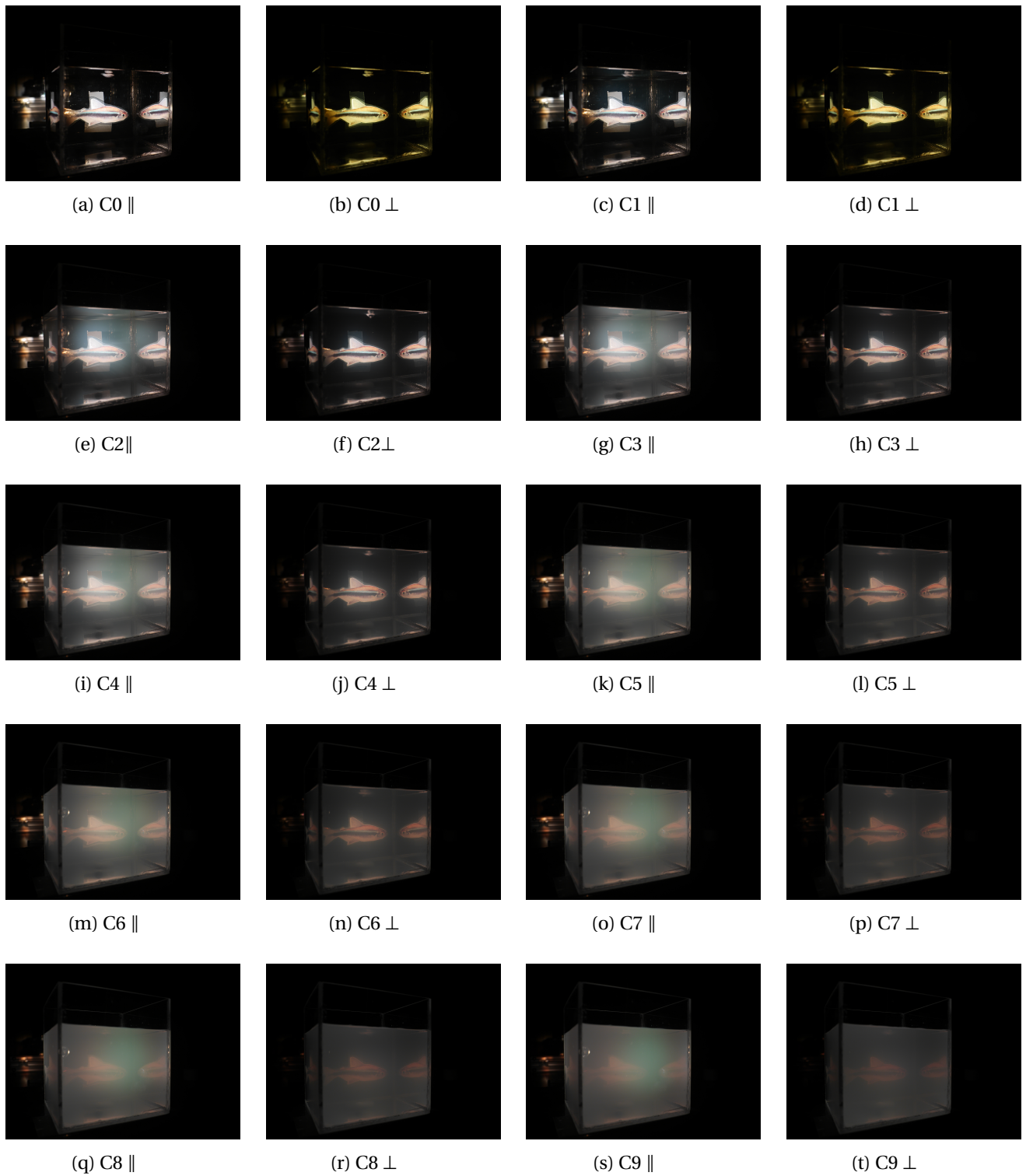
Figure 4.1: C1-C9 indicates the different concentrations from the serial dilution in Table 3.5. The content in the container in (a) and (b) is just Milli-Q Water. ∥ indicates that the polarizing filter in front of the LED is parallel to the one in front of the camera. ⊥ indicates cross-polarization.

By studying the result for case 1 in Figure 4.1, one can observe that the visibility in the container becomes poorer with increasing concentration of scattering particles, which is due to the scaled optical depth in the container increasing. The probability of scattering at the different optical depths can be calculated to study how the probability of scattering is changing with increasing (scaled) optical depth. Optical depth is given by Eq. 3.3: $\tau = \beta \cdot L$, where β is the scattering coefficient, and L is the length of the container. β is obtained from the scattering script and is calculated based on the particle used. Table 4.10 shows that the probability of scattering will increase with increasing (scaled) optical depth. The probability of survival is given by "$e^{-\tau}$", and the probability of scattering is given by "$1 - $ Probability of Survival". A higher probability of scattering gives a higher probability for multiple scattering. Multiple scattering is assumed from image C7 (Figure 4.1 (o)-(t)), here one can observe from Table 3.3 that the scaled optical depth (τ^*) is equal to 0.31, and that the probability for scattering is 85%.

Table 4.2: The scattering coefficient (β), scaled optical depth (τ^*), optical depth (τ), and probability of survival and scattering, for the concentration in each of the images.

Image	β [1/m]	τ^*	τ	Probability of survival	Probability of scattering
C0	-	-	-	-	-
C1	0.17	0.003	0.019	0.98	0.02
C2	2.91	0.054	0.33	0.72	0.28
C3	5.64	0.10	0.65	0.52	0.48
C4	8.44	0.16	0.97	0.38	0.62
C5	11.11	0.21	1.28	0.28	0.72
C6	13.83	0.26	1.59	0.20	0.80
C7	16.56	0.31	1.90	0.15	0.85
C8	19.00	0.36	2.18	0.11	0.89
C9	22.04	0.40	2.53	0.08	0.92

By studying the images in Figure 4.1, one can see a distinct effect of using cross-polarization, especially when single scattering is assumed (Figure 4.1(a)-(n), image C0-C6). Here the scaled optical depth (τ^*) is less than 0.30. As discussed in Section 2.4.7, linearly polarized light is preserved in the backward direction when light is scattered on a sphere, by using cross-polarization, it is thus possible to remove large parts of the backscattered light. By further studying the images

67

in Figure 4.1, it can be seen that the effect of cross-polarization decreases with increasing scaled optical depth. It does not seem to be an equally good effect of cross-polarization when there is multiple scattering in the container. As previously discussed, multiple scattering is expected from image C7 (Figure 4.1 (o)-(t)). When light is scattered multiple times, the polarization is not preserved in backward direction, and one thus does not expect an equally good effect of cross-polarization. One reason for this is that the polarizing filter in front of the camera does not block the backscattered light (which happens when there is mostly single scattering in the container), but it lets though some of the light, which is then captured by the camera.

One can especially for image C2 (Figure 4.1 (e) - (f)) observe a clear effect of cross-polarization. If one studies these images more closely, one can observe that the backscattered light almost is removed using cross-polarization. One way to study how much better it is to use cross-polarization instead of parallel polarization filters is to calculate the contrast. The contrast of these images is studied in the following section.

4.1.1 Uncertainties in Contrast Calculations

How contrast is affected by cross-polarization is studied in this section. As discussed in Section 2.1.3, it is assumed that the contrast is decreasing when there is an increasing amount of scattering in the container. As discussed, Bohren et al. [4] and Cartron et al. [3] states that polarization is known to improve the contrast in a scattering medium. Therefore it assumed that the contrast will be better when cross-polarization is used rather than parallel polarization filters. The contrast code described in Section 3.3 is used to study how the image contrast is affected by the increasing concentration. The images in Figure 4.1 is set as input parameters to the MATLAB script.

The contrast code calculates the contrast based on four different areas of the fish and the background. Furthermore, the average contrast and standard deviation are calculated for these areas. The results of the uncertainty calculations are summarised in Table 4.3. By assuming a normal distribution, 68.3% of the observations (contrasts) will be within one standard deviation. 95.3% of the observations will be within two standard deviations, and 99.7% of the observations

will be within three standard deviations. Uncertainty is usually expressed by one standard deviation and is expressed by $\bar{X} \pm \sigma$.

Based on the calculations from Section 3.1.3, one can expect multiple scattering in the container when the concentration is $8.6 \cdot 10^{13}$ $1/m^3$; here, the scaled optical depth (τ^*) is greater than 0.3. As discussed in the previous section, the scaled optical depth has been achieved from image C7 (Figure 4.1o and Figure 4.1p). When the scaled optical depth is greater than 0.3, it is assumed that cross-polarization will not give an equally good effect. By studying the different contrast in Table 4.3, one can see what is assumed; the contrast is decreasing with increasing concentration and scaled optical depth. By comparing the mean contrast $\bar{X}$ for cross-polarization and polarization in Table 4.3 one can observe that until image C6, one experiences a better contrast when photographing with cross-polarization. Although it was assumed that there is multiple scattering for the concentration in image C7, it is still possible that there is multiple scattering for the concentration in image C6. The limit for when multiple scattering can be expected in backward direction ($\tau^* > 0.3$) is not fixed.

Table 4.3: Uncertainty in the contrast measurements. $\bar{X}$ is mean contrast, and σ is the standard deviation calculated based on the mean contrast. Cross-Polarization

	Cross-Polarization		Polarization	
	$\bar{X}$	σ	$\bar{X}$	σ
Image C0	33	1.87	21	1.28
Image C1	22	0.76	12	1.01
Image C2	4.5	0.18	2.2	0.25
Image C3	2.5	0.099	1.5	0.14
Image C4	1.6	0.092	1.1	0.10
Image C5	1.1	0.075	0.89	0.081
Image C6	0.69	0.050	0.73	0.056
Image C7	0.45	0.036	0.60	0.036
Image C8	0.30	0.024	0.51	0.024
Image C9	0.19	0.012	0.44	0.020

Another factor that may have affected the contrast to deteriorate before assumed is the possi-

bility of erroneous reading of the imaginary refractive index of the spheres. The imaginary refractive index is obtained from Ma et al. [36]. The real part of the refractive index is given in the datasheet for the polystyrene spheres, shown in Table 3.3. Figure 4.2 illustrates the difference in scattering particles per volume if one has read the imaginary refractive index wrong with a difference of ±0.0002. By studying Table 4.4 one can see that there will be a difference in scattering particles per volume if the imaginary refractive index differs with ±0.0002. By comparing the scattering volume in Table 4.4 with the scattering volume in Table 3.5, it can be seen that the calculated scattering volume in table 4.4 is not small enough to match with the scattering volume for image C6 in Table 3.5. Thus, this is not why the contrast gets worse for image C6. The best explanation so far is, therefore, that the limit for multiple scattering is not completely set and that it is possible to have a high extent of multiple scattering in the container before the scaled optical depth has reached 0.3.
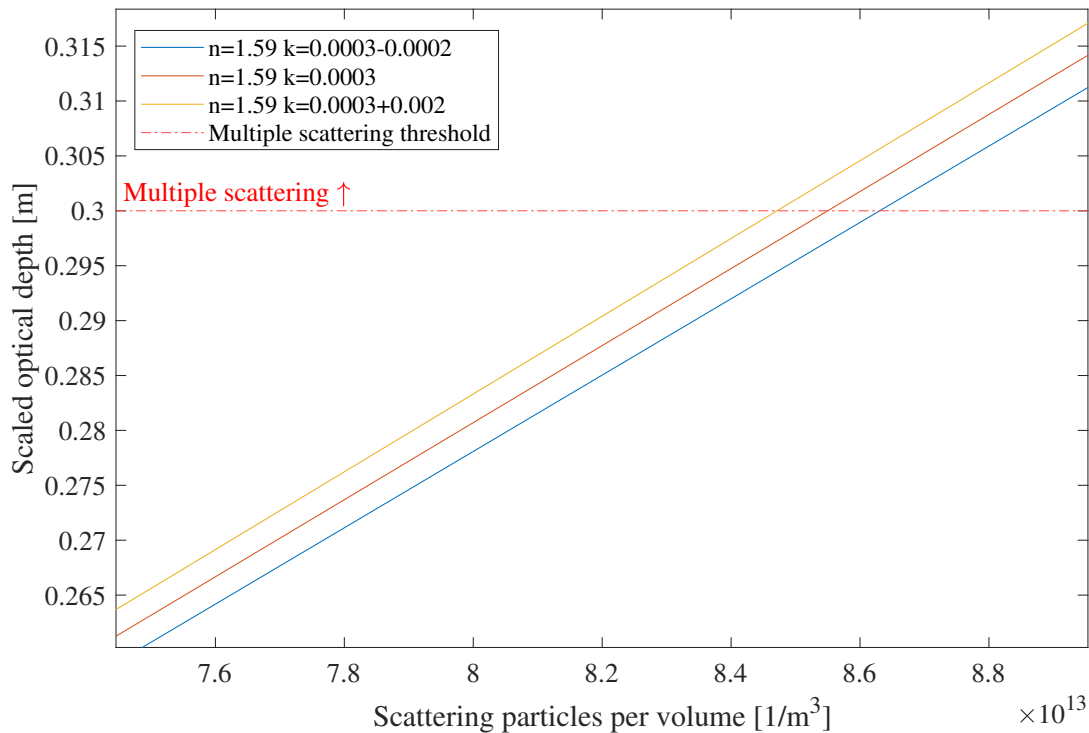
Figure 4.2: How the imaginary refractive index affects scattering particles per volume and scaled optical depth

Table 4.4: Complex refractive index affecting concentration and %Scattering volume. Real part (n) of the complex refractive index is equal to 1.59

	Concentration [1/m3]	%Scattering volume
k=0.0003-0.0002	8.47e13	5.88e-6
k=0.0003	8.55e13	5.94e-6
k=0.0003+0.0002	8.63e13	6.04e-6

4.1.2 Contrast Calculations Based on One Larger Area of the Object

In the previous section, the contrasts were calculated based on four different areas of the object. It is also desirable to study how the contrast differs if one chooses one larger area of the object instead of several smaller areas, as it is more user-friendly and reduces data processing time. The contrast is calculated by the use of the contrast code described in Section 3.3. The images in Figure 4.1 are selected as input parameters. The result of the contrast calculations is shown in Table 4.5. By comparing the values in Table 4.5 with the values in Table 4.3, one can observe that the calculations based on one larger area of the fish are within one standard deviation. Based on this, one can say that it is a good estimation to choose one large area of the fish instead of several areas when calculating the contrast of the images.

By studying Table 4.5, one can observe how the contrast is changing with increasing concentration, both with and without cross-polarization. Table 4.5 also contains a ratio that tells how much better or worse the contrast is when cross-polarization is used instead of polarization filters parallel. As discussed in the previous section, it was from image C7 that it was assumed that one could expect a worse effect of cross-polarization. However, after studying the contrast results in Table 4.3, it turns out that one gets worse contrast from image C6. The reason for this is most likely, as discussed, because the limit of scaled optical depth equal to 0.3 is not entirely set, and one, therefore, can have a high degree of multiple scattering in the container for image C6 as well. Based on this, the results are almost consistent with the assumptions that one will have a worse effect of cross-polarization when there is a great extent of multiple scattering.

By studying Table 4.5, one can observe that the contrast is 105% better for cross-polarization

than parallel polarization filters for image C2 (Figure 4.1 (e) - (f)). This agrees well with the fact that it was here that the best effect was seen. As discussed, a scaled optical depth greater than 0.3 has been obtained from image C7 (Figure 4.1 (o)-(p)). Based on this, by studying Table 4.5, it can bee seen that for $\tau^* < 0.3$ the contrast has been improved by 22-105% when cross-polarization is used. This indicates a good effect of cross-polarization when there is a high extent of single scattering in the container. The effect is not as good when there is multiple scattering in the container.

Table 4.5: Contrast calculated based on one larger area of the fish. The images used as input parameters are the images presented in Figure 4.1. Case 1 of the different camera settings.

Image	Contrast		Ratio	
	Cross-Polarization	Polarization	x	[%]
C0	33	21	1.57	57
C1	23	12	1.91	91
C2	4.5	2.2	2.05	105
C3	2.5	1.5	1.66	66
C4	1.6	1.1	1.45	45
C5	1.1	0.90	1.22	22
C6	0.70	0.73	0.96	-4
C7	0.45	0.60	0.75	-25
C8	0.30	0.51	0.58	-42
C9	0.19	0.44	0.43	-57

Figure 4.3 illustrates how the contrast is decreasing with increasing concentration. By studying the illustration, one observe that one gets a worse effect of cross-polarization when the concentration is greater than approximately $7 \cdot 10^{13}$ 1/m^3. Here the scaled optical depth is approximately 0.26. The concentration in image C6 and onwards are within this range, which agrees well with the assumptions for the contrast get worse when there is multiple-scattering in the container and thus having a scaled optical depth greater than 0.3.
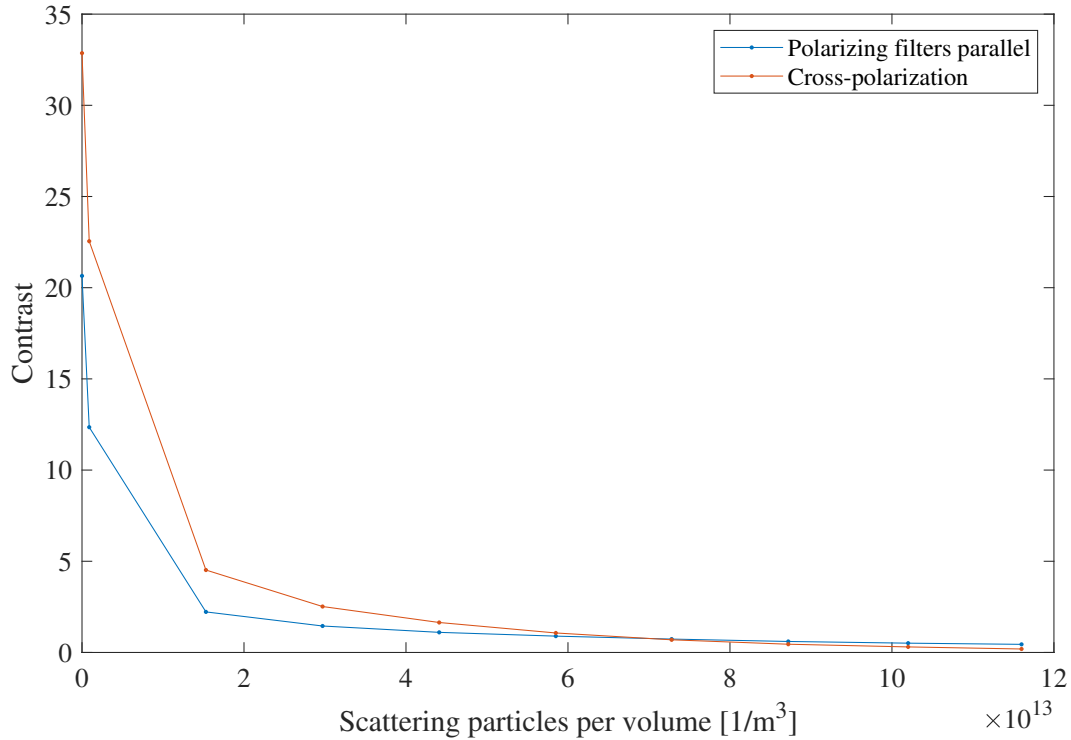
Figure 4.3: Contrast versus polyester spheres concentration

To study the scattering in the container in more detail, the mean free path can be calculated. The mean free path for scattering is a measure of the mean distance a light wave travels before it gets scattered. If the mean free path is greater than the length of the container, there will be mostly single scattering within the container. As discussed in Section 2.3, there will be dominating multiple scattering inside the container when the mean free path is less than the length of the container. The mean free path is calculated according to $l_s = 1/\beta$, $\beta = N \cdot \sigma_s$ is the scattering coefficient, N is number of scattering particles per volume and σ_s is scattering cross-section. β, N, and σ_s are all obtained from the scattering script, described in Section 3.1.3.

By comparing the mean free path in Table 4.6 with the length of the container (0.115 m), one can observe that from image C5 and onwards, there will be a mean free path shorter than the length of the container. The fact that the mean free path is less than the length of the container from image C5 and onwards helps strengthen the assumption that there may be multiple scattering in the container for image C6. The calculations also can indicate that the limit of scaled optical

73

depth equal to 0.3 is vague. Multiple-scattering may occur at the other concentrations, but the probability of it is way less for the smaller concentrations.

Table 4.6: τ^* is the scaled optical depth, N is the number of scattering particles per volume, β is the scattering coefficient, σ_s is the scattering cross-section of a single particle. The mean free path is the mean free path for scattering.

Image	τ^*	N [1/m^3]	β [1/m]	σ_s [m^2]	Mean free path [m]
C0	-	-	-	-	-
C1	0.003	8.90e11	0.17	1.90e-13	5.88
C2	0.05	1.53e13	2.91	1.90e-13	0.34
C3	0.10	2.97e13	5.64	1.90e-13	0.18
C4	0.16	4.41e13	8.44	1.90e-13	0.12
C5	0.21	5.85e13	11.11	1.90e-13	0.090
C6	0.26	7.28e13	13.83	1.90e-13	0.072
C7	0.31	8.72e13	16.56	1.90e-13	0.060
C8	0.36	1.02e14	19.00	1.90e-13	0.053
C9	0.40	1.16e14	22.04	1.90e-13	0.045

4.1.3 Which Camera Settings is Best Suited for the Setup?

The purpose of testing with different camera settings (Table 4.1) is to study which settings that are best suited for the setup. When studying the camera settings, the contrast code described in Section 3.3 has been used. The images for the different camera settings also are compared to each other. As discussed in the previous section, the contrast is within one standard deviation if one calculates the contrast based on one large area of the object instead of several smaller areas. Therefore, in these calculations, the contrast is calculated based on one larger area. The input parameter to the contrast code is the different images for each of the cases of camera settings. The result of the contrast calculations is shown in Table 4.7. By studying the contrasts in this table, one can, for case 1 and 4, observe that cross-polarization gives a worse contrast than for parallel polarizing filters from image C6. For case 2 and 4, the contrast gets worse from image C7. As discussed earlier, it is for the concentration around image C7 that one can expect multiple scattering. Based on this, the assumptions still hold true; the contrast gets worse in the area

74

where it goes from single to multiple scattering for all of the different cases of camera settings.

Table 4.7: Contrast overview for each of the cases. ⊥ is cross-polarization, and ∥ stands for parallel filters.

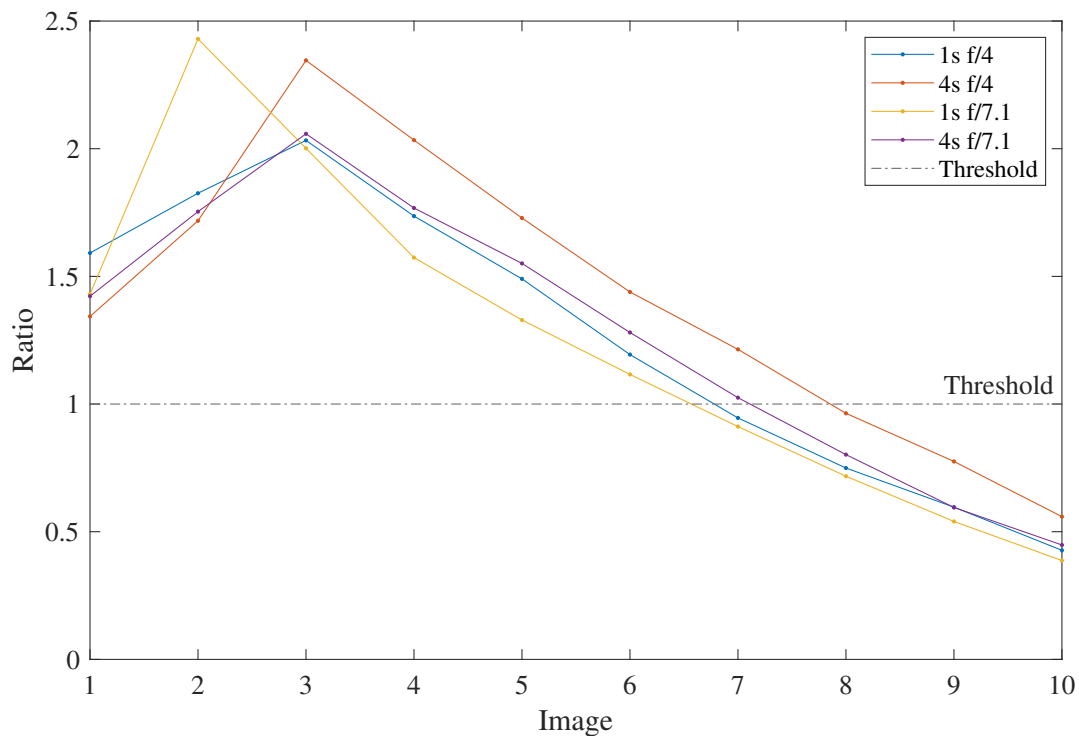| Image	Case 1		Case 2		Case 3		Case 4	
	⊥	∥	⊥	∥	⊥	∥	⊥	∥
C0	33	21	8.3	6.2	101	71	25	18
C1	23	12	6.1	3.5	76	31	17	10
C2	4.5	2.2	1.6	0.67	9.1	4.5	3.6	1.8
C3	2.5	1.5	0.94	0.46	4.5	2.9	2.1	1.2
C4	1.6	1.1	0.67	0.38	2.8	2.1	1.4	0.91
C5	1.1	0.90	0.47	0.33	1.7	1.5	0.94	0.73
C6	0.70	0.73	0.34	0.28	1.1	1.2	0.63	0.62
C7	0.45	0.60	0.23	0.24	0.66	0.92	0.42	0.52
C8	0.30	0.51	0.16	0.21	0.41	0.76	0.27	0.45
C9	0.19	0.44	0.11	0.19	0.25	0.65	0.17	0.37

Figure 4.4: How much better or worse it is to use cross-polarization for each of the concentrations. C0 is image 1, C1 is image 2, C2 is image 3 and so on.

Figure 4.4 illustrates how much better or worse it is to photograph with cross-polarization instead of parallel polarization filters for all four cases. By studying the figure, one can observe the same as what is observed from Table 4.7. Case 1 and 3 provide lower contrast for the concentration in image C6 (Image 7 in Figure 4.4) when using cross-polarization. While cases 2 and 4 provide lower contrast for the concentration in image C7 (Image 8 in Figure 4.4) when using cross-polarization. Based on the previous discussion, there is a considerable degree of multiple scattering in the container for these images. However, as mentioned above, it is desirable to study the images for each of the cases of camera settings (Table 4.1) to ascertain which camera settings are best suited to the setups used.

Three factors are central when choosing camera settings for an underwater imaging system: shutter speed, aperture and ISO. Shutter speed and aperture work together; therefore, it is necessary to balance them for the exposure to be good. The aperture is selected based on the distance to the object. The shutter speed is selected based on the motion of the object being photographed. Underwater, it is recommended to use shutter speeds of less than 1/30 s. For a fast motive, such as a shoal of fish, a shutter speed of 1/125 s is recommended. For a slower object, 1/60 s is recommended [37]. If the image still is perceived as dark after selecting these settings, the ISO value can be adjusted. ISO regulates the camera sensors light sensitivity. The higher ISO, the more noise. A constant ISO200 is therefore determined for this setup. The aperture and shutter speed is adjusted based on Table 4.1. Since the object used in this experiment is not moving, the lowest shutter speed used is 1 second. A good rule of thumb is to start with as low an ISO as possible and rather adjust the aperture and shutter speed. If one does not get the desired effect, one can adjust the ISO.

As previously discussed, the best effect of using cross-polarization can be seen for image C2 (Figure 4.1 (e)-(f)). Therefore choose to study image C2 for each of the different cases of camera settings. The images are presented in Figure 4.5. By studying the images, one can get an idea of the desired image quality for an underwater system. It is desirable to see as much details as possible of the object. Although the contrast ratio appears to be approximately the same for all four cases, it is thus not said that the details in the images are equally visible. In the following

paragraphs, the four different cases are studied.

| (a) Case 1: C2 ∥ | (b) Case 1: C2 ⊥ | (c) Case 2: C2 ∥ | (d) Case 2: C2 ⊥ |
| (e) Case 3: C2 ∥ | (f) Case 3: C2 ⊥ | (g) Case 4: C2 ∥ | (h) Case 4: C2 ⊥ |
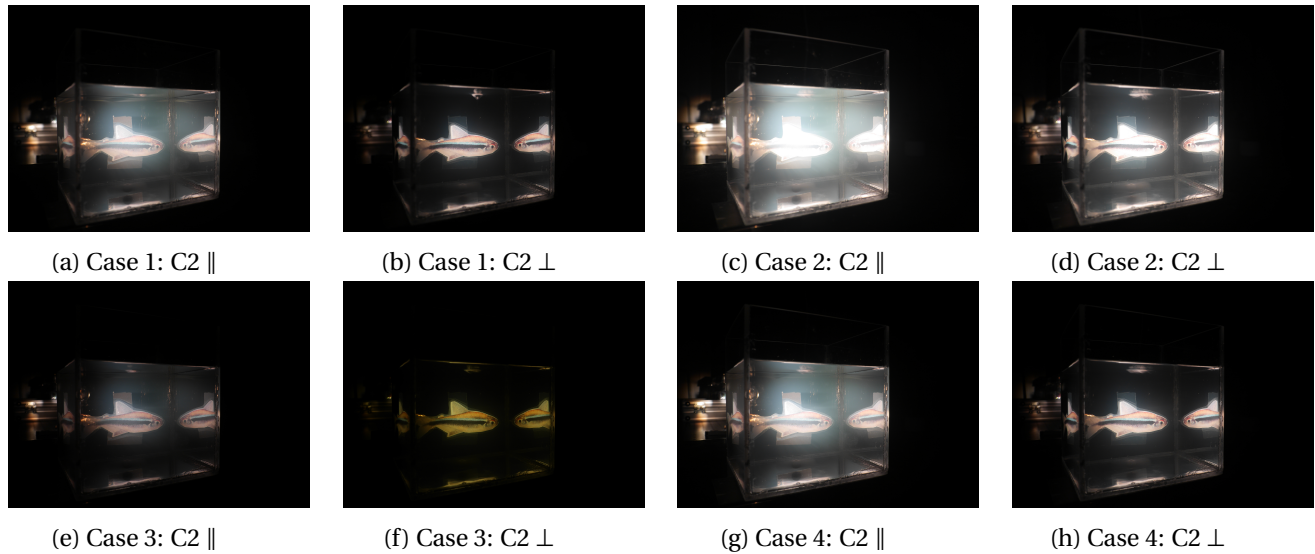
Figure 4.5: C2 indicate concentrations from the serial dilution in Table 3.5. ∥ indicates that the polarizing filter in front of the LED is parallel to the one in front of the camera. ⊥ indicates cross-polarization.

Case 1 - 1 s, f/4

The images captured with the camera settings in case 1 is shown in Figure 4.5 (a)-(b). The image quality seems great; details of the object can be observed. The colors of the object look the same as it is in real life. Since photographing in a dark environment, it is recommended to use a large aperture. For a large aperture, the depth of field is small, which results in the main being perceived sharply. The distance to the object is not large here, and a small depth of field is therefore OK. It looks like a good balance between aperture and shutter speed. It also looks like these two settings fit the constant ISO selected.

Case 2 - 4 s, f/4

Here the images seems overexposed (Figure 4.5 (c)-(d)). It is a larger aperture, resulting in more light hitting the camera sensor. A high shutter speed also increases the amount of light hitting the sensor. The balance is not great, and thus this is not an appropriate camera setting for imaging and observing the object.

Case 3 - 1 s, f/7.1

For this case, the images seem a bit darker than the others (Figure 4.5 (e)-(f)). The reason for this is the combination of shutter speed and aperture value, allowing less light to hit the camera sensor. An alternative here could be to adjust the ISO value. However, since constant camera settings are needed to study the optical phenomena, this is not an option.

Case 4 - 4 s, f/7.1

For case 4 the images seems similar to the images for case 1 (Figure 4.5 (g)-(h)). It looks like a good balance between shutter speed and aperture. Observing the background, one can observe it more visible here than in case 1. Since we are photographing at a smaller distance, the depth of field does not need to be that big - it may be smarter to choose a larger aperture where the object will be more focused.

Best choice

Based on the observations, the recommendation for this setup is to use camera settings: shutter speed 1 s, and aperture f/4, with fixed ISO200. Various factors influence this choice; the distance to the object being photographed and the depth of field required. It is also more appropriate to use a lower shutter speed and instead compensate with a larger aperture. Although these settings suit this setup, it is not sure it would fit as well if another camera were used. Therefore, it is crucial to investigate whether other camera settings may work better if one uses a different camera. However, it is a pointer. The camera settings in case 1 are used for the other experiments in this thesis.

4.1.4 Observations in the Images

By observing the images in Figure 4.1, one can observe blur in the images. The particles used in Experiment A have a diameter approximately equal to the wavelength of the incidence light ($d \geq \lambda$). As discussed in Section 2.3.3, it is a typical "Mie particle". For such a particle, there is a greater extent of forward scattering than backward scattering. As discussed in Section 2.1.3, a great extent of forward scattering in an underwater system will lead to a reduction in contrast as well as blur in the image. The blur may therefore be due to a greater extent of forward scat-

tering. However, most likely, the blur is caused by a combination of both forward and backward scattering, as well as masking of veiling light, and the fact that the scaled optical depth increases.

By studying the images in Figure 4.1 it also can be seen that the images are perceived as darker for increasing concentration. As discussed, the particles used in this experiment is typical Mie particles; there is more forward scattering than backscattering. This can be a factor why it gets darker for increasing concentration. Light is also scattered in other directions, which may also cause less light to be scattered backwards for increasing concentration. Another factor that may also cause the images to appear darker for increasing concentration is the use of polarization filters, as discussed in Section 2.4.5, the polarizing filter is reducing the light intensity as it only allows a specific polarization of light to let through the filter, and thus there is less light perceived by the camera. The medium is perceived as white, and thus there seems like there is little absorption in the container. It seems like the spheres scatter all the wavelengths.

Although the contrast is worse for the multiple scattering regime when cross-polarization is used, the eyes may tend to observe something else. By studying image C6-C9 (Figure 4.1 (m) - (t)), one may perceive the contrast as better when using cross-polarization. This may be due to the contrast difference between the dark background and red-orange fish. It seems like the eyes have a harder time distinguishing between a white background and an bright object. Thus, the eyes may have a different way of calculating contrast than the contrast code. Also, the contrast only is calculated based on one or several areas of the fish and one or several areas of the background. It could perhaps have been different if the contrast were calculated based on the whole object and the whole background. The method used to calculate the contrast may be simple, but a more advanced contrast code is outside the scope of this thesis. A more advanced contrast code is a suggestion for further work.

White balance

By observing the images in Figure 4.1, one can observe a yellowish ting in image (b) and (d). For image (b), there is only Milli-Q water in the container, and for image (d), there is a small number of polystyrene spheres. Since it just was for the images with cross-polarization, the first thought

was that this was due to the polarization filter. After researching, it turned out that the camera was not set to a constant white balance, and it is assumed that this is the cause of the yellowish tinge in image (b) and image (d). A MATLAB code was written to study the white balance. The code is in the GitHub attached to this thesis [30]. The MATLAB code retrieves the pixels from an area known to be outside the tank.

Furthermore, the code calculated the average of these pixels. The result is one average value for R, one for G, and one for B, for each of the images. If there is a constant white balance, the average values for these RGB values should be approximately equal for all images. In this case, it turned out that this is not true. The image with the best white balance (in relation to how it is perceived if one is studying the setup with own eyes) is set as a reference image. In this case, image (e) is selected as the reference for the parallel polarization filter. Image (f) is selected as the reference for cross-polarization. Another factor underlying this choice of images is that the average value of the RGB values in the selected area is approximately equal for the rest of the images (g)-(t). The white balance is thus most different in the first images.

Furthermore, the average RGB values for each of the two images are used to calculate which value the other images must be multiplied with to get the average pixel value to be equal to the average of two selected images. Once this is done, the RGB values can be recombined into a new image. The result is now images with the same white balance, and one can observe the yellowish tinge to be gone. The fact that the white balance turned out not to be constant will not affect the contrast calculations, as the formula for contrast, takes into account both an area of the background and an area of the object (Eq. 3.13). Since these values are multiplied by the same factor, this factor disappears when calculating the contrast.

After testing with another camera for the same concentrations (image (b) and (d)), the images does appear yellow, which substantiate the claim that the yellowish ting is due to the automatic white balance.

Figure 4.6 illustrates the result from the white balance code. By comparing these images with the images in Figure 4.1, one can see that there are no major differences in terms of white balance.

The biggest difference is the adjustments in image (a)-(d). Here one can observe the yellowish ting to be gone. Apart from this, one can observe the same as discussed in the section above; the scaled optical depth increases, leading to a reduction in contrast. The images are getting darker as a result of scattering and the polarizing filters reducing the light intensity. By studying the images with the eyes, one observes a clear effect of cross-polarization in all cases, especially for image C2 in Figure 4.6 (e)-(f). Although the calculations from previous sections indicate that the concentration worsens with cross-polarization when there is multiple scattering in the container, the eyes, as discussed, may have a different way of observing the image contrast.

(a) C0 ∥   (b) C0 ⊥   (c) C1 ∥   (d) C1 ⊥

(e) C2 ∥   (f) C2 ⊥   (g) C3 ∥   (h) C3 ⊥

(i) C4 ∥   (j) C4 ⊥   (k) C5 ∥   (l) C5 ⊥

(m) C6 ∥   (n) C6 ⊥   (o) C7 ∥   (p) C7 ⊥

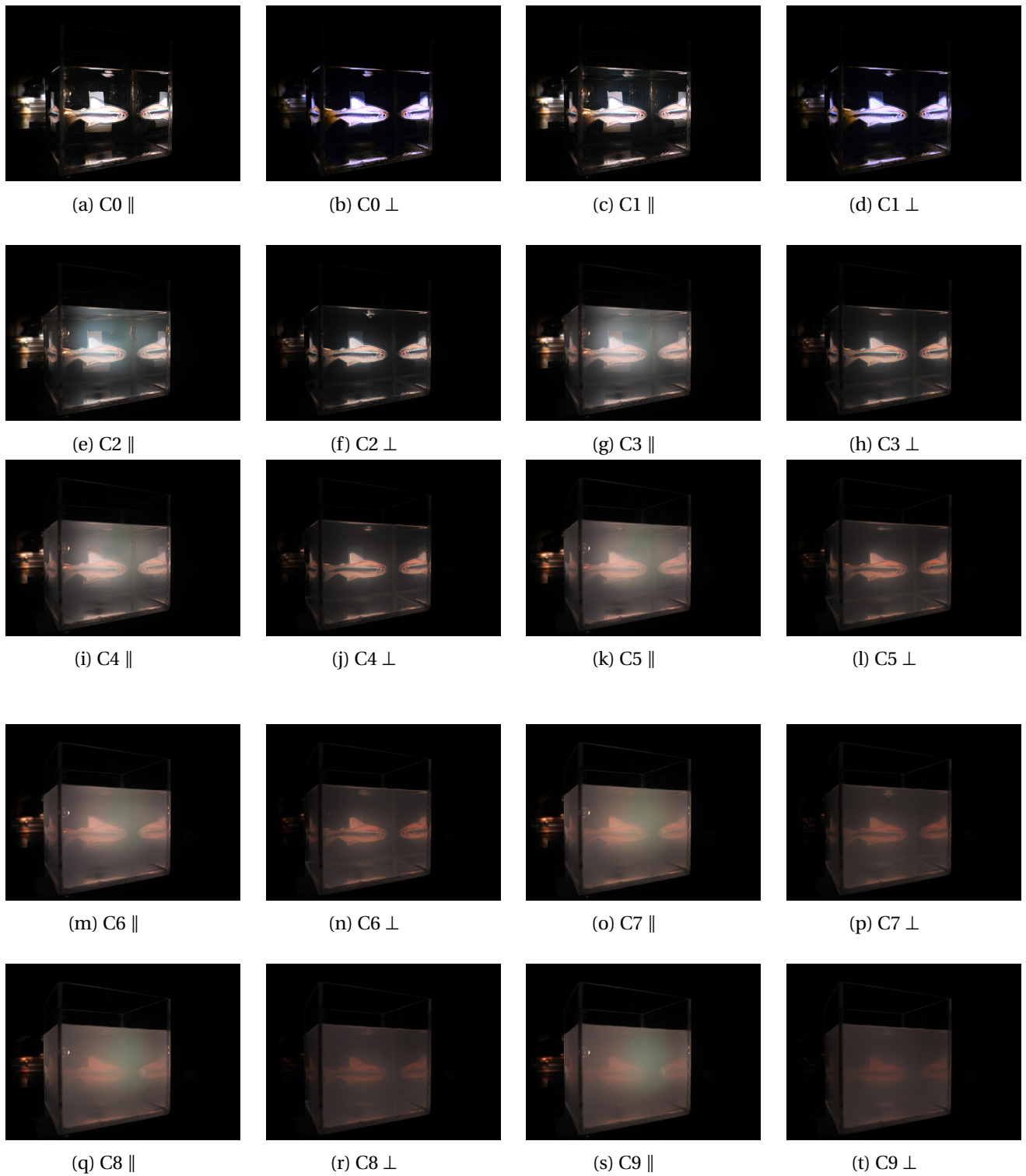(q) C8 ∥   (r) C8 ⊥   (s) C9 ∥   (t) C9 ⊥

Figure 4.6: C1-C9 indicates the different concentrations from the serial dilution in Table 3.5. The content in the container in (a) and (b) is just Milli-Q. ∥ indicates that the polarizing filter in front of the LED is parallel to the one in front of the camera. ⊥ indicates cross-polarization.

4.2 Experiment B - Algae

Whether it is possible to improve underwater imaging by using two polarizing filters, is further studied in experiment B. As discussed in Section 4.1.3, the shutter speed is set to 1 s, and the aperture is set to f/4. ISO200 is constant. The setup used is described in detail in Section 3.1.2. The algae are added to the container by a pipette according to the serial dilution shown in Table 3.6. As mentioned in Section 3.1.6, the algae are added logarithmic, which means that one can see a clearer effect of increasing the concentration versus in Experiment A. Two images are taken for each of the concentrations; one image with polarization filter parallel and one with cross-polarization. The images are shown in Figure 4.7.

By observing the different images in Figure 4.7, one can see a small effect of cross-polarization. By comparing the images in Figure 4.7 with the images taken in Experiment A (Figure 4.1), one does not see an apparent effect of polarizing filters as for the spheres. As discussed earlier, and as stated in Bohren et al. [4], polarization is said to be preserved in backward direction when light is scattered by spherical particles. Since the algae are not spherical, it is conceivable that the polarization is not entirely preserved in the backward direction for these particles. Thus, it is conceivable that the effect is not as good for the algae. Another factor that may be one reason one does not observe such a good effect of cross-polarization as in Experiment A is absorption. Absorption causes some of the incident light to be absorbed, and this may lead to less backscattered light, and therefore less backscattered light to be removed. A combination of this, may be the reason why the effect of cross-polarization is not as visible as in Experiment A.

By studying the images in Figure 4.7, it can also be seen that the images are pretty blurry for the low concentrations compared to the images from Experiment A. As the diameter of the algae is larger than the wavelength (and also larger than the particles used in Experiment A), there is a higher degree of forward scattering. As discussed in Section 2.1.3, a great extent of forward scattering results in blur in the images. However, it is not just forward scattering that can lead to blurring in the image; absorption also can. For an increasing concentration, it becomes challenging to observe details of the object. This is because the algae absorb some of the light, which makes it challenging to observe the details of the object. Although one experiences less effect of

cross-polarization when algae are used, it is desirable to study the contrast to see how it changes and how much better or worse the contrast one gets by using cross-polarization. In the following section, the contrast will be studied.

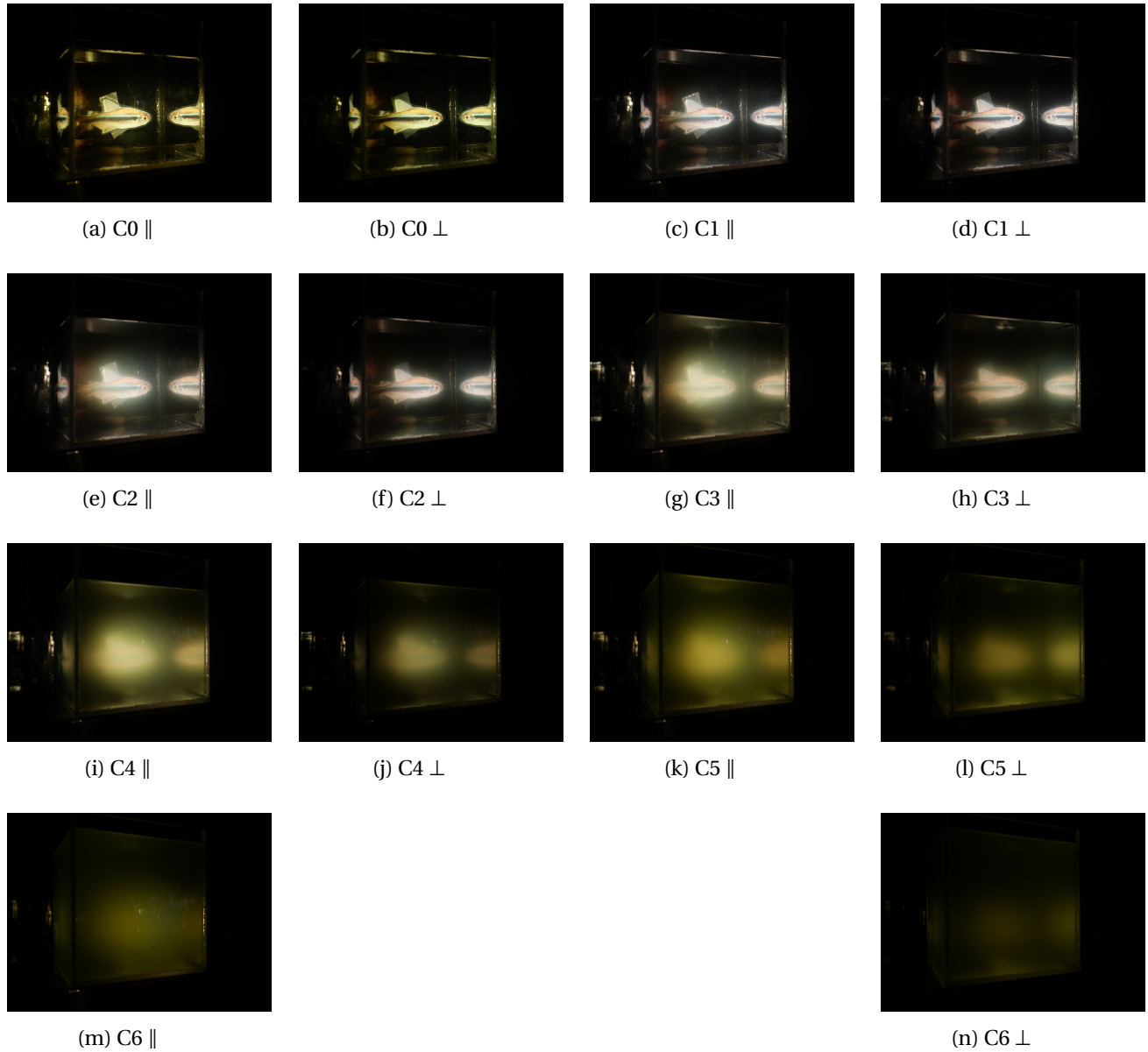| (a) C0 ∥ | (b) C0 ⊥ | (c) C1 ∥ | (d) C1 ⊥ |
(e) C2 ∥	(f) C2 ⊥	(g) C3 ∥	(h) C3 ⊥
(i) C4 ∥	(j) C4 ⊥	(k) C5 ∥	(l) C5 ⊥
(m) C6 ∥			(n) C6 ⊥

Figure 4.7: C1-C7 indicates the different concentrations from the serial dilution in Table 3.6. The content in the container in (a) and (b) is just seawater. ∥ indicates that the polarizing filter in front of the LED is parallel to the one in front of the camera. ⊥ indicates cross-polarization.

4.2.1 Contrast calculations

The images in Figure 4.7 are set as input parameters for the contrast code. The code is described in Section 3.3, and can be found in the GitHub attached to the thesis [30]. Based on previous discussions, the contrast is calculated based on a larger area of the fish instead of several smaller areas. The contrast calculations are shown in Table 4.8. How contrast is decreasing with increasing concentration is illustrated in Figure 4.8. Based on the assumptions from Section 3.1.6, a high extent of multiple scattering can be assumed from image C5 (Figure 4.7 (k)-(n)). By observing the results shown in Table 4.8 and Figure 4.8, it can be seen that the results show what was assumed; better contrast when using cross-polarization. As discussed multiple scattering ($\tau^* > 0.3$) is assumed from image C5. Based on Table 4.8, it can be observed that for $\tau^* < 0.3$ the contrast has been improved by 63-132% when cross-polarization is used. Although the object is not observable due to absorption, the contrast in the images is nevertheless improved using cross-polarization.

By observing Table 4.8 it can be seen that the contrast is better for cross-polarization in all cases. Based on what was experienced in Experiment A, it was not entirely expected that it would be better to use cross-polarization when there is multiple scattering in the container.

Table 4.8: Contrast calculated based on one larger area of the fish. The images used as input parameters are the images presented in Figure 4.7.

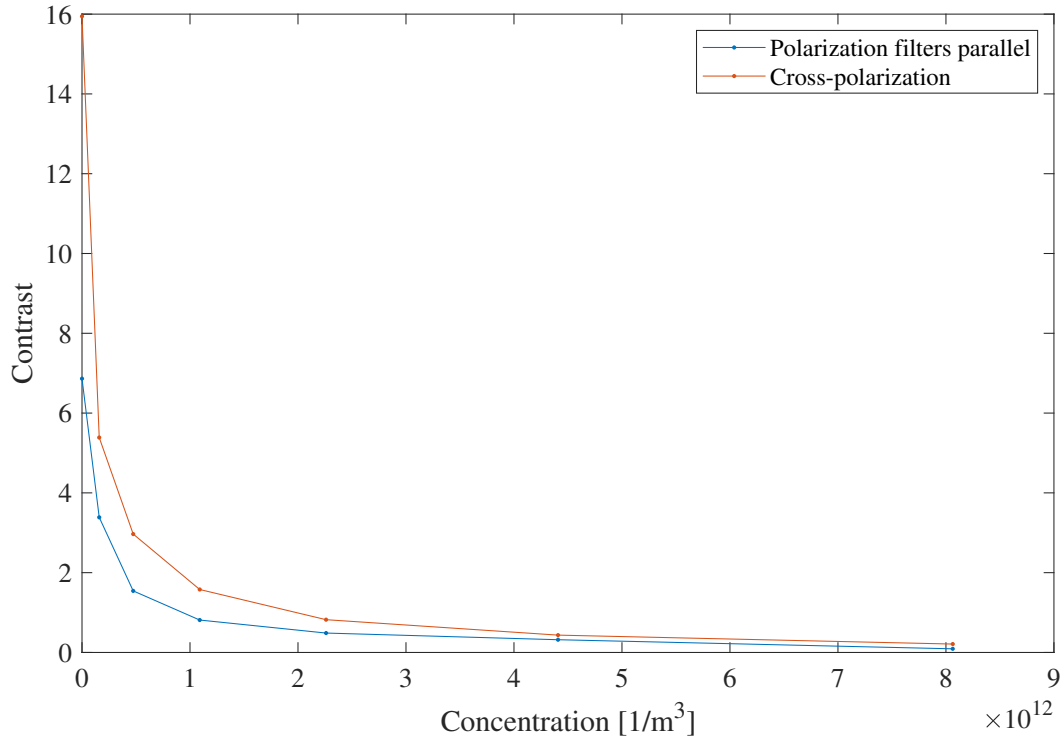| Image	Contrast		Ratio	
	Cross-Polarization	Polarization	x	[%]
C0	16	6.9	2.32	132
C1	5.4	3.3	1.63	63
C2	2.9	1.5	1.93	93
C3	1.6	0.81	1.98	98
C4	0.82	0.49	1.67	67
C5	0.43	0.32	1.34	34
C6	0.21	0.09	2.33	133

Figure 4.8: Contrast versus algae concentration

There is various hypothesis why the results are not quite as expected. As discussed, linearly polarized light is preserved in the backward direction when polarized light gets scattered by a sphere. Since the algae are not spherical, the backscattered light most likely is not linearly polarized. As a result, the linear polarization filter in front of the camera will block some of the backscattered light and allow light that oscillates parallel to the polarization axis to pass through. Since light passes through the polarizing filter in front of the camera, the camera will capture backscatter for both cases, and one will thus not experience the same effect of cross polarization here.

Another factor that may affect the contrast to be better in all cases of cross-polarization is the particle size. The size of the algae is much larger than the wavelength ($d \geq \lambda$), there will be an even greater degree of forward scattering for such type of particle compared to the particle size used in Experiment A. This result in less light being scattered backwards and thus less backscattered light to remove. The effect is thus not as significant here, and one does not see the

contrast get worse when there is multiple scattering in the container. The asymmetry parameter g indicates back, forward or isotropic scattering. Backscattering is assumed for $-1 < g < 0$, isotropic scattering is assumed for $g = 0$ and forward scattering assumed for $0 < g < 1$. For this type of alga, the asymmetry parameter g is equal to 0.97, which may indicate that there is much forward scattering. This strengthens the claim of little backscattered light. In addition to the fact that there is a greater extent of forward scattering here, it is worth mentioning that light is also scattered other ways. There is also a greater extent of absorption for the algae versus the polystyrene spheres used in experiment A.

As discussed in the previous section, one hypothesis as to why one does not see an equally good effect of cross-polarization in Figure 4.7, may be because of the combination of a great extent of forward scattering, absorption and the fact that polarization is not preserved in backward direction when the light is scattered on the algae. It is also conceivable that this combination may cause the contrast to be better in call cases, even when there is multiple scattering in the container. How absorption affects the limit for multiple scattering $\tau^* > 0.3$, as well as to what extent the backscattered light not is preserved when scattered on the algae, is out of the scope of this thesis but is a suggestion for further work. However, the contrast calculations show that better contrast is obtained by imaging with cross-polarization, which is in line with the assumptions.

As discussed in Section 4.1.1, and illustrated in Figure 4.9, scattering particles per volume depends on the complex refractive index of the algae used. If the refractive index is incorrect, one can assume multiple scattering for the wrong concentration. The complex refractive index of the algae used is obtained from Kandilian et al. [31]. The real part of the refractive index (n) is equal to 1.371, and the imaginary part (k) is equal to 0.0005. In Figure 4.9, one can study the outcome if one have read the wrong complex refractive index $n \pm 0.005$, $k \pm 0.0002$. Table 4.9 illustrates the %Scattering volume for the different cases. By comparing the values in Table 4.9, one can observe that the multiple scattering limit sill will be for the concentration in image C4. Based on the calculations, it is thus not for a different image this limit could have been, but one can observe that the refractive index affects the results.
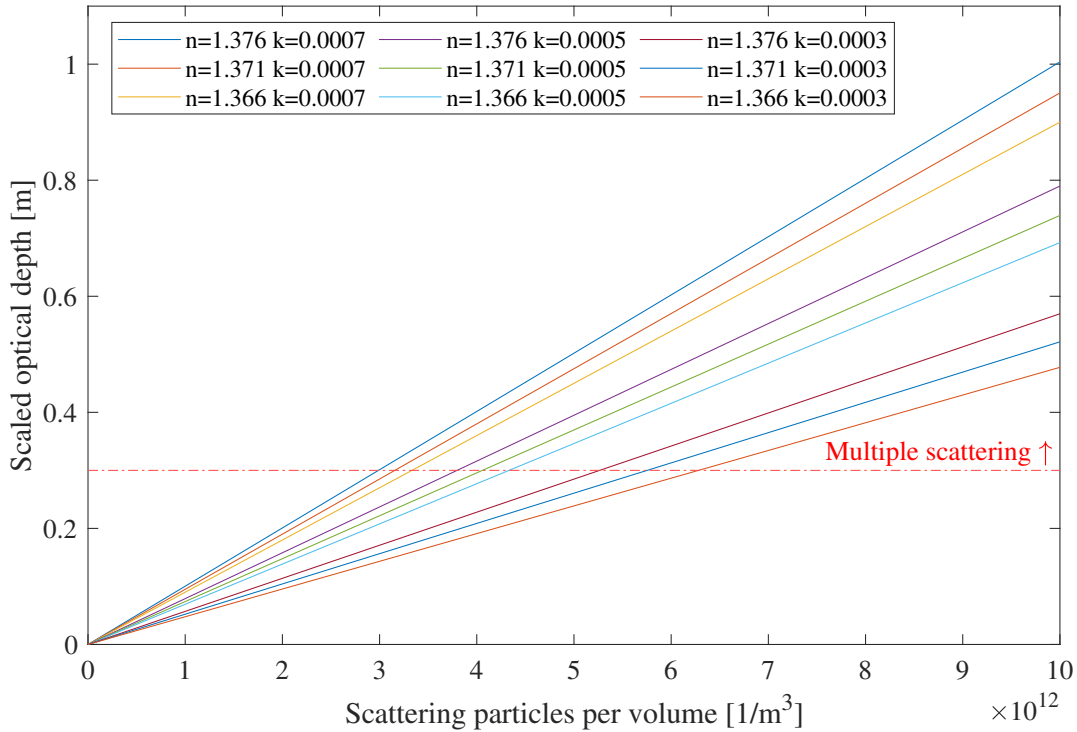
Figure 4.9: How refractive index affects scattering particles per volume at the scaled optical depth limit

Table 4.9: How concentration for scaled optical depth equal to 0.3 varies with complex refractive index.

	k=0.0005+0.0002		k=0.0005		k=0.0005-0.0002	
	Concentration	%S. Volume	Concentration	%S. volume	Concentration	%S. volume
n=1.371+0.005	2.99e12	1.35e-4	3.80e12	1.72e-4	5.27e12	2.38e-4
n=1.371	3.16e12	1.46e-4	4.06e12	1.84e-4	5.76e12	2.60e-4
n=1.371-0.005	3.34e12	1.50e-4	4.33e12	1.96e-4	6.28e12	2.84e-4

4.2.2 Observations

As previously discussed, one can, by studying the images in Figure 4.7 observe an increasing blur. As discussed, blur may result from forward scattering, but backward scattering and absorption can also cause blur in images. For an increasing concentration, one can not observe details of the fish anymore, and it is therefore conceivable that much absorption can be seen. An example illustrating that there is more absorption here than in Experiment A can be seen

by comparing the images in Figure 4.1 (o)-(p) with the images in Figure 4.7 (k)-(l). The scaled optical depth is approximately similar for both of the images, but the details of the fish in Figure 4.1 is more apparent. A transmission measurement has been made in order to study how much of the light is transmitted for the highest concentration (C7) of algae (Figure 4.7(m)-(n)). The method described in 3.2.4 is used to process the results. The result is shown in Figure 4.10.
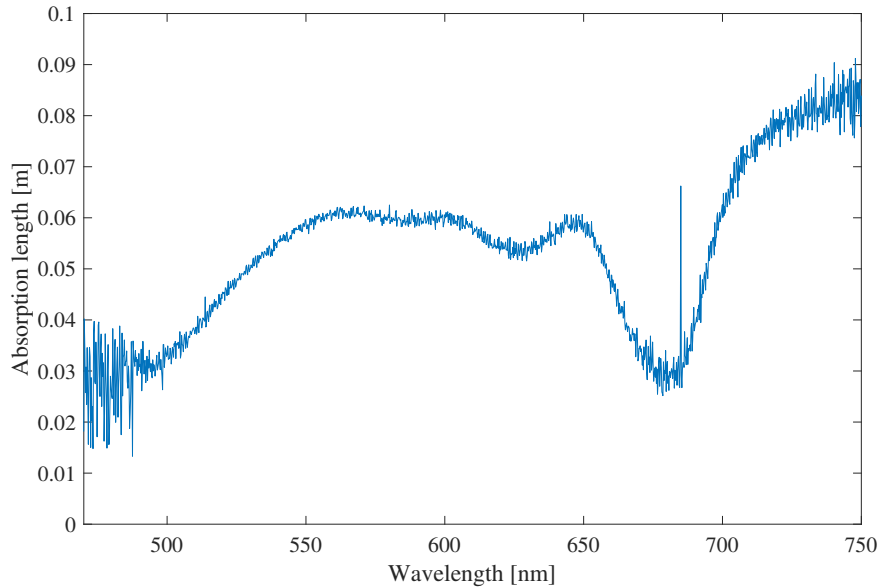
Figure 4.10: Absorption length for the concentration in image C6

As discussed in Section 2.1.4, absorption length is the distance where approximately 64% of the light intensity is absorbed. By comparing the length of the container (0.115 m) with the absorption length in Figure 4.10, it can be seen that most of the light is absorbed within the container for the concentration in Figure 4.7 (m)-(n). A result of light being absorbed is darker environments. By observing the images in Figure 4.7 one can observe the images to appear darker for increasing concentration. As absorption is increasing with increasing concentration, it may look like the increasing darkness is caused by absorption, but also the fact that there is a higher extent of forward scattering than backscattering for the algae used.

As discussed in previous sections, one can observe that the visibility in the container deteri-

orates with the increasing concentration of algae, which is caused by the optical depth in the container increasing and a greater degree of absorption. It has been assumed that one has multiple scattering in the container from image C4 (Figure 4.7 (i)-(n)). However, by calculating the probability of scattering, it can be seen that for image C3, there is a 95% chance of scattering. Due to this high probability, there is also ha higher chance of multiple scattering. Thus, it is conceivable that here one has multiple scattering in the container before assumed.

Table 4.10: The scattering coefficient (β), scaled optical depth (τ^*), optical depth (τ), and probability of survival and scattering, for the concentration in each of the images

Image	β [m^{-1}]	τ^*	τ	Probability of survival	Probability of scattering
C0	-	-	-	-	-
C1	3.72	0.01	0.43	0.65	0.35
C2	11.10	0.04	1.28	0.28	0.72
C3	25.50	0.08	2.93	0.05	0.95
C4	52.86	0.17	6.08	3e-3	0.997
C5	103.16	0.33	11.86	7.046e-6	0.999
C6	188.69	0.60	21.70	3.77e-10	0.999

The mean free path for scattering can also be studied in order to study the scattering in the container. The result is shown in Table 4.11. By comparing the mean free path with the length of the container (0.115 m), one can observe that the mean free path for the concentration in image C2 is less than the length of the container. When this value is shorter than the length of the container, there dominating multiple scattering in the container. Therefore, it may indicate that there is much multiple scattering already for image C2.

Table 4.11: τ^* is the scaled optical depth, N is the number of scattering particles per volume, β is the scattering coefficient, σ_s is the scattering cross-section of a single particle. The mean free path is the mean free path for scattering.

Images	τ^*	N [1/m^3]	β [1/m]	σ_s [m^2]	Mean free path [m]
C0	-	-	-	-	-
C1	0.013	1.59e11	3.72	23.40e-12	0.27
C2	0.035	4.74e11	11.09	23.40e-12	0.09
C3	0.081	1.10e12	25.50	23.40e-12	0.04
C4	0.17	2.26e12	52.86	23.40e-12	0.02
C5	0.33	4.41e12	103.16	23.40e-12	9.70e-3
C6	0.60	8.063e12	188.69	23.40e-12	5.30e-3

Although the probability of scattering in Table 4.10, and mean free path for scattering in Table 4.11, indicates that there is a great extent of scattering in the medium, and thus also a high probability of multiple scattering, it is not experienced the same way as in Experiment A. As discussed, this probably is due to the combination of a high extent of forward scattering, absorption and the fact that polarization is not preserved in backward direction when light is scattered by the algae. A suggestion for further work is to study these causes in more detail.

White balance

By observing the images in Figure 4.1, one can observe a yellowish-ting in (a)-(b). In this case, there is only seawater in the container, no algae. After examining the same concentration with another camera where the white balance is set as constant, it has been found that it is the automatic white balance that causes the yellowish color. The same code and procedure as described in Section 4.1.4, are used to change the white balance in the images so that the white balance is constant for each of the images. As discussed in this will not affect the contrast calculations, but the images will get a slightly different hue. The input parameters to the white balance code are the images depicted in Figure 4.7. The result from the white balance code is illustrated in Figure 4.11.
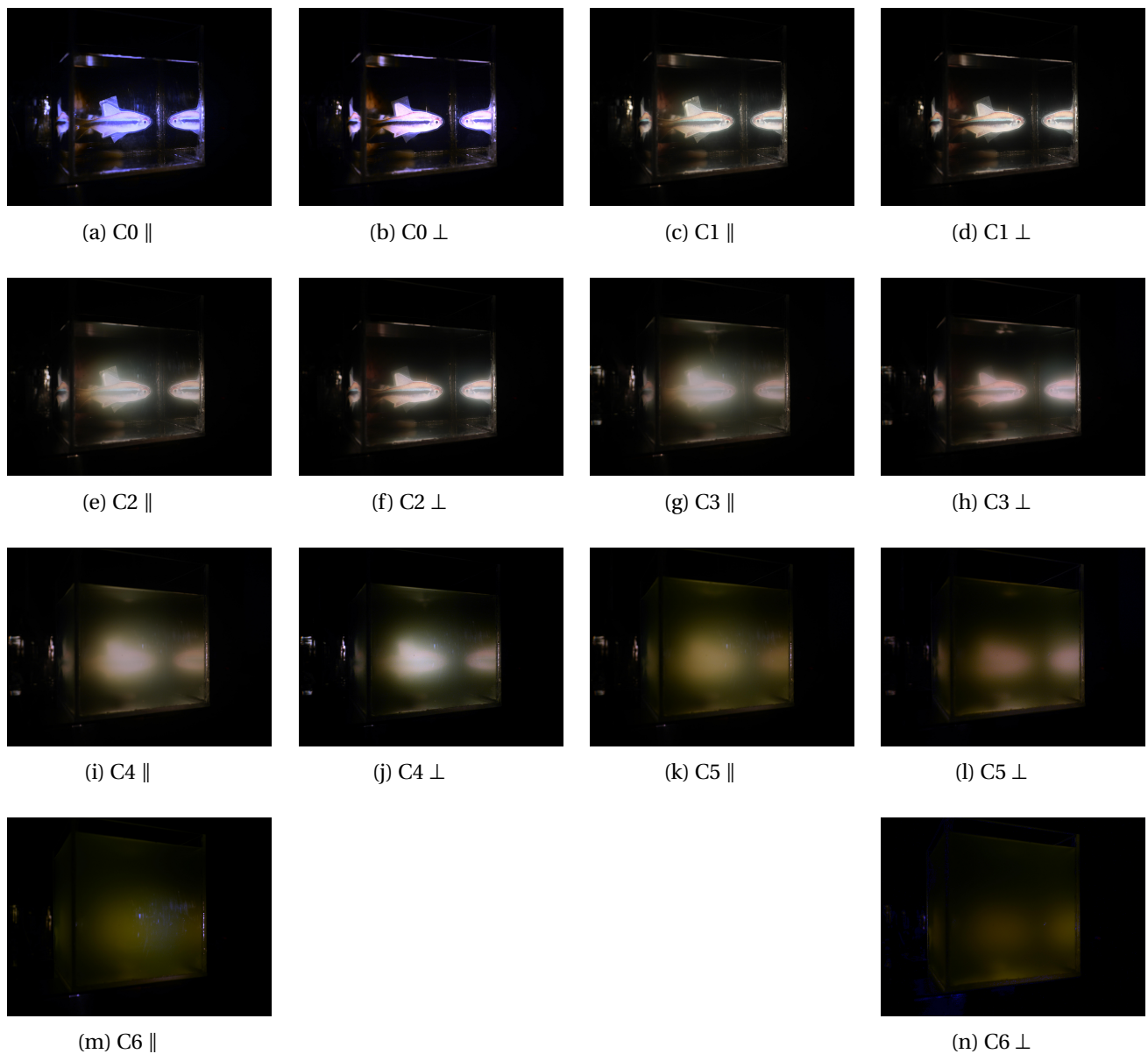
Figure 4.11: Recombined images after constant white balance. C1-C7 indicates the different concentrations from the serial dilution in Table 3.6. The content in the container in (a) and (b) is just seawater. $\parallel$ indicates that the polarizing filter in front of the LED is parallel to the one in front of the camera. $\perp$ indicates cross-polarization.

Studying the different images, the same thing as previously discussed can be observed; there is an increased absorption for increasing concentration, which causes the images to appear darker. Due to the particle size, there is also a great extent of forward scattering. The combination of a great degree of forward scattering and absorption causes less backscatter here than

for experiment A, and thus also less backscattered light to be removed. This may be a reason for the effect of cross-polarization not to be observed as well here as it was in Experiment A. One can see an effect of cross-polarization, but due to absorption, one does not observe details of the object for the higher concentrations.

4.3 Experiment C - CDOM

The purpose of Experiment C is to study how CDOM affects underwater imaging. In order to do that, the absorption coefficient and absorption length for the different CDOM materials used are determined. The different CDOM materials used are listed in Table 4.12. Case 1 consists of Earl Gray Tea made on 1.5 L water boiled to 100 °C, where the three tea bags used have been in the water for 15 min. Case 2 consists of Earl Gray Tea made on 1.5 L water heated up to 37 °C, where the three tea bags used have also been in the water for 15 min. In case 3, Fun Light Ice Tea Peach has been used. The setup for the experiment is shown in Figure 3.5. The procedure for the experiment is explained in Section 3.2.3. The results for each of the cases are presented in the following sections.

Table 4.12: The different cases of CDOM

Case	Tea	Amount
1	Earl Gray Tea (100 °C, 15min)	1:5 + 1:10
2	Earl Gray Tea (37 °C, 15min)	1:5 + 1:10
3	Fun Light Ice Tea Peach	1:5 + 1:10

(a) ∥ 1:5　　　　(b) ⊥ 1:5　　　　(c) ∥ 1:10　　　　(d) ⊥ 1:10

Figure 4.12: Case 1

| (a) ∥ 1:5 | (b) ⊥ 1:5 | (c) ∥ 1:10 | (d) ⊥ 1:10 |

Figure 4.13: Case 2

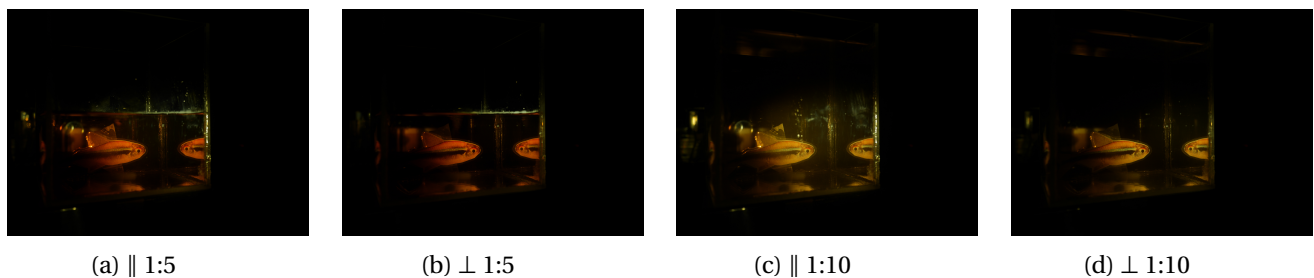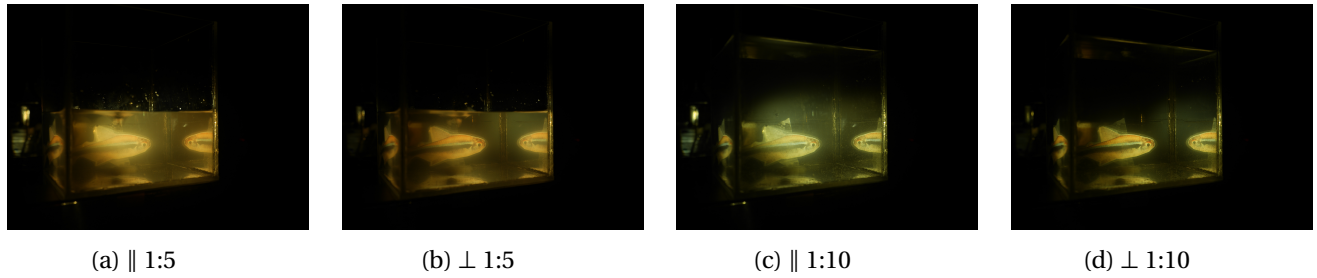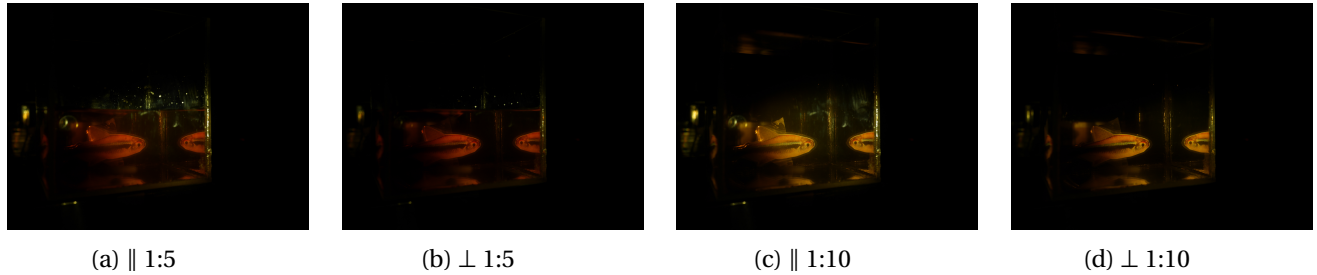| (a) ∥ 1:5 | (b) ⊥ 1:5 | (c) ∥ 1:10 | (d) ⊥ 1:10 |

Figure 4.14: Case 3

The images in Figure 4.12, Figure 4.13 and Figure 4.14, are set as input parameters to the contrast code described in Section 3.3. ∥ indicates parallel polarizing filters, and ⊥ indicates cross-polarization. The result is presented in Table 4.13. If one studies the three different cases, it can be observed that it gives a higher contrast to photograph with cross-polarization for all the concentration of tea. By observing the images, there is thus not as clear a difference using cross-polarization as for the other two experiments. One reason for this is probably because there are not enough particles to experience a significant backscatter, and it is thus little backscatter to remove.

Table 4.13: Contrast calculations

	Case 1		Case 2		Case 3	
	⊥	∥	⊥	∥	⊥	∥
Image 1 (Water)	7.1	3.8	7.1	3.8	7.1	3.8
Image 2 (1:5)	7.8	3.2	0.59	0.42	4.1	0.97
Image 3 (1:10)	3.8	1.1	1.2	0.66	4.4	1.6

In order to study how CDOM is affecting imaging underwater, the absorption coefficient and absorption length for the different CDOM materials used is studied in the next sections.

4.3.1 Case 1 - Absorption Coefficient and Absorption Length

As described in the experimental procedure in Section 3.2.3, transmission measurements have been performed. These measurements have been processed with the absorption code described in Section 3.2.4. The script plots absorption length and absorption coefficient against wavelength. The absorption coefficient and absorption length from case 1 are depicted in Figure 4.15.
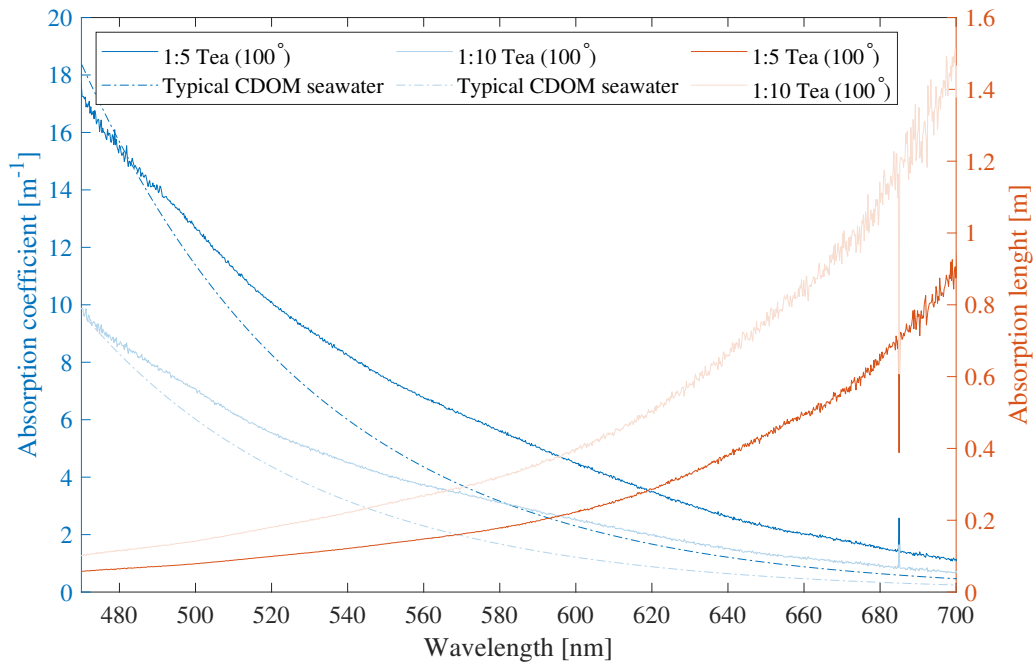

Figure 4.15: Absorption length and absorption coefficient for case 1. CDOM Parameterization is based in equation 3.12

By studying Figure 4.15, it can be seen that the short wavelengths are the ones that are absorbed first. This is consistent with typical CDOM. The longer wavelengths survive the longest. Since the absorption length is greater than the length of the container (0. 115m) for the longer wavelengths, most of the wavelengths will pass through, but it may look like some of the smaller wavelengths gets absorbed in the container. The dotted lines in Figure 4.15, is the CDOM pa-

rameterization for 1:5 and 1:10. One can see that the calculated absorption coefficients (1:5 and 1:10) do not match the CDOM parameterization. It is a similar type of curve, but it has a different slope. This may indicate that the particles used is larger than typical CDOM. CDOM is by definition what passes through a filter with a pore size of 0.02 μm. Therefore, it may look like the CDOM used has particles larger than 0.02 μm.

A high concentration of CDOM can result in darkening in the images due to absorption. By studying the images in Figure 4.12, one can see how images taken in typical CDOM water looks like; the images are appearing yellow-brownish. CDOM causes color degradation, and also causes one to not be able to see the original colors of the object being imaged.

4.3.2 Case 2 - Absorption Coefficient and Absorption Length

Figure 4.16 illustrates the absorption coefficient and absorption length for case 2. As for case 1, the same things can be observed here: the shorter wavelengths are absorbed first, while the longer ones are the one surviving longest. Here, the absorption length is longer for the shorter wavelengths than for case 1. Because the tea bags are dissolved in water at 37°, there is not as much color as when the tea bags are dissolved at 100°. This results in the medium having a higher absorption length, The absorption coefficient here does not correspond to CDOM parameterization, as discussed in the previous section, this is due to the particle size of the CDOM used.

By studying the images in Figure 4.13, it can also for case 2 be observed that the CDOM results in a yellow-brownish color in the image, which results in one not being able to see the original colors of the object.
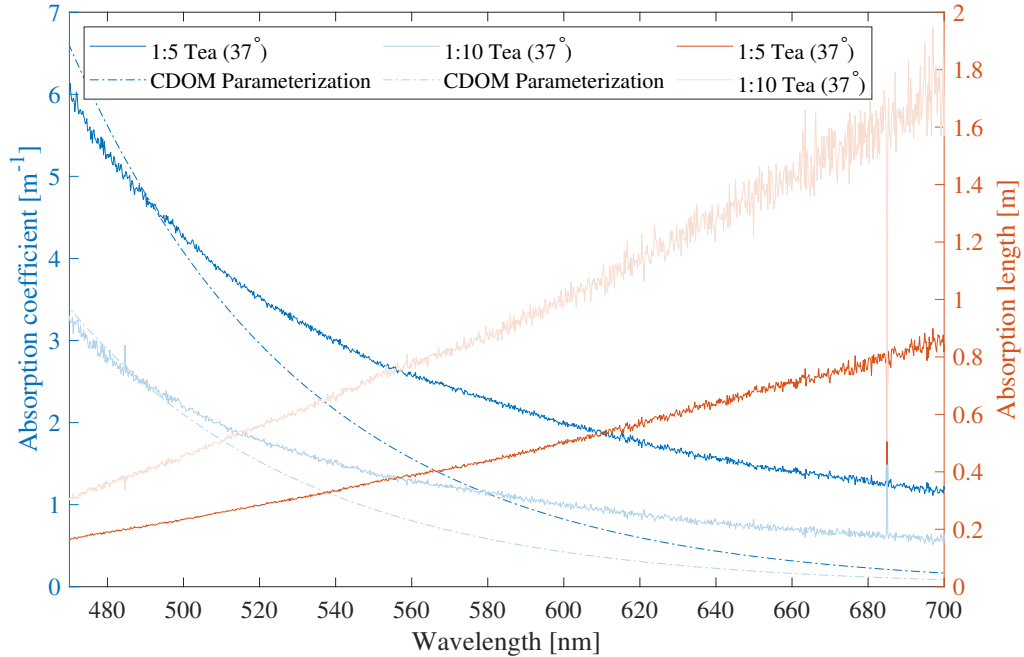
Figure 4.16: Absorption length and absorption coefficient for case 2

4.3.3 Case 3 - Absorption Coefficient and Absorption Length

Figure 4.17 illustrates the absorption coefficient and the absorption length of the CDOM materials used for case 3. One can observe the same thing here, as for the other cases; the short wavelengths are absorbed first, and the long ones can survive the longest. If one compares the absorption length with the absorption length in Figure 4.15 and 4.16, one can observe that the absorption length is shorter here. This is caused by the CDOM materials used; there is a greater extent of absorption here. Since the absorption coefficient is the inverse absorption length, it can be seen that the absorption coefficient is also higher here than in the other cases. The measurements from case 3 do not seem to correspond with the CDOM parameterization here either, as a result of the particles size being larger than typical CDOM. It has a typical CDOM curve, just with a different slope.

By studying the images in Figure 4.14, it can also for case 3 be observed that if one are imaging in a CDOM medium the images will be appearing yellow-brownish.
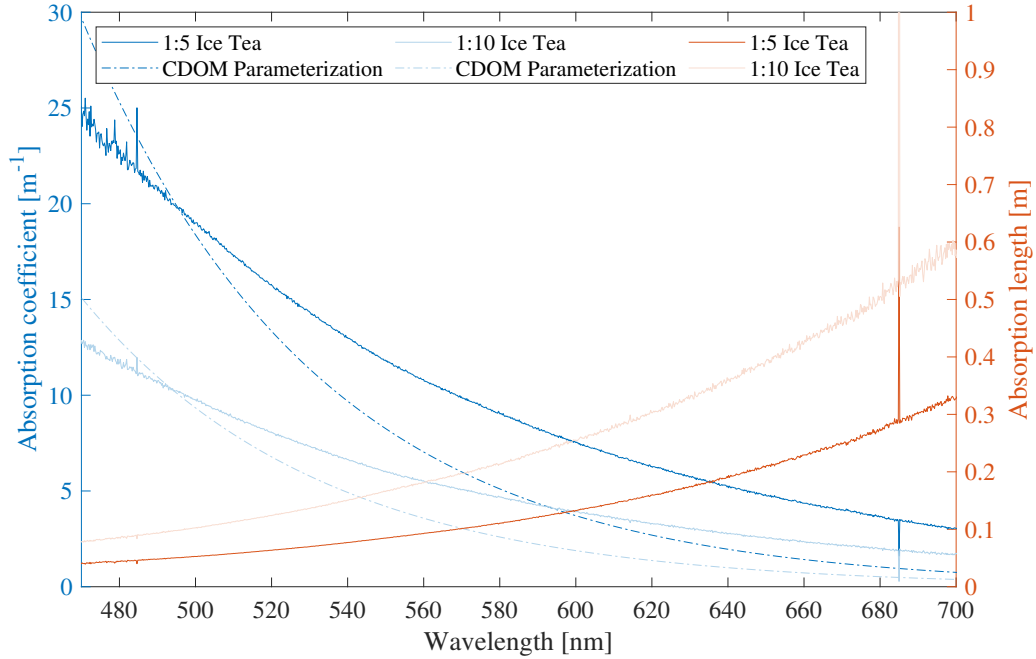
Figure 4.17: Absorption length and absorption coefficient for case 3

4.4 Sources of Error

Various sources of error may have influenced the results. As discussed in previous sections, one of these error sources may be misreading the refractive index. As discussed, this will have an effect on which concentration multiple scattering can be expected.

Another factor that may have influenced the result is that the polarization filters may not have been rotated completely 90° on each other or rotated completely parallel to each other when the images have been taken. This will allow unwanted scattered light to let through the filters or to be blocked, which may lead to an error in the contrast calculations, as well as the observations that have been made. Marks have been set on the filters to indicate that these are rotated correctly, so it should not have affected the results that much, but one cannot be entirely sure. Other sources of error can be that one has touched the camera when the polarizing filters was getting adjusted. This can result in the contrast code not retrieving the exact same area of the fish for the different images, which may affect the contrast calculations. Have studied the ex-

tracted area for all of the images, and it seems to be almost exact, but it may deviate a bit. Small reflections from the container may also have affected the results slightly, but no large reflections have been observed.

Another source of error is that constant white balance was assumed. During the process of studying the results, it turned out that the white balance was set to automatic. This resulted in different white balances in the images, but as discussed previously, this does not affect the contrast calculations. A code has been written to set the automatic white balance to constant. This reduces the possibility of sources of error in the observations of the images.

For the transmission measurements, a reference spectrum has been set, so it is not intended that there should be many sources of error related to this. However, one may experience noise in the measurements. One reason for this may be due to calibration and that the layout may have been changed slightly after the reference spectrum was set. The LED light only emits light in the range of 470-850 nm, resulting in noise for the other wavelengths. As mentioned, noise in the measurements can be caused by tiny changes, such as when adding tea to the container, there may be bubbles in the water, which can cause noise in the measurements. The setup is calibrated to an empty container. When adding water and tea, this may result in some noise.

5 Conclusion

The main objective of the thesis was to study whether it is possible to improve underwater imaging utilizing the polarization properties of light. By using two polarizing filters, one in front of the light source and one in front of the camera rotated 90° (cross-polarization), one should be able to remove most of the unwanted scattered light. Three different experiments have been performed to study the effect of cross-polarization in different types of water.

In Experiment A, the container consists of spherical polystyrene particles and Milli-Q water. It was assumed that the use of polarization filters would work best when there was single scattering in the container, as polarization is preserved in backward direction when light is scattered on spherical particles. For multiple scattering, the backscattered light is not preserved, and the effect is thus assumed to be as good here. In order to determine whether it is single or multiple scattering, a limit was set. When the scaled optical depth is greater than 0.3, one could expect multiple scattering in backward direction. The results from Experiment A indicates an apparent effect of using cross-polarization when there is single scattering in the container. For $\tau^* < 0.3$ the contrast has been improved by 22-105% when cross-polarization is used.

Since polarization is preserved in backward direction when scattering by spheres, it was assumed that cross-polarization should not give an equally good effect in Experiment B since the algae used is not spherical. The algae absorb more than the spheres, making it more challenging to observe the object in the area where multiple scattering is expected. The particle size of the algae is much larger than the wavelength, which leads to a greater extent of forward scattering. The combination of absorption, great extent forward scattering and the fact that polarization is not preserved in backward direction when light is scattered by the algae, results in not observing an equally good effect of cross-polarization in Experiment B as was observed in Experiment A. Although one did not observed an equally good effect in Experiment B as in Experiment A, contrast calculations indicates that it was better to image with cross-polarization. For $\tau^* < 0.3$ the contrast has been improved by 63-132% when cross-polarization is used. Although the object is not observable due to absorption, the contrast in the images is nevertheless improved using

cross-polarization.

In Experiment C, it was studied how CDOM is affecting underwater imaging. Absorption length and absorption coefficient was calculated for the various CDOM materials used. CDOM typically absorbs the short wavelengths first, while the longest survives the longest. This can also can be seen in the results. The results also shows that CDOM typically makes the images appear yellow-brownish. As a result of the images appearing yellow-brownish, one does not observe the correct colors of the object being imaged. CDOM also makes it more difficult to photograph objects at longer distances than if the medium only was consisting of pure water or seawater. Results from the contrast calculations shows an improvement in contrast when cross-polarization is used, but by observing the images one does not see as clear an effect of cross-polarization as for the other experiments. The reason for this is because there is not a large enough concentration of particles to have a significant backscatter, and there is thus little backscatter to remove.

All three experiments indicate that one experience a better contrast when imaging with cross-polarization underwater, especially in cases where the scaled optical depth less than 0.3. Based on results from these experiments, it can be seen that an underwater system affected by unwanted backscattering can benefit from utilizing the polarization properties of light.

6 Further Improvements

The contrast code written in connection with this thesis may be seen as a straightforward method. Nevertheless, it is a good indicator of how the contrast changes with increasing scaled optical depth. The calculations could have benefited from more advanced algorithms. For further work, one could create a more advanced method of calculating the contrast. For example, a method that retrieves the entire object from the background, and calculated the contrast based on the whole object and the whole background.

As discussed in section 2.4.7, linear polarization is preserved in backward direction when scattering by a sphere. The polarization is not linearly preserved for other directions than backward direction (180°). A suggestion for further work is to study how much of the backscattered light that can be removed at other angles, by moving the camera around using the same setup as in these experiments.

The challenge of underwater imaging can also be further researched with great advantage. There is still a long way to go if it is ever going to be as easy to photograph underwater as it is on land.

References

[1] Y. Y. Schechner and N. Karpel, "Recovery of underwater visibility and structure by polarization analysis," *IEEE Journal of Oceanic Engineering*, vol. 30, no. 3, pp. 570–587, Jul. 2005, Conference Name: IEEE Journal of Oceanic Engineering, ISSN: 1558-1691. DOI: `10.1109/JOE.2005.850871`.

[2] F. Liu, P. Han, Y. Wei, K. Yang, S. Huang, X. Li, G. Zhang, L. Bai, and X. Shao, "Deeply seeing through highly turbid water by active polarization imaging," *Optics Letters*, vol. 43, no. 20, pp. 4903–4906, Oct. 15, 2018, Publisher: Optical Society of America, ISSN: 1539-4794. DOI: `10.1364/OL.43.004903`. [Online]. Available: `https://www.osapublishing.org/ol/abstract.cfm?uri=ol-43-20-4903` (visited on 03/31/2021).

[3] L. Cartron, N. Josef, A. Lerner, S. D. McCusker, A.-S. Darmaillacq, L. Dickel, and N. Shashar, "Polarization vision can improve object detection in turbid waters by cuttlefish," *Journal of Experimental Marine Biology and Ecology*, Cephalopod Biology a special issue compiled under the auspices of no-profit research organization CephRes, vol. 447, pp. 80–85, Sep. 1, 2013, ISSN: 0022-0981. DOI: `10.1016/j.jembe.2013.02.013`. [Online]. Available: `https://www.sciencedirect.com/science/article/pii/S0022098113000658` (visited on 05/22/2021).

[4] C. F. Bohren and E. E. Clothiaux, *Fundamentals of Atmospheric Radiation: An Introduction with 400 Problems*. Wiley-VCH, Jan. 3, 2008, ISBN: 978-3-527-40503-9. DOI: `10.1002/9783527618620`. [Online]. Available: `https://pennstate.pure.elsevier.com/en/publications/fundamentals-of-atmospheric-radiation-an-introduction-with-400-pr` (visited on 03/05/2021).

[5] J. Watson and O. Zielinski, *Subsea Optics and Imaging*. Jordon Hill, UNITED KINGDOM: Elsevier Science & Technology, 2013, ISBN: 978-0-85709-352-3. [Online]. Available:

http://ebookcentral.proquest.com/lib/bergen-ebooks/detail.action?docID=1574931 (visited on 03/31/2021).

[6] J. S. Jaffe, "Underwater optical imaging: The past, the present, and the prospects," *IEEE Journal of Oceanic Engineering*, vol. 40, no. 3, pp. 683–700, Jul. 2015, Conference Name: IEEE Journal of Oceanic Engineering, ISSN: 1558-1691. DOI: 10.1109/JOE.2014.2350751.

[7] E. G. Reynaud, *Imaging Marine Life: Macrophotography and Microscopy Approaches for Marine Biology*. Weinheim, GERMANY: John Wiley & Sons, Incorporated, 2014, ISBN: 978-3-527-66420-7. [Online]. Available: http://ebookcentral.proquest.com/lib/bergen-ebooks/detail.action?docID=1568428 (visited on 01/18/2021).

[8] N. G. N. G. o. a. d. s. i. Mexico, i. a. P.-c. o. w. s. instructor is a, and T.-c. f. c. d. i. o. e. p. N. Gibb. (). "Factors affecting visibility when scuba diving," LiveAbout. Section: LiveAbout, [Online]. Available: https://www.liveabout.com/factors-that-affect-visibility-underwater-2963268 (visited on 11/17/2020).

[9] H. S. Ugulen, H. Sandven, B. Hamre, A. S. Kristoffersen, and C. Sætre, "Analysis of multiple scattering errors in LISST-VSF volume scattering function measurements using monte carlo simulations and experimental data," *Optics Express*, vol. 29, no. 8, pp. 12 413–12 428, Apr. 12, 2021, Publisher: Optical Society of America, ISSN: 1094-4087. DOI: 10.1364/OE.419116. [Online]. Available: https://www.osapublishing.org/oe/abstract.cfm?uri=oe-29-8-12413.

[10] F. Liu, Y. Wei, P. Han, K. Yang, L. Bai, and X. Shao, "Polarization-based exploration for clear underwater vision in natural illumination," *Optics Express*, vol. 27, no. 3, pp. 3629–3641, Feb. 4, 2019, Publisher: Optical Society of America, ISSN: 1094-4087. DOI: 10.1364/OE.27.003629. [Online]. Available: https://www.osapublishing.org/oe/abstract.cfm?uri=oe-27-3-3629 (visited on 05/22/2021).

[11] C. LibreTexts. (May 3, 2015). "12.6: Spectroscopy and the electromagnetic spectrum," Chemistry LibreTexts, [Online]. Available: `https://chem.libretexts.org/Bookshelves/Organic_Chemistry/Map%3A_ Organic_Chemistry_(McMurry)/12%3A_Structure_Determination_- _Mass_Spectrometry_and_Infrared_Spectroscopy/12.06%3A_Spectroscopy_and_ the_Electromagnetic_Spectrum` (visited on 04/24/2021).

[12] P. Classroom. (). "Physics tutorial: Specular vs. diffuse reflection," [Online]. Available: `https://www.physicsclassroom.com/class/refln/Lesson-1/Specular-vs- Diffuse-Reflection` (visited on 01/18/2021).

[13] E. Hecht, *Optics*, 5th ed. England: Pearson Education Limited, 2016, ISBN: 1-292-09693-4.

[14] Feynman. (). "The feynman lectures on physics vol. i ch. 26: Optics: The principle of least time," [Online]. Available: `https://www.feynmanlectures.caltech.edu/I_26.html` (visited on 11/23/2020).

[15] T. Treibitz and Y. Y. Schechner, "Active polarization descattering," *IEEE Transactions on Pattern Analysis and Machine Intelligence*, vol. 31, no. 3, pp. 385–399, Mar. 2009, Conference Name: IEEE Transactions on Pattern Analysis and Machine Intelligence, ISSN: 1939-3539. DOI: `10.1109/TPAMI.2008.85`.

[16] C. Nima, Ø. Frette, B. Hamre, J. J. Stamnes, Y.-C. Chen, K. Sørensen, M. Norli, D. Lu, Q. Xing, D. Muyimbwa, T. Ssenyonga, K. H. Stamnes, and S. R. Erga, "CDOM absorption properties of natural water bodies along extreme environmental gradients," *Water*, vol. 11, no. 10, p. 1988, Oct. 2019, Number: 10 Publisher: Multidisciplinary Digital Publishing Institute. DOI: `10.3390/w11101988`. [Online]. Available: `https://www.mdpi.com/2073-4441/11/10/1988` (visited on 04/20/2021).

[17] J. S. Jaffe, "Underwater optical imaging: The design of optimal systems," *Oceanography*, vol. 1, no. 2, pp. 40–41, 1988, Publisher: Oceanography Society, ISSN: 1042-8275. [Online]. Available: `https://www.jstor.org/stable/43924421` (visited on 03/06/2021).

[18] J. S. Jaffe, "Computer modeling and the design of optimal underwater imaging systems," *IEEE Journal of Oceanic Engineering*, vol. 15, no. 2, pp. 101–111, Apr. 1990, Conference Name: IEEE Journal of Oceanic Engineering, ISSN: 1558-1691. DOI: `10.1109/48.50695`.

[19] S. Harris and R. Ballard, "ARGO: Capabilities for deep ocean exploration," in *OCEANS '86*, Sep. 1986, pp. 6–8. DOI: `10.1109/OCEANS.1986.1160528`.

[20] C. F. Bohren and D. R. Huffman, "Introduction," in *Absorption and Scattering of Light by Small Particles*, Section: 1 _eprint: https://onlinelibrary.wiley.com/doi/pdf/10.1002/9783527618156.ch1, John Wiley & Sons, Ltd, 1998, pp. 1–11, ISBN: 978-3-527-61815-6. DOI: `10.1002/9783527618156.ch1`. [Online]. Available: `https://onlinelibrary.wiley.com/doi/abs/10.1002/9783527618156.ch1` (visited on 04/22/2021).

[21] Hyperphysics. (). "Blue sky and rayleigh scattering," [Online]. Available: `http://hyperphysics.phy-astr.gsu.edu/hbase/atmos/blusky.html` (visited on 04/27/2021).

[22] E. Optics. (). "Introduction to polarization | edmund optics," [Online]. Available: `https://www.edmundoptics.com/knowledge-center/application-notes/optics/introduction-to-polarization/` (visited on 02/16/2021).

[23] C. F. Bohren and D. R. Huffman, "Electromagnetic theory," in *Absorption and Scattering of Light by Small Particles*, Section: 2 _eprint: https://onlinelibrary.wiley.com/doi/pdf/10.1002/9783527618156.ch2, John Wiley & Sons, Ltd, 1998, pp. 12–56, ISBN: 978-3-527-61815-6. DOI: `10.1002/9783527618156.ch2`. [Online]. Available: `https://onlinelibrary.wiley.com/doi/abs/10.1002/9783527618156.ch2` (visited on 02/01/2021).

[24] P. forums. (). "Zi2le-png.239279 (480×431)," Physicsforums, [Online]. Available: `https://www.physicsforums.com/attachments/zi2le-png.239279/` (visited on 04/30/2021).

[25] Microscopyu. (). "Introduction to polarized light," Nikon's MicroscopyU, [Online].
      Available: `https://www.microscopyu.com/techniques/polarized-`
      `light/introduction-to-polarized-light` (visited on 02/08/2021).

[26] Commonvisionblox. (). "Polarization > theory of operation," [Online]. Available:
      `https://help.commonvisionblox.com/Polarization/html_english_theory-of-`
      `operation.html` (visited on 04/28/2021).

[27] P. Classroom. (). "Physics tutorial: Polarization," [Online]. Available:
      `https://www.physicsclassroom.com/class/light/Lesson-1/Polarization`
      (visited on 02/19/2021).

[28] Pajs, *Brewster's angle*, in *Wikipedia*, Page Version ID: 1018229104, Apr. 16, 2021. [Online].
      Available: `https://en.wikipedia.org/w/index.php?title=Brewster%27s_angle&`
      `oldid=1018229104` (visited on 04/30/2021).

[29] J. A. Shaw and M. Vollmer, "Blue sun glints on water viewed through a polarizer," *Applied
      Optics*, vol. 56, no. 19, G36, Jul. 1, 2017, ISSN: 0003-6935, 1539-4522. DOI:
      `10.1364/AO.56.000G36`. [Online]. Available:
      `https://www.osapublishing.org/abstract.cfm?URI=ao-56-19-G36` (visited on
      04/29/2021).

[30] MalinStolsvik, *MalinStolsvik/mastersthesis*, original-date: 2021-05-26T20:08:15Z, May 26,
      2021. [Online]. Available: `https://github.com/MalinStolsvik/Mastersthesis`
      (visited on 05/26/2021).

[31] R. Kandilian, E. Lee, and L. Pilon, "Radiation and optical properties of nannochloropsis
      oculata grown under different irradiances and spectra," *Bioresource Technology*, vol. 137,
      pp. 63–73, Jun. 1, 2013, ISSN: 0960-8524. DOI: `10.1016/j.biortech.2013.03.058`.
      [Online]. Available:
      `https://www.sciencedirect.com/science/article/pii/S0960852413004264`
      (visited on 05/05/2021).

[32] A. R. Supply. (). "Nannochloropsis," Algae Research Supply, [Online]. Available: `https://algaeresearchsupply.com/pages/nannochloropsis` (visited on 05/11/2021).

[33] C. Nima, Ø. Frette, B. Hamre, S. R. Erga, Y.-C. Chen, L. Zhao, K. Sørensen, M. Norli, K. Stamnes, and J. J. Stamnes, "Absorption properties of high-latitude norwegian coastal water: The impact of CDOM and particulate matter," *Estuarine, Coastal and Shelf Science*, vol. 178, pp. 158–167, Sep. 5, 2016, ISSN: 0272-7714. DOI: `10.1016/j.ecss.2016.05.012`. [Online]. Available: `https://www.sciencedirect.com/science/article/pii/S0272771416301500` (visited on 05/20/2021).

[34] E. Pietka, "48 - image standardization in PACS," in *Handbook of Medical Imaging*, ser. Biomedical Engineering, I. N. Bankman, Ed., San Diego: Academic Press, Jan. 1, 2000, pp. 783–801, ISBN: 978-0-12-077790-7. DOI: `10.1016/B978-012077790-7/50056-4`. [Online]. Available: `https://www.sciencedirect.com/science/article/pii/B9780120777907500564` (visited on 05/28/2021).

[35] N. ames research center. (). "Luminance contrast," [Online]. Available: `https://colorusage.arc.nasa.gov/luminance_cont.php` (visited on 05/13/2021).

[36] X. Ma, J. Q. Lu, R. S. Brock, K. M. Jacobs, P. Yang, and X.-H. Hu, "Determination of complex refractive index of polystyrene microspheres from 370 to 1610 nm," *Physics in Medicine and Biology*, vol. 48, no. 24, pp. 4165–4172, Dec. 2003, Publisher: IOP Publishing, ISSN: 0031-9155. DOI: `10.1088/0031-9155/48/24/013`. [Online]. Available: `https://doi.org/10.1088%2F0031-9155%2F48%2F24%2F013` (visited on 11/05/2020).

[37] S. photo. (). "Fotografer under vann: 7 tips," [Online]. Available: `https://www.scandinavianphoto.no/inspirasjon/produkttips/fotografer-under-vann-7-tips` (visited on 05/19/2021).